Fakultät für Elektrotechnik und Informationstechnik
Technische Universität München

Widefield Multispectral Reflection and Fluorescence Imaging for Biological Applications

Panagiotis Symvoulidis

Vollständiger Abdruck der von der Fakultät für Elektrotechnik und Informationstechnik der Technischen Universität München zur Erlangung des akademischen Grades eines

Doktor-Ingenieurs (Dr.-Ing.)

genehmigten Dissertation.

Vorsitzender:
  Prof. Dr. Bernhard Wolfrum

Prüfende der Dissertation:
  1. Prof. Dr. Vasilis Ntziachristos
  2. Prof. Dr. Jakob Macke

Die Dissertation wurde am 02.07.2018 bei der Technischen Universität München eingereicht und durch die Fakultät für Elektrotechnik und Informationstechnik am 22.10.2018 angenommen.

TUM

Widefield Multispectral
Reflection and Fluorescence Imaging
for Biological Applications

Panagiotis Symvoulidis

Vollständiger Abdruck der von der Fakultät für Elektrotechnik und Informationstechnik
der Technischen Universität München zur Erlangung des akademischen Grades eines

Doktor-Ingenieurs (Dr.-Ing.)

genehmigten Dissertation.

Genehmigtes
Titelblatt

Technische Universität München
SSZ Ab 2/2 Prüfungsangelegenheit-
- Promotionen -
Arcisstraße 21, 80333 München

Vorsitzender:
    Prof. Dr.- *Bernhard Wolfrum*

Prüfende der Dissertation:
    1. Prof. Dr. *Vasilis Ntziachristos*
    2. Prof. Dr.- *Jakob Macke*

02.07.2018

Die Dissertation wurde am ~~15.12.2017~~ bei der Technischen Universität München
eingereicht und durch die Fakultät für Elektrotechnik und Informationstechnik am
22.10.2018 angenommen.

Acknowledgements

I am obliged to start these acknowledgments with an apology to all the people that I forget to mention here. During the last years I was fortunate to be exposed to multiple project and research collaborators along with persons outside my academic circle. I guess each of them contributed intentionally or unintentionally and directly or indirectly to shaping me to the person I have become and the decisions that brought me to the point of finishing this dissertation.

Before moving on to acknowledge by name some of the most important contributors to this works, I would like to also thank all my research collaborators and colleges. Some of the projects have already been published and thus the names of these people can be found as co-authors in my publication list. Apart from research collaborators the Chair of Biological imaging (CBI) of the Technical university of Munich and the Institute of Biological and Medical Imaging of Helmholtz Zentrum Munich that I was working in, must be thanked. Not only I found many open doors that keep providing academic feedback of the years (e.g. Dr. Deliolanis), but a great procedural framework (from ordering equipment to animal protocols) was in place as well. That framework was supported by few ,often overwhelmed but always friendly, technical assistants and secretariat personnel to whom I am grateful.

Having said that about the CBI, I owe to namely acknowledge the efforts of Prof. Ntziachristos who keep pushing the Chair forward. Not only is he great at securing the necessary funds, but most importantly ideas and perspective. I was lucky enough to be assigned by Vasilis at some point in a group that was directly supervised by him. Thus appart from a Chair, I feel the need to also thank him as a mentor. I feel privileged that I had the chance to experience the way he approached projects and learn from both his analytical thinking methodologies and strategies of optimal presentation of results.

It was through the trust that Prof. Westmeyer showed to my skill set that further empowered me and enabled me to undertake even more challenging projects, like the NeuBtracker. Gil shows an amazing ability to set worth-following goals and he has both the knowledge and motivation to work hands-on on those to achieve them. So I have to thank him both for giving me the option to work on such interesting projects and for being there at all times to enable me, support me, and always had my back to ensure the success of the projects.

Specially for the first two publication presented in this thesis I have to acknowledge the contribution of my predecessors on the project, Dr. Themelis and Dr. Sarantopoulos, for putting the bases of those projects and remaining available for feedback after they have distanced themselves from those. Our grumpy but humorful optical imaging team took over after them, lead by Dr. Alliende. Dr. Glatz and (Dr.?) Koch provided day-to-day feedback on my projects and all had excellent work and research ethics focusing on the actual long-term development of our project rather than short-term satisfaction of other stakeholders.

For the other two publications I moved to the multidisciplinary team at Westmeyer's lab. During our seminar, coffee-brakes and beers with Mrs. Stelzl, Mrs Myklatun, Mr. Massner, Mr. Sigmund, Mr. Cruz introduced me to their research topics, but also supported mine both sharing methodologies and mental support. It was Dr. Lauri, that undertook the responsibility to teach me about Zebrafish neuroscience and support accordingly the related projects. I am especially thankful to her, for over-simplifying biological concepts enough from me to understand them and enable my research and being there to provide the in depth discussion on top of our findings.

One of the reasons that I was able to enjoy this sort of exposure to a different field of research was that people like Dr. Jia, Dr. Cmyrov, Mr. Erdmann made themselves available for me offering solutions or guidance to the optical instrumentation problems I was facing during the development of the projects. Dr. Cappetta, Mrs. Stefanoiu and Prof. Lasser played a similar role on the computational

and data analysis part of the projects.

Having thanked the people that taught me one way or another, during those years, I would like to thank also my students for both helping me become a better teacher and producing results that were useful for the projects. Mo Azizian, Carlos Cruz-Perez, Thanos Alexiou, Bénédicte Archambault, Julian Fuchs, Steffen Schneider were just few of them.

Working in academia requires a high level of self-motivation and mental stability. While this can be derived from the project, mentors and collaborators, a fulfilling personal life is of equal importance. Trying to write down some of the name of people that have contributed to that, I will be biased toward the ones that I still interact with in an almost daily basis. So apologizes to the ones that I have to leave outside, like many old school friends , the EESTEC-crew from my university years and people that left Munich (e.g. Ms Eleftheriadou, Vletsi and Vavadaki). A special thanks must go to Maria Pappa who was not only available for friendly chats but happy to contribute supporting me with illustrations.

Probably of one of my first acquaintances in Munich, Dr. Vittorias, ended up not only becoming a good friend but also introducing me to many other including Dr. Daniilidis, Dr. Evangelou, Dr. Papadopoulos, Mr. Kipouridis (and their families). Despite theirs doctor's titles the discussions with them where far from sterile.

Having the opportunity to have such interesting discussions also inside the work environment was thanks to Dr. Tzoumas and Dr. Chekkoury. The discussions with them were extremely helpful since we were working in the same workplace and sharing the same challenges, and even more so since we have different personalitiesand were approaching those challenges in different ways. Further, they are great scientist and thus provided actual practical feedback and run interesting projects that I was happy to participate in.

Specially in the last years another Helmholtz Campus colleague Dr. Kyriakou introduced me to a joyful group of couples with whom I became friends. Speaking about couples, I consider myself lucky that during my PhD years a had partners that were understanding about the challenges of a research job in academia and not only showed patience but actively supported me. A special acknowledgment must be given to Ms. Nikoleta Mouriki that stands next to me the months of writing this Thesis. Despite the fact that I fail to compartmentalize my life and both stress and actual work duties (e.g. writing in afternoon and weekends) reach our home, she coped with that amazingly and helped me to both relax and work efficiently.

Before thanking the family back home (since I do not come originally from Munich), I would like to acknowledge the importance of a place which felt like home during those years. "Anti" a cozy restaurant in Munich, and its personnel where opening their doors and hearts to host spontaneous meetings in cases of both depression and celebration. Walking spontaneously into "Anti" after the submission of a paper and requesting a table for two, hoping that someone from the aforementioned friends would be available to join me, was usually ending up in a ten people feast.

Finally, the almost invisible contribution from my family must be acknowledge. Not visiting them often, I might have created the impression of weak bonds with them. The truth is exactly the opposite. During all those years I knew, both as gut feeling and through proof (e.g. my sister's proof-readings -pun intended) when needed, that all my family members completely trusted me and where supporting my decisions. From overtaking a high-risk project almost at the end of my PhD (which worked out fine in the end), to skipping Christmas Holidays to collect data for a paper (that will never be published). This type of support enabled all the hard work that all the projects needed. Since any amount of words would be too little for the gratitude they deserve, I will just conclude this section with a big thank you to my grandparents and to Stelios, Panagiota, Alexia, Nikos, Loulou Maya and Vera Jo.

Abstract

   Novel optical imaging probes enable quantification of molecular process in a variety of biomedical applications ranging from cancer imaging to neuroscience and beyond. Camera-based widefield fluorescence imaging allows us to capture this molecular information at high speeds using flexible yet simple and robust instrumentation enabling easy penetration of this technology to both operating rooms and biological laboratories. Contrary to x- or gamma-rays photons interact with human tissue. Moving to infrared acquisitions only partially alleviated the problem of having to perform a reversion of the captured image to deconvolve the real biodistribution of the fluorescence probes from the optical effects of the tissue they lay in. Aiming to understand the foundation of such a reversions process we proceeded with: (a) modeling such effect of underlying optical properties of tissue to formed image using theoretical formulas and phantoms experiments and (b) creating a robust and user- friendly validation pipeline based on an imaging cryotome that allowed capturing 3D information of bulk tissue and comparing it with gold-standard thin slices. Based on our findings a roadmap was desinged towards Hi-Fidelity fluorescence imaging, in both terms of localization and quantification of e.g. target fluorescence probes that highlight protein over-expression of cancerous tissues during surgeries. While working on medical research projects has direct impact, working on basic research ones offers higher flexibility with experimental designs. Such an example is the use of transparent model organism, like zebrafish larvae, to bypass the bottleneck of effects of scattering and absorption on the captured images. We identified two major engineering bottlenecks that affected the design and analysis of neuroimaging data from zebrafish larvae. The first was the scanning methodologies that are commonly used to acquire three-dimensional information across the brain, resulting in volumes where is spatial location was sampled at different time points. Co-current volumetric acquisitions are needed to enable imaging of fast processes in fast moving animals and as an easy way to achieve single-snapshot 3D imaging, we used a microlens array that allows the capturing of the whole light field of an imaging scene, allowing its volumetric reconstruction, providing depth information in the expense of lateral resolution. The second challenge the researchers faced the need to comply with was the trade-off of resolution and field of view, forcing them to either stick to low resolution (mainly behavioral) monitoring of freely swimming animals or higher resolution brain imaging of restrained ones. While tracking microscopes that break this trade-off by compensating for the movement of slower animals repositioning it under the field of view of a microscope existed in the literature, such solution would affect the behavior of Zebrafish larvae who have a developed motion perception system. Thus we engineered NeuBtracker, a closed-loop system, where two mirrors and a tunable lens guided by a tracking algorithm, focus a microscope on the brain of the fish, which swims freely. NeuBtracker offers microscopic resolution($<1~\mu$m) across a macroscopic arena (>10 mm), thus enabling a series of novel neurobehavioral experiments. We showcased that with multiple examples (including default swimming activity, odor avoidance, pharmacological stimulation of neurons and photostimulations), along with alternative design options proving its modularity and further expandability towards high throughput and optogenetics experiments. All presented projects in this thesis showcase the importance of multidisciplinary research where engineers are asked to improve the available imaging equipment to better exploit novel biochemical tools to enable progress in both fronts of clinical intervention and basic research.

Contents

1 Preface

A PhD Dissertation that tries to summarize the work of a PhD student in a multidisciplinary field, that expands across a time period of years and often includes several projects that superficially appear unrelated, might appear *scattered*. In this thesis a different sort of scattering, the scattering of photons from tissue during optical imaging, is actually the binding thread of all the presented projects. All the projects in this work lay in two groups: (a) trying to understand optical scattering in order to propose methods that will allow in the future to alleviate its effects in (pre-) clinical imaging or (b) trying to bypass its effect using either suitable imaging modalities or a transparent model organism to answer specific biological questions. Those biological questions, ranging from imaging for applied cancer drug/therapy development to basic neuroscience, are not in the focus of this specific document. But brief and simplified description will be provided to illustrate the motivation for this work.

To make the reading of the thesis easier, the projects are not presented in chronological order. But it could be useful to provide here for reference a quick overview of the work as it evolved over the years.

The original question posed can be phrased as: "Is there an algorithm that can use the information regularly acquired by current intra-operative imaging systems to compensate for the contribution of scattering and absorption on the final fluorescence image allowing better quantification and localization of the distribution of the agents?". To answer this question we pursued two parallel approaches. The first was to model those effects, using a series of tools ranging from simulation to theoretical formulas, that had to be validated and adjusted based on bio-mimicking phantom data. The second was to create an imaging pipeline that would allow the acquisition of datasets from real biological samples along with some sort of ground-through information. Those datasets were used to both provide insight in the phenomena of interest and as benchmarks for the experimentation with novel algorithms.

Part of the pipeline that created those datasets was an ex-vivo imaging system based on a cryotome that enabled volumetric imaging of a whole sample in reflection and fluorescence mode across multiple combinations of wavelengths. This modality was also used over the years as an independent tool. Fellow colleagues that were working on developing a novel in-vivo optical imaging modality (optoacoustics) that is only minimally affected by the scattering since the detection of absorbers is done through ultrasound detectors. The cryoslicer-based ex-vivo validation pipeline was used by them as a gold-standard. In parallel collaborating research institutes and pharmaceutical companies asked us to provide whole body biodistribution of drugs or expressions patterns. Note that each of those project was requiring -at least at some degree- custom optimization of our default pipeline, from unmixing of overlayed signals to segmentation of specific structures of interest. An example of such structures were neurons highlighted by expression of a fluorescence protein. The resulting imaging and the context of the project was inspiring and its limitation (ex-vivo and at samples limited by diffusion of light) were intriguing. Luckily the opportunity to get involved in a project involving in-vivo imaging of "firing" of neurons across the whole brain with almost cellular resolution came up. And this was achieved by changing the model organisms and moving from mice to small transparent fish.

With a group of colleagues and an industry-collaborator we investigated the use of light-field technology (camera that can acquire volumetric images in a single snap-shot using an array of microlenses and computer vision algorithms) for in-vivo imaging of zebrafish larvae expressing

a responsive fluorescence protein that increased it signal when the calcium concentration in neurons is high (an indicator of neuronal activity). Despite the fact that the optimization of both imaging -eg. characteristics of microlenses- and reconstruction is ongoing, the imaging of restrained animals itself was easy. But it is also restricting the biological questions that can be asked. Thus for the next couple of years I focused on developing an imaging system that can image freely swimming animals with four main specification: high resolution, across a big field of view, with minimal perturbation of the animals and allowing not only imaging but also optical stimulation of fish (eluding to optogenetics application proteins are not used as indicators but as actuators of neuronal activity). Based on those specifications and with the help of scientists with experience in microscopy and image processing, we builded a tracking microscope that tracks and magnifies the brain of larvae while it swims in an arena several times its size and after registration of the acquired images extract neural signal that can be correlated to natural activity or external stimulation.

In the next chapters, we will first shortly introduce the concept of (fluorescence) optical imaging. A brief discussion about the different types of optical probes will be made, ranging from unspecified to targeted systemically injected fluorochromes to genetically expressed responsive fluorescence proteins. Then a generic core-system for widefield imaging will be introduced and based on this we will present the most important additional components we used to generate our tools. Finally we will present the two research programs that our tools used, namely cancer imaging using fluorescence probes and systems neuroscience using zebrafish. Hopefully after all these concepts are superficially introduced the attached papers that consist the core of this thesis will provide the needed level of details for a PhD Disseration.
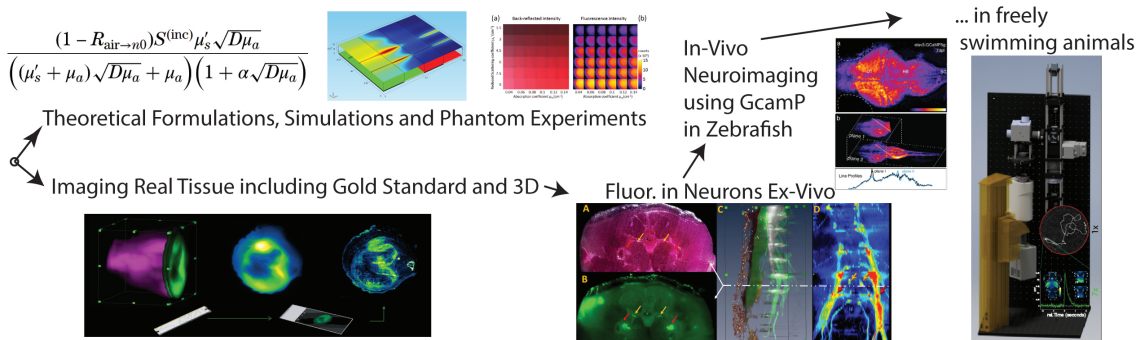

Figure 1.1: An overview of the transition between project during the PhD.

2 Publication Record

This cumulative ,publication based, dissertation includes the following four published works with me as a first author:

1. **Symvoulidis, P.***, Jentoft, K. M.*, Garcia-Allende, P. B., Glatz, J., Ripoll, J. and Ntziachristos, V. (2014) 'Steady-state total diffuse reflectance with an exponential decaying source', *Optics Letters.* Optics InfoBase Publications, 39(13), pp. 3919–22.

2. **Symvoulidis, P.** and Perez, C. (2014) 'Serial sectioning and multispectral imaging system for versatile biomedical applications', *2014 IEEE 11th International Symposium on Biomedical Imaging (ISBI), Beijing, 2014, pp. 890-893. doi: 10.1109/ISBI.2014.6868014*

3. Perez, C. C.*, Lauri, A*., **Symvoulidis, P.***, Cappetta, M., Erdmann, A. and Westmeyer, G. G. (2015) 'Calcium neuroimaging in behaving zebrafish larvae using a turn-key light field camera', *Journal of biomedical optics.* International Society for Optics and Photonics, 20(9), p. 96009.

4. **Symvoulidis, P.**, Lauri, A., Stefanoiu, A., Cappetta, M., Schneider, S., Jia, H., Stelzl, A., Koch, M., Perez, C. C., Myklatun, A., Renninger, S., Chmyrov, A., Lasser, T., Wurst, W., Ntziachristos, V., Westmeyer, G. G. and others (2017) 'NeuBtracker - imaging neurobehavioral dynamics in freely behaving fish', *Nature Methods.* Nature Research, 14(11), pp. 1079–1082. doi: 10.1038/nmeth.4459.

Some of the systems and methodologies developed during those projects were used (with proper modification and expansion) to generate data for a series of other publications which are either not published yet (5) or I am not the first author of the publication (6-17). The introductions of this dissertation though aims to familiarize the reader also with the general field of widefield fluorescence optical imaging, to understand the connections of the presented projects to this related work.

5. Koch, M.*, **Symvoulidis, P.***, Ntziachristos, V. (2018) "High-fidelity fluorescence imaging: Definition, Standardization and Reversion", Accepted (In Press), Nature Photonics.

6. Koch, M., de Jong, J. S., Glatz, J., **Symvoulidis, P.**, Lamberts, L. E., Adams, A. L. L., Kranendonk, M. E. G., van Scheltinga, A. G. T. T., Aichler, M., Jansen, L. and others (2017) 'Threshold analysis and biodistribution of fluorescently labeled bevacizumab in human breast cancer', *Cancer research.* American Association for Cancer Research, 77(3), pp. 623–631.

7. Stritzker, J., Kirscher, L., Scadeng, M., Deliolanis, N. C., Morscher, S., **Symvoulidis, P.**, Schaefer, K., Zhang, Q., Buckel, L., Hess, M., Donat, U., Bradley, W. G., Ntziachristos, V. and Szalay, A. A. (2013) 'Vaccinia virus-mediated melanin production allows MR and optoacoustic deep tissue imaging and laser-induced thermotherapy of cancer', *Proceedings of the National Academy of Sciences.* National Acad Sciences, 110(9), pp. 3316–3320. doi: 10.1073/pnas.1216916110.

8.   Tzoumas, S., Nunes, A., Olefir, I., Stangl, S., **Symvoulidis, P**., Glasl, S., Bayer, C., Multhoff, G. and Ntziachristos, V. (2016) 'Eigenspectra optoacoustic tomography achieves quantitative blood oxygenation imaging deep in tissues', *Nature Communications*. doi: 10.1038/ncomms12121.

9.   Roberts, S., Seeger, M., Jiang, Y., Mishra, A., Sigmund, F., Stelzl, A., Lauri, A., **Symvoulidis, P.**, Rolbieski, H., Preller, M. and others (2017) 'Calcium Sensor for Photoacoustic Imaging', *Journal of the American Chemical Society*. American Chemical Society.

10.   Chekkoury, A., Nunes, A., Gateau, J., **Symvoulidis, P**., Feuchtinger, A., Beziere, N., Ovsepian, S. V, Walch, A. and Ntziachristos, V. (2016) 'High-Resolution Multispectral Optoacoustic Tomography of the Vascularization and Constitutive Hypoxemia of Cancerous Tumors', *Neoplasia*. Elsevier, 18(8), pp. 459–467.

11.   Omar, M., Schwarz, M., Soliman, D., **Symvoulidis, P**. and Ntziachristos, V. (2015) 'Pushing the Optical Imaging Limits of Cancer with Multi-Frequency-Band Raster-Scan Optoacoustic Mesoscopy (RSOM)', *Neoplasia*. Elsevier, 17(2), pp. 208–214.

12.   Chekkoury, A., Gateau, J., Driessen, W., **Symvoulidis, P.**, Bézière, N., Feuchtinger, A., Walch, A. and Ntziachristos, V. (2015) 'Optical mesoscopy without the scatter: broadband multispectral optoacoustic mesoscopy', *Biomedical optics express*. Optical Society of America, 6(9), pp. 3134–3148.

13.   Barapatre, N., **Symvoulidis, P.**, Möller, W., Prade, F., Deliolanis, N. C., Hertel, S., Winter, G., Yildirim, A. Ö., Stoeger, T., Eickelberg, O., others, Ntziachristos, V. and Schmid, O. (2015) 'Quantitative detection of drug dose and spatial distribution in the lung revealed by Cryoslicing Imaging', *Journal of pharmaceutical and biomedical analysis*. Elsevier, 102, pp. 129–136. doi: 10.1016/j.jpba.2014.09.001.

14.   Glatz, J., **Symvoulidis, P.**, Garcia-Allende, P. B. and Ntziachristos, V. (2014) 'Robust overlay schemes for the fusion of fluorescence and color channels in biological imaging.', *J. Biomed. Opt.*, 19(4), p. 40501. doi: 10.1117/1.JBO.19.4.040501.

15.   Tapfer, A., Bech, M., Zanette, I., **Symvoulidis, P.**, Stangl, S., Multhoff, G., Molls, M., Ntziachristos, V. and Pfeiffer, F. (2014) 'Three-dimensional imaging of whole mouse models: comparing non-destructive X-ray phase-contrast micro-CT with cryotome-based planar epi-illumination imaging', *Journal of microscopy*, 253(1), pp. 24–30.

16.   Garcia-Allende, P. B., Glatz, J., Koch, M., Tjalma, J. J., Hartmans, E., van Scheltinga, A. G. T., **Symvoulidis, P.**, van Dam, G. M., Nagengast, W. B. and Ntziachristos, V. (2014) 'Towards clinically translatable NIR fluorescence molecular guidance for colonoscopy', *Biomedical optics express*. Optical Society of America, 5(1), pp. 78–92.

17.   Garcia-Allende, P. B., Radrich, K., **Symvoulidis, P.**, Glatz, J., Koch, M., Jentoft, K. M., Ripoll, J. and Ntziachristos, V. (2016) 'Uniqueness in multispectral constant-wave epi-illumination imaging', *Optics letters*. Optical Society of America, 41(13), pp. 3098–3101.

3 Introduction

3.1 Engineering Optical Imaging for Biomedical Applications

At the core of clinical practice and basic biological research we can find imaging. In engineering and sciences quantifying parameters of the observed systems is essential to understand them and efficiently interact with them. Quantification does not have to be image-based and can be either as simple as measuring the temperature of a patient or calculating the concentration of biomarkers in their blood or as complex as sequencing their genetic information. However, biomedical imaging offers simultaneously information across many locations of the samples, ranging from a whole human or animal to a slice of an excised tissue for histopathological evaluation. Relatively new technologies like Magnetic Resonance Imaging, Computed Aided Tomography with X-rays and Positron Emission Tomography offer valuable data to the physician or researcher and found their way in everyday pipelines. However biomedical imaging is by no means a recent advancement.

To form an image, we do not need to build high-tech instrumentation. Actually, we come equipped with one: the eye. A composite organ, with a lens at the front and an array of photodetectors in the back, enabling our brain to form images based on the distributions of detected photons (ranging approximately from wavelengths between 380 nm and 700 nm). The remaining of the thesis can be considered just as an effort to replace the eye with an improved electronic version (cameras with sensitivity at different regions and better interpreting the acquired data Chapter 1-2), while going back to its actual design to get inspired and overcome technical limitations (volumetric imaging and the trade-off between field of view and resolution 3-4). But before that, we will introduce the principle and importance of optical imaging in the clinical practice.

Although in present times the term "optical" in the biomedical context probably refers to either miniaturized wearable sensors that reveal blood oxygenation[119] or novel non-ionizing tomographic modalities like Fluorescence Molecular Tomography (FMT)[6, 130] or Multispectral Optoacoustic Tomography (MSOT)[147], an optical inspection of the patient or biological sample is (and probably has been since the beginning of medicine) the first step of any study. When medical personnel looks at a patient, the back-starred light collected across multiple wavelengths (exploiting the tri-color vision of humans which seems to be accordingly optimized by evolution[29, 79]) is analyzed by the brain which tries to infer if the tissue colorization is physiological or not. A pale patient might infer circulatory problems and a burst region might reveal inflammation[145], while the density and appearance of a mole might hint to melanoma[200]. In laboratory framework, the opacity of a dilution of a substance or a sample is indicative of its concentration or compositions[168], while visual monitoring of animals is used to study behavioral phenotypes[23]. Those are just examples of both biological and medical applications where a simple visual inspection with the naked eye is helpful or necessary. But the human vision system (including eyes and the processing of visual information) has limitations that technology comes to overcome. Additional optical components are placed in front of the researcher's eye, and the eye itself is being replaced by imaging sensors with increased sensitivity.

However as any movie director would argue, it is not (only) the equipment that makes a good movie. There are also limitations on the information that can be revealed from the biological samples just by their inherent visual appearance. Thus in the recent years, bioengineering methods and tools (from chemical substances to genetically modified organisms)

are created to translate the state of a tissue at a molecular level to an optical contrast that can be captured by the advanced instrumentation that we currently have at hand (or eye).

In the next paragraphs, we will briefly discuss technological advances in both fronts of **(1) optical detection instrumentation and (2) methods that improve the information that our biomedical samples emit**. After this introduction it will be apparent that, depending on the application, we can benefit from both a better understanding of the physical principles that governs light propagation in tissue (e.g., mathematical formulation of tissue optics) and from instrumentation that is optimized to capture it efficiently (e.g., tracking fluorescence microscopes). Finally, we will present our work, the way it was published in peer-reviewed journals.

3.1.1   How to better capture the scene? Transitioning for the Eye to Electronic Imaging Systems

Lenses - From Macro to Micro: One of the first bottlenecks that humans realized their vision has was the range of scales they could capture information from. Indeed their eye was able to see from the rough outlines of large stuff (including celestial bodies) even many kilometers away to things as small as thin hairs if they could bring them close enough to their eyes. Even in ancient times [134] people realized that objects placed behind properly shaped glasses appeared bigger. But it was only after the 15th century that glass-craftsmanship reached a level allowing those magnifying lenses to be clean enough and accurately shaped to create sharp images. Since then progress focused on both optimizing such single lenses and building compound microscopes made of multiple optical elements[40] . Such microscopes (and telescopes) enabled researchers of the time to observe objects of completely different scales. While the quality of the microscope kept improving, the way that those observations were documented and shared with the world stayed the same until recently. The microscopists were hand-drawing the objects and although we can argue that the level of abstraction of those images has educational value as is the case in the neuronal networks drawn by Ramon y Cajal [27, 26], it is a cumbersome procedure with obvious limitations like the inability to properly depict dynamic events. So having a system to automatically depict the output of a microscope to a piece of paper or other archiving medium was crucial to expand the usability of microscopy (and optical imaging generally) .

Film and Digital Photography: Having augmented the lens of the human with additional ones, the next step in the progress of microscopy was to improve on the capturing of the image by replacing the photoreceptors of the eye. While the film-cameras were an improvement over the hand-drawing progress, it was the development of digital sensors that revolutionized optical imaging. The ever-increasing resolution and sensitivity of camera sensors and the simplicity of the image acquisition, previewing and storing pipeline tend to make eyepieces on conventional microscopes obsolete (similar to the transition to mirror-less consumer cameras). For the rest of the thesis we will focus on acquisition methodologies that exploit the flexibility of manufacturing and controlling such digital sensors to acquire images that would not have been possible using the eye as a detector -even augmented with a microscope. Capturing however even simple color images is important and possibly life-saving[124]. Documenting any form of "optical inspection" of biomedical samples (a photo of a mole or a pathology slice) was always crucial for archiving reasons. Thanks to the increased connectivity of high-tech hospital sites to patients with mobile phone cameras and the new generation of deep-learning algorithms, this accumulation of optical imaging data can also result in an automated diagnosis, even in remote regions[53] .

IR-sensitivity & Multispectral: Using electronic pixels rather the eye's photoreceptors does not only allow us to automatically acquire a digital copy of the image. It additionally gives us flexibility on what information will be captured in the first place. While the photoreceptors of the eye are sensitive to a specific spectral region and have a (vast but) fixed

sensitivity and dynamic range, we can tailor our digital sensors based on our needs. We can properly decide which (combinations) of wavelength we want to capture and we can also detect invisible to the human eye photons like the ones in the infrared regions of the spectrum. This capability of visualizing infrared photons opened new venues for optical imaging. Most biological tissues absorb and scatter light and thus they are not see-through (contrary to the jelly-fish for example), but both absorption and scattering are lower in the infrared range allowing us to capture information from few millimeters to centimeters deep inside the body. While the traditional optical inspection that a doctor performs is limited to external or internal (through endoscopy) surfaces or a surgically exposed region of interest, the capability to see non-invasively deeper inside the body using infrared sensor redefined the field of optical imaging the beginning of the 21st century[129, 131, 197]. A new generation of sensors, based Indium gallium arsenide (InGaAs) rather than silicon photodetectors, enables imaging at even higher wavelengths were scattering is increased providing sharper images even from highly scattering tissues like the brain, even through the mouse skull [170, 80].

From static 2D depiction to dynamic 3D acquisitions and reconstructions: One of the major advantages of the human eyes is that they are connected to/with a powerful real-time vision processing unit that can not only interpret the acquired signals but also control the acquisition (and their "tripod" –the human dipod) to ensure the proper information is captured. Optical engineers are trying, in a similar way to optimize their acquisition pipeline to make sure that they capture as much information as possible from a scene (e.g., moving the camera around the same way that a human might walk around a strange object or try to autofocus to ensure sharpness) and they have to develop algorithms to combine this information in an optimal way and -if possible- finally interpret it. Most of the modern optical imaging system are not just a sensor, but complex devices incorporating both automations[156] (from simple stages to adaptive optics elements) and reconstruction algorithms[12].

Back to the Eyes as source of inspiration: The last paragraphs might have created the impression that the eye is an obsolete imaging sensor when it comes to modern medical imaging. While this is true in many aspects, evolution has given smart solutions to optical problems thus the human (and other animals) vision system can be used to draw inspiration for improved biomedical imaging[162, 144, 3]. For one of our applications we wanted to observe in high detail a tiny organism moving in a big arena. But in traditional imaging systems a trade-off between the resolution and the field of view exists. Looking back to the vertebra eye[202] , we realized that there the photoreceptors are not distributed uniformly in the retina. There are two distinguished regions: one with a higher density of color-sensitive cells in a small region around the center of our optical field; and many more monochromatic cells distributed all around sampling a much bigger region. This inspired us to build a two camera system that we will present in detail in Chapter 5.4. .

3.1.2 How to better design the scene? Enabling Molecular Imaging.

Our discussion so far has focused on why and how we can replace the eye of the doctor with a system that offers higher magnification, higher sensitivity at specific bands, and automatic digitization of the images. But where are the photons that the optical imaging system captures coming from? What do those images tell us about the tissue's state? And most importantly, what is the combination of biochemistry, bioengineering and optical instrumentation that can allow us to recover even more information?

It is no coincidence that the field of optical imaging was virtually reborn in the last 20 years together with the field of molecular imaging[152, 198]. The term "molecular imaging" refers to a set of techniques that help researchers capture information regarding processes at the molecular level from biological samples. While molecular imaging can also refer to positron emission tomography or other imaging modalities, the low cost and relative simplicity of building optical molecular sensors make optical methods the technology of choice for many
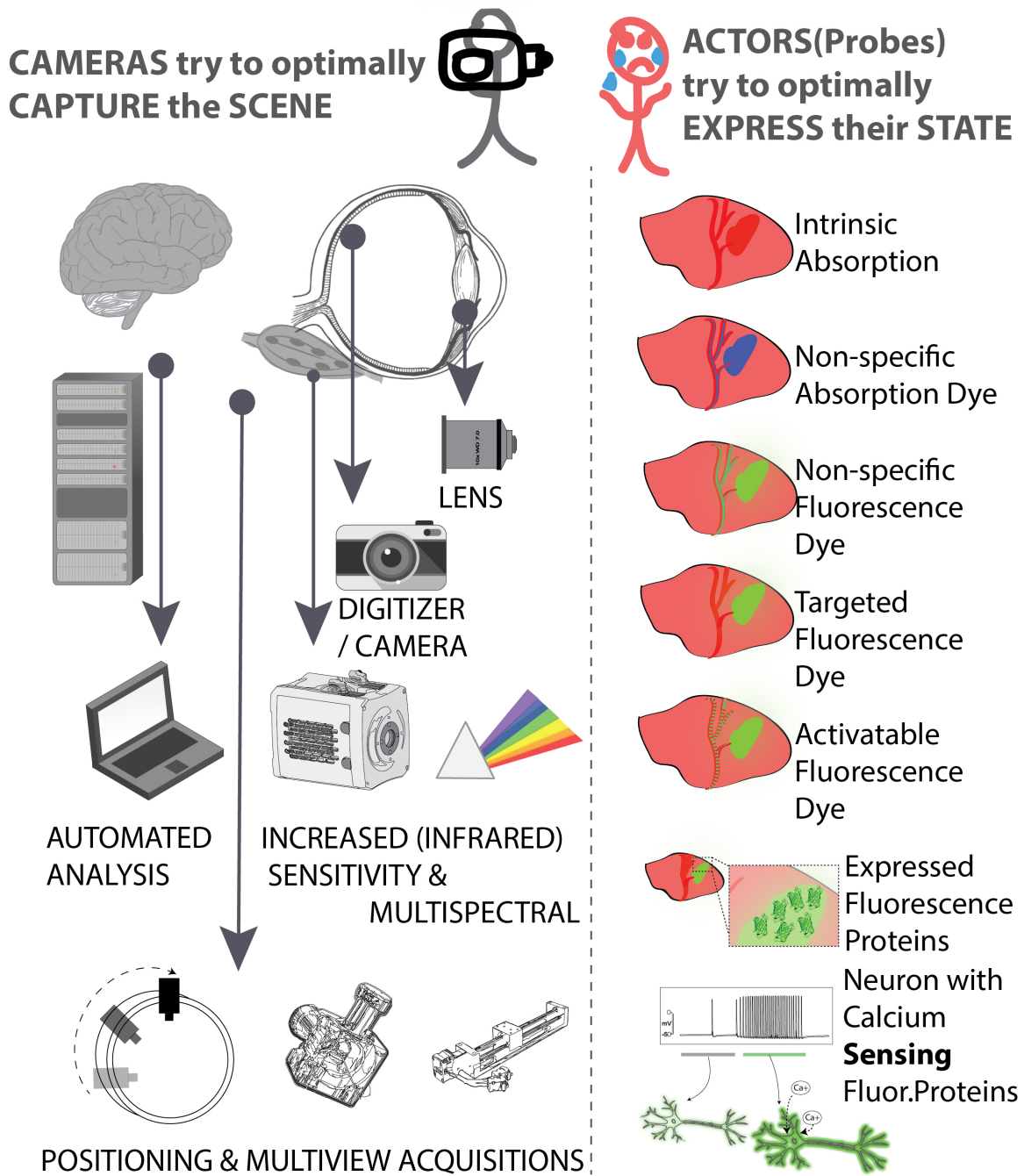
Figure 3.1: Schematic overview of the progress in optical imaging. On the left side we see how different component of the human visual imaging system, can be expanded or replaced to allow improved imaging of the sample. On the right the evolution from simple intrinsic contrast to advanced activatable genetic probes is shown, to convey the importance of novel probe that enable the proper visualization of the state of imaged sample.

applications. That application ranges from quantifying protein over-expressing at canceric tissues[130] to monitoring calcium fluxes of firing neurons[70]. While the state-of-art systems might sound futuristic (e.g., viral transfection of living samples to alter their genetic code and force expression of fluorescence proteins as indicators disease[173]), the basic idea remains the same as it was at the beginning of the 18th century when the first dyes for histopathology were discovered. Find *something* that when *added* in tissue will create some *contrast* informative for the application of interest. In the next two paragraphs we will shortly discuss what the information that is encoded in same basic types of images is.

Multispectral back-scattered reflection: From blood to dyes: Most[102, 201] of the photons we see when looking at biological samples are generated from sources outside the body. They interact with the tissues being elastically or inelastically scattered by those or absorbed depending on their wavelength and the composition of the tissue. Due to the scattering and absorption (mainly from blood), most biological tissues are not transparent, thus using conventional imaging systems (human eye or camera) we can sample relatively superficial tissues. Thus the superficial blue-looking[97, 189] veins under our skin disappear when they go deeper. Still, valuable information can be revealed both from the shape of the structure of interest (e.g. a melanoma or a mole) and its color (circulation problem result in pale limps or an inflammation resulting in rubor).

While the abundance or not of blood at specific locations has clinical value (and our trichromatic color vision is well suited for resolving that[29, 79]), the fact that surrounding tissue is also blood-like deteriorated our capability for interpretation of the visual appearance of the sample. This can be better showcased with an example from cancer research. Most tumors have increased but abnormal vasculature, thus substances traveling through the vasculature reach the tumor site but do not return to circulation properly. This is called Enhanced Permeability and Retention (EPR)[125, 117]. The vascular network itself can be used to identify cancer using advanced optical techniques[87, 28, 133], but just the visual appearance of accumulated blood might be inconclusive. Thus doctors are trying to "color" the tumor using extrinsic dyes that can provide better contrast. Studies delivering blue dyes (like methylane blue) have appeared in the literature since the 40s[111, 64]. Such coloring of the sample can be done through systemic administration, e.g., intravascular injection, through local administration, e.g., spraying[22] or ex-vivo staining or even genetic manipulation[173], but still unmixing those colors from back-scattered images is problematic (despite the huge progress in the field[184, 115]). What if we could use dyes that work with a different mechanism and thus provide better contrast? Similarly to how a fluorescence highlighter makes the passage of interest in a text pop-out.

Fluorescence Contrast and Molecular Imaging: There are indeed many substances that when they absorb a specific wavelength of energy get excited and then re-emit at a different wavelength. The main reason that we do not observe this phenomenon easily is that the amount of emitted photons is often low (compared to the detected backscattered reflection). To see the first we have to minimize the latter. While this is done in imaging systems with excitation and emission filters, we also clearly see fluorescence with naked eyes if we use a UV-light for excitation. From teeth in night-clubs with black-lights to biological liquids stains in forensics, we already know that biological samples have fluorescence, called auto-fluorescence[74, 207, 8].

In some animals, autofluorescence might have added an evolutionary advantage[72]. While this is most probably not the case for humans, there are still multiple substances in our body that emit fluorescence photons. Probably the most interesting of those is Nicotinamide Adenine Dinucleotide (NAD) which is used in cell metabolism[20] Since deregulated cell energetics are a hallmark of cancer[75, 76], the level of NAD and the resulting level of autofluorescence level has been proposed for detecting cancerous lesions[135, 104, 112].

In order to exploit the similar principle of increased metabolic activity of malignant tumors, researchers decided to use external substances. 5-Aminolevulinic acid hydrocloride (5-ALA), after being administered orally reaches through the blood-brain barrier glioma tumors and there it is used by the cells to produce Protoporphyrin IX (PpPiX) which has strong fluorescence that can be detected by surgeons and guide the surgery[73] (or used for photodynamic therapy[59]). While PPiX guided brain tumor resections are being performed regularly (and tried with other tumours[19]), achieving better labeling of tissue is of high interest[164].

We have already discussed the use of EPR effect for absorbing dyes. A similar practice with fluorescence dyes (e.g., like indocyanine green- ICG[5]) has already been used for cancer localization[105, 183]. Since the level of autofluorescence is lower than backscattered light from tissue, using fluorescent dyes offers higher contrast compared to simple chromophores. Apart from cancer, such unspecific dyes can be used for a series of other medical examination procedures, when highlighting the perfusion of blood is of interest, e.g., examining vascularization of limps in case occlusions are suspected[14] or of transplanted organs or tissues[88, 36].

One of the current directions of the field is to engineer smarter probes that can increase the specificity of the labeling of either molecules or even molecular processes of interest. Two main strategies are used to achieve that: Either target probes that are binding only to specific regions of interest(Giepmans et al. 2006) or activatable probes(Kobayashi and Choyke 2010) that while they might be everywhere, their fluorescence characteristics change in the presence of specific substances in their environment. Examples of both approaches exist in the cancer research field. It has been documented that specific tumors over-express some proteins responsible for angiogenesis (the increased metabolic need of proliferating tumors must be covered by nutrition and thus increased angiogenesis is another hallmark of the disease). This has been exploited to develop anticancer drugs like Avastin, that target cancer cells and block the function of the proteins preventing the growth of tumors. Binding fluorochromes on such drugs allows clinicians to see where they are accumulated and thus properly localize the tumors[159].

Tumors consist of cells that have specifics characteristics -like the overexpression of proteins. Those cells give rise to abnormal processes and thus subsequently create the so-called tumor microenvironment where researchers observe abnormal concentrations of other substances (e.g., enzymes like proteases that degrade proteins like the ones used on extracellular matrices and thus facilitating invasion and metastasis). So a second strategy to target cancer is to aim not for the cells themselves, but for the microenvironment they form around them. A second approach of labeling is to create fluorescing substances that selectively accumulate there and more specifically a type that only if they reach such an environment they increase their fluorescence. Those are called activatable probes since they are normally fluorescing only minimally and they increase the number of re-emitted photons if specific substances are present[101, 186].

Aiming to some consistency of the text, it is focused on mainly clinical applications and a macroscopic scale (the size of multicellular lesions). The reality is though that fluorescence labeling is equally important for pre-clinical and biological applications and can offer subcellular specificity. Not only can we use similar methods to both animal models and clinical samples, but the different regulatory frameworks enable faster adoption of novel probes in the everyday laboratory framework as well. A great example of such probes that revolutionized the field of neuroscience is calcium-sensitive probes[70, 181]. Similar to the activatable probes, calcium-sensitive probes change their fluorescence level as a function of the calcium concentration inside the cells. Since when neurons get activated we observe a calcium influx, the fluorescence level we record from each neuron corresponds to its activity level[205, 169]. A new generation of probes is aiming to even capture the voltage changes that are observed during neuronal signaling[100, 182, 60], while other substances can work as actuators, en-

abling the opening of calcium channels (and thus forcing the firing of the neurons) when light is shined into them[43, 42]. The combination of light-based sensors and actuators of neural circuits of live animals gives rise to the field of all-optical electrophysiology[155, 51], that offers great advantages (number of concurrently interrogated cells, specificity of acquires signals, etc) compared to electrode-based approaches.

One final note regarding fluorescence probes must be given for the ways that those are delivered to the location of interest. That could be among others: a tumor of a patient, the brain cells of an animal model in-vivo, an in-vitro cell culture or organoid/organ-in-chip, or a histopathological slice ex-vivo. Protocols exist for a variety of combinations of probes-samples. For slices or small tissues sample staining can be as easy as dipping the sample in a solution with the probe. The probes themselves are engineered in a way to selectively bind (at least with higher affinity) to substances of interest. Still, there are applications that the brute-force approach of selectively loading a (often responsive) probe inside a cell using micro-pipetting with micromanipulators and a microscope for guidance is preferred. For in-vivo application on animals and humans, administration of the probes either systemic (e.g., with intravenous injection) or local (e.g., spraying on a possible interesting tumor) is used in practice and is often enforced by regulations (weighting the kinetics of the probes and other safety concerns). Especially for cell-culture or animal experiments, genetic tools have enabled researchers in the last years to engineer organisms that express fluorescence proteins at specific cells of interest. This can also be done for dynamic fluorescence proteins that change their fluorescence level (like the calcium indicators) and offers great flexibility. Some of the ways that those genetic manipulations are done could be potentially used also on humans (e.g., through viral transfections). Similar techniques are currently tested for gene-therapy[94] but genetic theranostics can be rendered of equal importance, especially in the context of personalized medicine where a smart imaging probe can be tailored to highlight only cancerous cells with the specific mutation of the patient[165, 159].

3.1.3 Optical Imaging Beyond Digital Photography. Alternative Contrasts Mechanisms and Computerized Acquisition and Reconstructions.

One can argue that what we have described so far as optical imaging is nothing more than photography. Maybe using a special lens and some filters along with a scientific grade camera, and by investing quite some effort to properly setup and illuminate the sample to allow to capture its state properly (next Chapter will introduce those instrumentation in more details). But still photography. Indeed this Thesis is focus on just this sort of optical imaging. There is though a series of techniques that are not camera-based but still depend (at least partially) on the interaction of light with tissue. Briefly mentioning some of them bellow is essential not only for completion of this introduction to biomedical optical imaging, but to help the reader better understand the connection between the actual topics of the thesis as well. While the presented papers of this work, range from macroscopy to microscopy and from cancer imaging to neuroscience all the included papers focus on camera-based widefield fluorescence imaging where backscattered reflection is used to either augment or even drive the fluorescence acquisitions. This thesis is not about optoacoustics, Raman scattering, coherence tomography or two photon imaging, but in the next paragraphs we will briefly discuss those.

As we will see in more details in Chapter 3.3.1., both reflection and fluorescence imaging of thick tissue-like samples have resolution limitations defined by the sample and not by the optics. As the light (either back-scattered or emitted by a structure inside the sample) travels through the sample to our detector, it undergoes multiple scattering events before escaping the surface of the tissue and reaching our sensor. The number of scattering events depends on the composition of the tissue and the depth of the structure of interest, but trying to capture an image below a few mm results in extensive blurring of the image. To alleviate the problem of scattering researchers have developed an optical imaging system based on acoustic detection.

It has been observed that when light is absorbed by molecules part of its energy is converted to thermoelastic expansion which results in acoustic waves in the ultrasound range, that can be captured by conventional ultrasound detectors. This way imaging the (wavelength-specific) absorption signatures of molecules deep inside the tissue with ultrasound-like resolution is possible. While researchers are still optimizing the ultrasound detector geometries[194], the reconstruction algorithms[121], absorbing molecular probes[196] and applications[178] there is a need for a Gold Standard Imaging for such imaging . The system presented in Chapter 5.2. has been used for this purpose. Being ex-vivo allows optical access deep inside the tissue (by sequential removal of tissue) and both reflection and fluorescence can be correlated with the absorption.

Elastic scattering (where the scattered photon is not losing its energy and thus retains it wavelength), was presented in the last paragraph as a bottleneck of optical imaging. But the truth is that with proper instrumentation we can use the elastic scattering to recover important information about the subsurface structure of the tissue with resolution down to $10mum$A technique called Optical Coherence Tomography[161] is using the interference of the incident beam with the one escaping the tissue to recover the composition of the tissue with depths up to 2mm. Despite the fact that the molecular information that can be recovered by OCT is limited[132], it has been widely used in clinical practice both for ophthalmology[47] and dermatology[199].

However not all scattering events are elastic. Inelastic (Raman) scattering results in small changes of the wavelength of the light, since the photons are losing energy. Assuming a homogeneous sample (or high enough resolution to probe homogeneous regions of a complex sample), the shift of the wavelength can reveal information about the chemical substances that compose the sample, each having a very specific spectrum[106]. Not only the specificity with which Raman can reveal the composition of the tissue is high, but additionally, due to the relatively low number of inelastic scattering events from tissue when extrinsic probes[96] (properly designed nanoparticles) are used, the sensitivity of the system and their multiplexing capabilities[34, 114] are higher than the fluorescence (since auto-fluorescence is present). Traditionally Raman-scattering measurements were point-measurements with spectrometers but advances in both instrumentation and compressed sensing algorithm might enable real-time Raman imaging in the coming years[18, 65], that will allow its transition from bench to bedside[99].

More complex nonlinear optical phenomena than what we described before can also be used for imaging, offering significant advantages, like increased focusing capabilities both in terms of focus and depth of imaging and of reaching intrinsic contrast from biological tissues without labeling. For better focusing researchers are using nonlinearfluorescence effects where absorption of two (or more photons) of lower intensity must be absorbed to enable the excitation of the molecule and the re-emission of fluorescence photons. Since those photons are of higher wavenumber their penetration depth in biological tissue is bigger and because the statistical probability of excitation non-linearly depends on the excitation light, much tighter focus points can be achieved minimizing out-of-plane signals[77, 83, 210]. Some anisotropic molecules (found abundant in highly structured tissue like collagen, muscles or microtubules) allow another nonlinear phenomenon, called second harmonic generation, where two(or more[41]) lower power photons rather than being absorbed (and re-emitted) are combined in one photon of lower energy.

Indeed non-linear optics can provide tight focus, but these focus points have physical limitations due to diffraction. Super-resolution microscopy[84, 157] is an umbrella-term referring to several optical microscopy modalities where using a combination of optics, biochemical properties of samples and algorithms, resolutions higher than the smallest focus point can be achieved, allowing us to resolve even sub-cellular structures. The main issue with all these

techniques is that due to the need for point focusing in order to achieve image or volume formation, scanning is required which is generally slower than widefield acquisitions.

This is by no means an extensive review of state-of-the-art bioimaging using optical methods and thus we will not enumerate all the recent developments in the field. We will just give two more examples showcasing that the tighter the collaboration between optical engineers and bio-researcher (biologists \biochemist \biotechnologist \biophysists etc.), the more improved the formulation of problems and thus the easier it is to find a solution,either from the imaging system or the sample perspective. For example, when optical engineers faced the challenge of scattering of thick samples that was preventing microscopes from achieving the resolution that they were designed for, they realized that something similar is happening also in astronomy (where the atmosphere create aberrations) and are now modifying adaptive optics[89] and wavefront shaping[190] techniques to create microscopes that compensate for those. On the other front, in the recent years biochemists managed to optimize sample preparation by minimizing scattering by removing lipids from tissue[167] or (/and) by physically expanding the sample[32] before trying to image it. Thus we can foresee optical imaging pipelines of high ingenuity that can both answer basic science questions and improve everyday clinical practice.

3.2 Instrumentation for Widefield Reflection and Fluorescence Imaging

3.2.1 The core-setup

To enable the reader better understand our contributions on an instrumentation level, we provide in the next paragraph a short primer of widefield fluorescence imaging based on a core setup. Modifications of this core geometry resulted in the four different instruments presented and used in the publications that compose this thesis.

Filters The main difference between a fluorescence imaging system and a regular reflection camera is the need to ensure the collection of only fluorescence photons and not the ones that are coming from specular or backscattered reflection events. To separate them we are using optical filters[148, 52]. The excitation filter, placed in front of the light source, makes sure that we shine to the sample only the wavelengths that are needed to excite the fluorescence and the emission filters block all wavelengths of light apart from the ones coming from the de-excitation process of the fluorochrome. If those filters overlap they also capture reflections from the overlap region. Generally they must have high transmission in order to ensure proper coupling of excitation light and detection of emission light. Additionally they need to have high cut-off the reason being that since the quantum yield of fluorochromes might be lower than 1%, if the cut-off is at that range, our camera would collect bleed-through signals as well. Tunable filters[68] exist and offer a flexibility in prototyping novel imaging systems, but their characteristics (lower transmittance, higher bleed-through and imaging aberrations) make less appealing for actual systems with defined specifications.

Light Sources: Depending on the application of interest, different light sources can be used[13]. For a multispectral \hyperspectral imaging system a broadband white light source can be used and then properly filtered to ensure a specific wavelength is reaching the sample. This also offers flexibility in experimenting with different probes. But for many cases, the user knows already at the design phase the wavelengths that they want to work with. If this is the case, monochromatic sources can be chosen. Depending on the wavelength, LEDs (Light Emitting Diodes) or Lasers might be the most cost-effective solution in terms of price/Watt. Lasers, being coherent, are suitable for setups where the light must pass through multiple optical elements positioned apart while retaining the possibility of fine focusing on the sample.
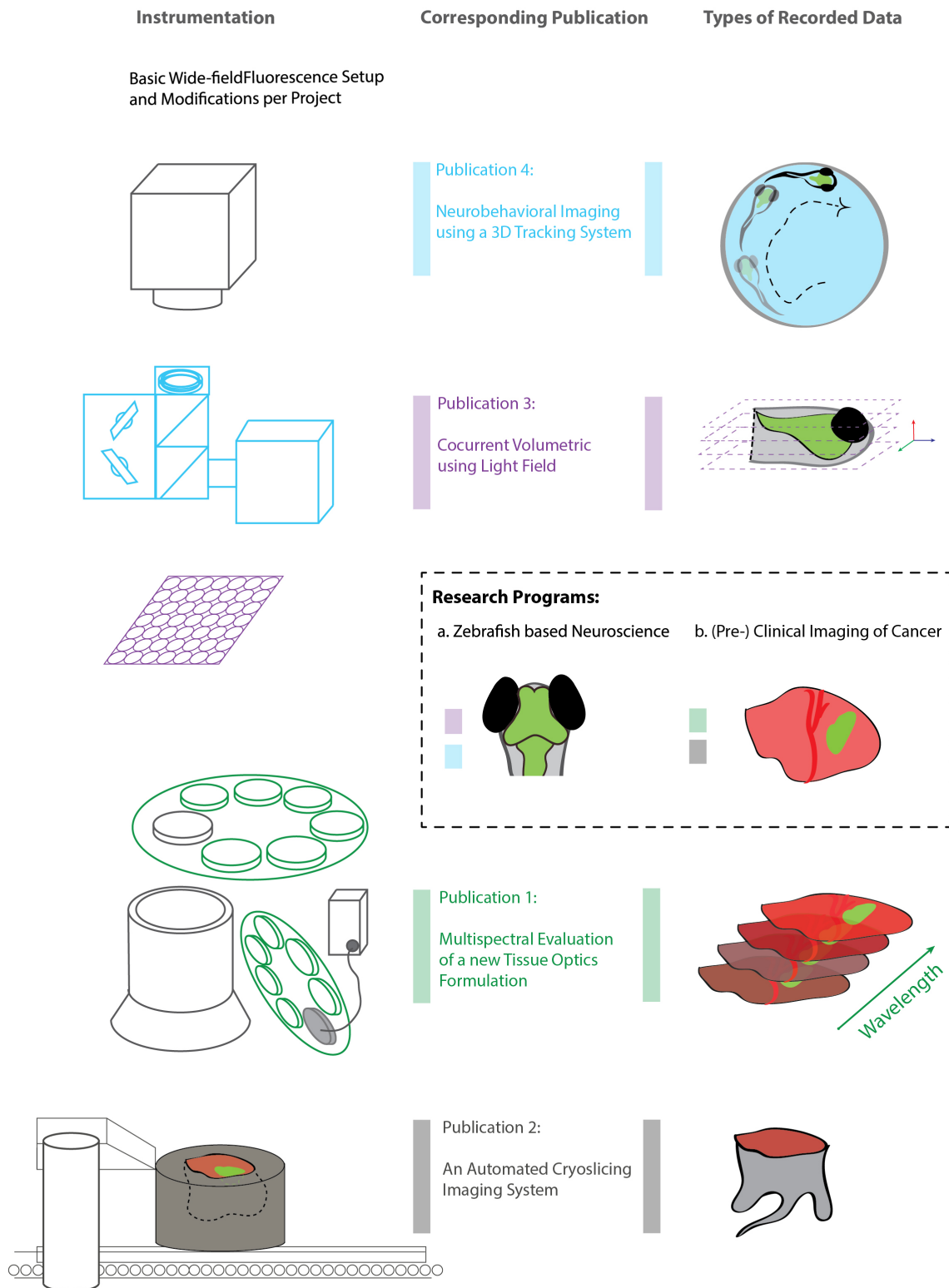
Figure 3.2: Schematic Overview of the modification of a basic wide-field fluorescence imaging setup (left side), to allow acquistions of special type of data (right side) to enable the research programs (middle).

The coherence gives rise to speckles patterns due to interferences but those can be alleviated (e.g. with dynamic defocusing elements and rotating diffusers).

Objective Lenses: The objective lens of the imaging depends greatly on the field of view requirements on of the application[166]. Simple telescopes with a single lense, a pair of lenses, or more complex composite microscopy objectives (together with the needed tube lenses) and macroscopy lenses (photography) can be used. The composite lenses offer a smaller footprint and advanced performance (offering minimal aberrations), but the user should ensure that they perform acceptably in their application framework. The two main issues are: (a)the chromatic aberrations in the infrared (including infrared blocking coatings) since most of those lenses are designed for visible light applications and (b) possible autofluorescence of the lens, which is generally low, but it might be comparable with the fluorescence of challenging samples, like in-vivo administered micro-doses of targeted fluorochrome in clinical samples. We note here that with the use of dichroic mirrors, the objective lens can also be used for coupling the excitation light which can be beneficial, e.g., to ensure that the illuminated area matched the imaging area in case the zooming of the systems is changed. Replacing or combining the objectives with an endoscopes (rigid, imaging fiber, etc) enables imaging inside the body[69].

Camera: Due to the low ratio of conversion of excitation photons to emitted ones and the low concentration of fluorescence molecules per pixel for most applications (either due to low targeting efficiency of administrated probes or the number of fluorescence proteins that genetically modified cells can synthesize and sustain), cameras with high sensitivity are required[9]. In the recent years we observe a transition from Electron Multiplying Charge Coupled Devices (EMCCD) to scientific-graded Complementary Metal–Oxide–Semiconductor (sCMOS), due to the increase of the sensitivity of the later. While those two types of camera dominate the market of fluorescence imaging for biomedical application, depending on the application Image Intensified Camera[180] (in cases were fast getting is of the essence) or InGas Sensors[81, 170] (for imaging above 1000nm where a second window exists in the electromagnetic spectrum where tissue absorbs and scatters minimally) are also used. What is of high importance when choosing a fluorescence camera is a proper evaluation of the specification for the application of interest, since the requirements for, high sensitivity, low exposure times \high frame rates might be mutually exclusive (to fit many pixels in the area of a sensors, those must be small and thus the number of photons that hit each ,at a specific amount of time, is decreasing). Often the limitation of imaging are imposed by the scence rather than the camera, e.g. imaging a fluorescence in a diffusive tissue results in low resolution images independently of the number of pixels of the sensors, while the dynamics of fluorescence calcium indicators are in the hundreds of ms scales therefore increasing the acquisition speed does not increase the number of detected firing events of neurons.

For all the publications included in this thesis, we were based in the above core setup and engineered solutions to extend it in order to enable or optimize acquisitions schemes needed to enable research in the fields of interest. While more details can be found in the papers, we briefly present bellow our add-ons to this core setup, to bring the four different systems in a common instrumentation framework.

3.2.2 Multispectral Imaging using automated excitation and emission filtewheels

Acquiring spectral information from a sample is traditionally done as (a series of) point measurements using a spectrometer. Spectrometers are prism or grating-based instrument that analyzes a single beam of light to its spectral components and measures their intensities. The first efforts to provide spectral(in terms of color) information in images was motivated more by the need for proper aesthetic representation of the colors that human can perceive rather than quantification of spectral information. Still, the Bayer-filter mosaic found in most modern color consumers cameras, provide spectral information at 3 different bands (red,

green, blue). An easy approach to achieve multi-spectral imaging, is to use more complex micro-filter pattern, which relatively easy using modern manufacturing techniques[45, 179, 50].Another way to simultaneously capture multiple images on a single sensor is the use of image splitters instrumenting which combine dichroic mirrors that project differently filtered images at different locations of the sensor (devices like Optosplit). Both methods share the common drawback of the inability to change the image acquisition parameters for each channel individually, possibly resulting in suboptimal imaging in terms of noise-rate for each of the channels or in need for High-Dynamic Range acquisitions protocols. Nonetheless, this solution can still be suitable for multispectral reflectance imaging (especially with the modern megapixel sensors), but for fluorescence imaging we have to filter both excitation and emissions lights, which complicate the acquisition, creating the need to overlay a notch filter at other excitation bands or temporal multiplex excitations at different wavelengths using either tunable light sources or rotating filter-wheels. Of course, if cost is not an issue and the number of wavelengths is small, using multiple cameras each with a single filter, is a solution that offers flexibility in term of acquisition parameters (especially since each of the cameras might have different characteristics).

We can group the filter-wheels-based solutions in two groups: continuous vs. sequential movement of the wheel. The first approach can be faster since the sensor acquires continuously and can benefit from actual wheel-shaped filters, while in the second approach we can specify the location and duration of each stop. This second solution allows for: (1) use of normal circular filters positions in a wheel-like holder, (2) individually modifying the time spend at each filter based on the specimen requirements (to do so in the continuous movement wheels with uneven segments must be manufactured) (3) easier control of the acquisitions pipeline. For the above reasons it is preferred in a research framework where flexibility might be of interest. One additional benefit of the sequential filter-wheel solution (and the main reason we choose it for the setup presented in publications 1-2 of this thesis), is that the images for each individual channel are identical to the ones that would have been acquired from a single filter-sensor pair and thus any finding (as, e.g. optimal combination of filters for imaging a specific sample), can be then applied to multi-cameras setups without the need for temporal multiplexing (at least at the detection).

It must be noted, that although our solution of choice for our multispectral system was driven mainly by the need of applicability of the findings on a clinical setup for intraoperative fluorescence imaging where few wavelengths are sufficient, other applications (e.g. like Raman scattering) might require denser wavelength sampling (even with the expense of spatial resolution). The field of multispectral-hyperspectral imaging is quite active with new dynamic optical elements (like acoustooptics tunable filters[68] that might potentially replace filter wheels), smart setups combining sensors \sample scanning with 1-D hyperspectral sensors and new algorithms using the principles of compressed sensing[137, 113].

3.2.3 Volumetric imaging using Automated Cryo-Imaging Setup

One of the main challenges of optical imaging is the limited penetration depth, with many applications focusing on surface imaging (external and also internal surface -endoscopic methods, or exposed tissue) with minimal or no volumetric information. Some novel tomographic all-optical[6] and hybrid (e.g. optoacoustic[147]) modalities can potentially provide full-body 3D imaging of small animals, but validating the imaging capabilities of those modalities also requires imaging tools based on the same optical-contrast mechanism that can provide ground truth. One way to address the need for both imaging in deep tissue and acquire volumetric information is to replace the "optical sectioning" (referring to the capability of an optical imaging system to discriminate between different planes) with actual mechanical sectioning. Mechanical sectioning of biological samples already exists in the pipelines of most medical and biological labs, where few thin slices of the sample are excised and investigated under a

microscope. Modern solutions allow though both: (a) the reconstruction of a volume from many excised slices imaged separately[58] and (b) incorporating in the same device both a sectioning device and an imaging one. The destructiveness of such imaging systems forced them to be applied only ex-vivo, but can still generate valuable information. To do so, the experiments must be designed properly, with educated decision about the euthanization time points and \or complementary in-vivo measurements.

Many different combinations between sectioning devices (cryotomes, microtomes, vibrotomes) and imaging systems (wide field reflection[122] and epifluorescence[151, 82], confocal[163] or two-photon[146], or even optoacoustic[203] and electron-microscopy[78, 44]) can be made, each with significant advantages and disadvantages that make them suitable for specific applications. For example, while vibratomes are suitable for slicing unfrozen sample like excised brains, they can not cut through bones and thus are not suitable for full body sectioning. Similarly, two-photon microscopes offer high spatial resolution being minimally affected by diffusion but are much slower than widefield imaging methods.

For our applications, we decided to stick to combining the multispectral widefield reflection and fluorescence imaging system presented in the previous paragraph with cryotomes imaging systems. The motivation for this was three-fold driven by the application, which was mainly the improvement of validation of other optical imaging modalities. (1) Cryoslicing followed by staining of the thin slices and microscopy imaging is an established validation method, so adding imaging on top-off it would not require modification of the pipeline or preparation of additional samples (2) Since cryoslicing can be performed across the whole body of small mammals, it is ideal for validating in-vivo full-body biological imaging modalities like fluorescence molecular tomograpy and optoacoustics and (3) the imaging setup of choice has a imaging geometry and parameters similar to the ones used in the clinics during intraoperative fluorescence imaging, and thus potential development done on that (e.g. from optimization of imaging to post-processing algorithms) can be almost directly applicable in clinics.

One of the main challenges we addressed during the development of both a manual and a fully automated version of cryo-slicer imaging systems, was the need to engineer a user-friendly front-end that could allow users (even ones without technical background) to easily define their image (and slicing) protocols based on the specific studies of interest. The software we developed allows the user to select a series of pre-defined images (RGB, narrow-band reflectance at multiple wavelengths, fluorescence for most commonly used fluorochrome, multispectral fluorescence acquisition for unmixing of fluorochromes and autofluorescence) at different modes (fixed exposure, automatic exposure definition per slice, HDR (High Dynamic Range) imaging) or define new acquisitions (e.g. by individually selecting the excitation and emissions filters and the parameters of acquisition). This enabled the transition of the cryotome from an experimental setup to a "core-facility" type of instrument, where both internal and external collaborators run studies with minimal support from our scientist.

3.2.4 Light Field Imaging using microlens-arrays

While imaging tissue in high resolution in the diffusive regime requires mechanical sectioning, acquiring 3D information from transparent samples can be done using optical sectioning methods. A lot of samples ranging from small living brains (c. elegance, zebrafish larvae, etc) to chemically cleared ex-vivo samples (mammalians brains and tumor biopsies)meet those requirements and thus nondestructive volumetric optical imaging is of higher interest. Most of the volumetric imaging modalities require some sort of scanning of one[140] or multiple beams[48] or sheets of lights[2] (and focus points \planes) across the three spatial dimensions. Apart from the increased complexity of such imaging systems, the fact that the information is not acquired simultaneously from each of the sampling points can be problematic and thus research on modalities that can offer co-current acquisitions of volumes (even at lower resolution or even frame-rates is of interest) is blooming.

A simple stereoscopic imaging system with two (properly aligned and calibrated) cameras is a basic solution to retrieve depth information from a sense, but due to phenomena like occlusions (where an object hide the object behind it) a denser sampling of the imaging space is required, acquiring both intensity and angular information from many rays in order to reconstruct the whole "light field". While the concept of such acquisitions and the principle of the reconstruction of scenes from their light-fields have already been described almost a century ago[86], it was only recently that the instrumentation enabled such acquisition. Just few years after the first meaningful attempts to acquire light field using huge arrays of multiple cameras[187], micro-manufacturing techniques of both sensors and optics allow for doing so. This is achieved with a single assembly consisting of a microlens array (an optical element with size comparable with the imaging sensors hosting of multiple -hundreds or more- of tiny lenses) and an imaging sensor with dozens of millions of pixels. Finally, the processing power of current computers (including embedded microprocessors) enabled reconstructions of volumetric scenes in real-time, even on consumers cameras.

Apart from the apparent benefit of the co-current acquisition that will be discussed in the context of the possible application in Chapter 3.3.2. in more detail, there is a series of advantage that render light-field imaging (and generally computational imaging) an appealing imaging technique. The first advantage being the simplicity of the instrumentation. A simple addition of a microlens array in the proper position of the optical path results in the acquisition of light fields. This can be done on both macroscopic imaging systems (even conventional digital cameras[126]) and microscopes[110]. Consideration regarding the ratio of number of pixels and number of microlenses, the aperture size of the optical system and the microlenses must be taken into account to achieve meaningful axial and lateral resolution and depth of fields. The second advantage is the flexibility that modern micro-manufacturing techniques offer in terms of the microlens array designs. It is possible to modify each of the lenses, giving different focal length to each of those (e.g. for extending the depth of field[139]) or to overlay spectral filters and to acquire multispectral 4D data (XYZ,wavelength) from a single snapshot[204]. Finally, researchers are working on improving the reconstructions, using either wave-optics modeling[24] (better suitable for microscopy application compared to wave optics), coding masks in the optical paths[37] or compressed sensing principles using either prior information from the dynamics of the sample[136] (e.g. firing patterns of neurons) .or . Some of the computations needed for such reconstructions would have been difficult with the previous generation of computers. But today's computers using proper algorithms are able to reconstruct even less structured images, thus in the forefront of the field of "computational imaging" (that includes light field imaging) we find lenslet imaging systems where the sensors capture complex interference patterns and computers apply phase retrieval algorithms to reconstruction the path of light until it reaches/has reached the sensor[118, 208, 11, 1, 171].

3.2.5 Tracking Microscopy controlling galvanometric mirrors in close-loop

There is an inherent physical trade-off between the resolution and the field of view that a sensor can acquire with a single snapshot. The number of sensing elements of the sensor (from the photoreceptive cells of an eye to the pixels of a camera), can either capture high resolution details of a small region or lower resolution information from a bigger field of view. This is a limiting factor that many applications face and the solution of scanning can be used to capture many high resolution images and then stitch them together. This can be done either by moving a small field with steps comparable to the field of view[116] (capturing information outside the field of view of the first image) or with moving a large field of view with steps comparable to the pixel size[128](capturing information between the pixels of the first image, a technique named geometric super-resolution imaging not to be confused with optical super-resolution microscopy). Depending on the application it might be easier to move the imaging instrumentation itself or the sample relative to each other. All

scanning methods are relatively slow and the speed is decreased proportional to the increase of resolution and field of view, which make them not suitable for live scenes. But in some of those scenes the change is not happening across the whole field of view simultaneously. Thus a tracking solution following a changing region of interest, while it moves around the big field of view, is of interest.

In biomedical field tracking microscopes have been proposed for high resolution monitoring of behaving animals, that are allowed to move in space much bigger than the actual size of the field of view of the imaging system. In the case of simple organisms like worms, stages that move under the animal to compensate its crawling trajectory and ensure that it remains in the fixed field of view of a (fluoescence) microscope are prefered. While for faster moving or more sensitive animals it is actually easier and prefered to move the aiming point of the imaging system without interacting with the animal. This can be done by the users of the instrumentations, but automated systems have been proposed recently to automate the process, which offer both unattended use of the instrument and more reproducible results, especially in case the reaction times of the animals are too fast for a human observer to react. Automated systems have been proposed in the literature both based on stages for monitoring the neuronal activity of c.elange[109, 191, 127, 93] and hydras[49] by placing stages under either con-focal or even two-photon microscopes[93], and for capturing the behavioural information flying of flies[153] and of the whiskers of walking mice[123]. A couple of years ago, a tracking macroscope based on xy-mirrors was introduced to neuronal information of walking flies as well, requiring the creation of a cranial window[71].

Aiming to engineer a system suitable for Zebrafish larvae, we aimed for both microscopy level capabilities (since the resolution is not limited by diffusion as in the fly brain) and without stages, since zebrafish have complex movement perception systems (combining information from visual inputs[138, 142], flow sensing through the lateral line[35, 174] and sensing of acceleration with the otolith in their vestibular system[57, 21]). Thus we designed a widefield imaging system, where after the main objective an xyz-scanner, receiving information from a second camera, and displacing the formed image ensuring that the head of the fish remains at the focus point of the zooming system that magnifies it. At the moment of publication of this setup (along with a series of biological experiments as a showcase of its capabilities), two more zebrafish focus systems based on stages (one based on light-field technology[38] and one structure illumination[98]) appeared in the literature, which are complementary to ours offering volumetric imaging of higher resolution but stimulate the fish while moving its swimming arena under the microscope.

3.3 Related Research Programs

The reason for developing the instruments presented above (and in more details in the attached papers), was not to do a tour-de-force showcasing capabilities of modern optical imaging but to enable studies with application both in clinics and in basic research. Thus at least at some of the specs, the system might lack behind state-of-art imaging, but they satisfied -sufficiently if not optimally- the specifications that we put in the first place to enable our research programs. To make this more clear, we will present in the following paragraphs those research fields aiming to a level of abstraction and simplification suitable for a dissertation at an engineering faculty. Especially for the first two chapter publications, where follow-up work based on those two publications are either pending or driven by fellow colleagues(e.g., the incorporation of the ex-vivo imaging validation pipeline in a clinical framework [103]), we present a bird-eye-view of the topic and our approach to it which is necessary to put the herein presented publications in context.

This first topic is the (clinically applicable) imaging of fluorescence probes in the diffusive regime, which results in raw-images which are not a direct depiction of the location and

concentration of the probes, but capture convolved information depending on the optical properties of the underlying tissue as well. Addressing this problem either in algorithms or instrumentation level is crucial for clinical application, but for basic research, like probing brain circuits functions, researchers have found workarounds \shortcuts. One of them is using transparent model organisms, like zebrafish larvae and imaging those is our second research program. The limitations there are not coming from the light transportation inside the tissue, but from the need to ensure the optimal trade-offs between spatiotemporal resolutions, field of view and animal handling for the specific experiment.

3.3.1 Quantification and Localization of Fluorescence Signals for Cancer Imaging

Recent advances in biochemistry allow researchers to tag specific molecules with fluorescence dyes. The portofolio of the taggable molecules, the efficiency of the tagging mechanism and possible activation mechanisms (only fluorescence under specific background) keeps expanding allowing us to envision a clear path toward personalized tumors resection[165, 159]. A biopsy of a patient's cancer can allow physicians to identify what was the molecular mechanism of a specific cancerous lesion and then highlight any other cells in the body that seem to have the same issue (overexpression of the same protein) at a sufficient degree to render them possible candidates for future lesions. While already the current combination of dyes (even the non-targeted dyes that highlight some tumours due to their Enhanced Permeability and Retention effect) and imaging systems is proven a useful tools in the health of the physicians, we can foresee that both the spatial specificity (cellular) and their possible dynamic signal changes (e.g level of protein expression or other micro-environments parameters like pH[186]) will further benefit from advances in both accuracy of localization and quantification of the detected signals. Those are currently limited by the diffusion of both the excitation and emission light inside the tissues[131]. Furthermore those tissues might be heterogeneous, both because e.g. tumors grow in different organs and because the composition of the tissue might change because of the disease in unknown ways (even a superficial reading of the "hallmarks of cancer" papers[75, 76] that present basic cancer mechanism reveal that different cancers might have completely different characteristics, like vasculature, accumulation of necrotic tissue etc). It must be further noted that the visual appearance of tissue in the naked eye is often misleading since (for most application) we use infrared fluorescence probes in a wavelength range that the blood absorbs minimally. Even highly vascularized tumors, appearing deep red, might only minimally absorb -at least compared to melanomas with similarly dark appearance. This counter-intuitive finding that similarly looking tumors might result in different changes of fluorescence signals also expands on the multiplexed effects of absorption and scattering.

Finally, possible solutions have to be able to be implemented in a clinical setup from both technical and regulatory aspect, thus our first attempt is to better understand the information already included in the images we currently acquired with the approved instrumentation (combination of an RGB (Red Green Blue) reflection camera and a fluorescence one) and work either based on that or with minimal modifications (e.g., optimizing the filter, adding another camera or some specialized illumination, but not much more complex system). To do so we followed multiple interconnected paths, including theoretical modeling of light transport in tissue[175], experiments with tissue phantoms under both the multispectral imaging system and the cryo-slicer (able to resolve depth information) and finally tissue experiments both with mice cancer models[176] and ex-vivo human samples. Since ,contrary to the phantoms, for the clinical samples we were lacking gold-standard information, we established an imaging pipeline that included apart from the epi-fluorescence setup, cryo-slicing, thin-slice imaging, and histopathology[103].

Before providing further details regarding those methods, we can briefly summarize the conclusion of our research in this field. Based on our theoretical framework: (1) the fact that diffusion is equally important with absorption since appart from quantification proper localization of the sources of signals are crucial (2) contrary to past approached were pixels were treated individually, we showcased that any solution should take into account the neighborhood of the pixel as well (and it is important to experiment with non-homogeneous phantoms), (3) a non-uniqueness exists in term of visual appearance (=reflection images) and underlying optical properties[67], meaning that two different combinations of scattering and absorption might result in exactly the same image. To address that we have to either look for solutions in subspaces of parameters (assuming known scattering for specific tissues of interest), or perform additional measurements like multispectral fluorescence imaging or imagining under structured illumination.

Theoretical Modeling and Simulations: One path toward better quantification and localization of fluorescence is the use of theoretical formulas that describe how it is affected by the optical properties (mainly absorption and scattering) of surrounding tissue. Even then, measuring the optical properties of the tissue is not trivial (especially in an intraoperative setup), so formulas that describe how we can retrieve optical properties from e.g. multispectral or structured illumination images are equally important (and challenging). Based on our experience, a possible shortcut for actual corrections are formulas that combine such additional measurements to correction factors (e.g., normalizations of fluorescence using measurements at different wavelengths), without actually estimating the optical properties. One of the challenges that researchers face is that in order to derive analytic forms of such equations from the basic Helmholtz Equations, assumptions must be made. When we started working on our problem the analytic solutions that existed predicted back-scattered reflection based on the absorption and scattering of tissue assumed wave and point-source illumination[85, 55, 56, 54], thus with our collaborators, we reformulated those formulas to account for homogeneous planar illumination concepts like the ones we find in the widefield epi-illuminations clinical applications. Of course, this formulation had to be validated.

One validation concept are **Monte-Carlo simulations**. Similar to how Monte-Carlo simulations are employed to other fields, for optical simulations the trajectories of millions of photons are tracked, after assigned probabilities to a specific event (e.g. absorption by a molecule, or change of trajectory to scattering on another) depending on the optical properties of the simulated tissue[195, 61, 192]. Contrary to theoretical formulas that their range of applicability is limited (a complete theoretical model must include parameters for both ballistic and diffusive photons, but depending on the application -e.g. Microscopy vs. mesoscopy- one of the two is often both negligible and neglected), a properly set-up Monte-Carlo model can accurately predict light propagation across different regimes. The issue with them though is that although they can be used to generate look-up table (or to validate formulas), they are not directly applicable for the inverse problem (the prediction of underlying composition based on a measurement) .While in the past they were time-consuming, modern multicore CPUs and GPUs[149] on either local machines or accessible workstation on the cloud[46], enable time-efficient simulation. An additional benefit is the capability to simulate complex geometries, albeit this might require some level of expertise or familiarity with existing suites.

Finite elements methods provide numerical solutions to physics problems, without the need of exact analytical solutions to the governing equations. And since they are widely used in many contexts, software suites exist that offer simple importing of complex geometries and high parametrization capabilities[108, 16]. Despite not being featured in any of the herein presented publications, the simplicity of modifying the geometries on simulation based on two Helmholtz Equations (one for propagation excitation light and one for the emission light) provided us with important intuitions about the light propagation in non-homogeneous, complex

geometries that was necessary to explain phenomena that we observed in the experiments on real tissues.

Measurements on tissue-mimicking phantoms and biological tissues: The assumptions used for the theoretical frameworks must be tested on actual measurements. It is not uncommon for such measurements to hint to possible modification of the theoretical framework and further testings. Two main types of measurements can be used: (a) measurements on tissue-mimicking phantoms of known properties and (b) measurements on tissue accompanied by the acquisition of some gold-standard information.

There is a huge variety of **phantoms** for optical imaging[141, 7]. The main benefit of working with them is that at least some of their parameters can be considered known. For example, using proper concentration of blood and intralipid we can make liquid phantoms with known optical properties while by inserting a tube filled with fluorochrome inside an excised tissue we know the exact location of the source of the fluorescence. Furthermore, it is quite simple to change those parameters to acquire measurements across a wide range of the parameter space of interest, either by making multiple phantoms or even by modifying a single phantom (e.g. in a titration like a framework where we slowly increase the concentration of absorbers). One way to categorize phantoms is distinguish them to those being based on biological material, like homogenized tissue or extracted blood and those based on pure chemicals (e.g. absorbing dyes and scattering particles). While the later can be more controllable, it is extremely challenging to combine them in a way that accurately simulates tissue across a wide range of wavelength and care must be taken that assumptions made for biological tissues stand (Can their scattering be omitted as we do with blood?). Finally, if those phantoms are either stable over time, or if a specific preparation protocol can be described that ensures exact replications, they can also be used to standardize imaging pipelines, including instrumentation and corrections algorithms. It must be noted that ensuring exact values of the parameters of interest is not trivial, since there might be variabilities on both the basic substances used (e.g., absorption of a blood phantoms depending on the hematocrits of the blood used and often unstandardized milk is used as scattering rather than intralipid due to cost) and the procedure (e.g. shielding/not shielding a liquid blood-based phantoms might result in oxygenation changes). Thus it is advised to use additional measurements to characterize the phantoms properly. But even so, to do that is often easier in phantoms compared to actual biological samples.

The main issue with **real tissue** experiments is that we are lacking exact knowledge of the composition of the tissue, or a gold-standard regarding the final image of interest (for our application being the true distribution of fluorochromes). Although cryoslicer-imaging has been used as such for other imaging modalities or biological studies, the reality is that due the imaging of bulk tissue, diffusive light propagation and absorption affect the images. Using the images from the deeper layer[15] we were able to improve on that, but probably the most valuable contribution (due to its clinical relevance) was the development of a whole pipeline from planar epi-fluorescence imaging, to cryoslicing and then imaging of thin slice to provide real ground truth. The excised slices, having a thickness less than the mean free path, can provide diffusion-free imaging, which is closer to the real distribution inside the tissue. The low-volume of fluorochrome in that required improvement of the imaging systems (minimizing background noise level from ambient light, bleed-through of the filters and backscattered fluorescence). Additional staining of those thin slices also reveals additional information regarding the tissue (morphology of cells using H&E staining and reflection imaging or distribution of proteins using secondary fluorescent antibodies).

Studying novel imaging probes and validating in-vivo imaging modalities: While capturing as accurately as possibly the distribution of a fluorescence probe is of high interest, actually ensuring the proper labeling both in terms of its specificity and emitted signal (often proportional to an underlying biological process) is of equal -if not higher- importance.

Thus our cryoslicer-centered imaging pipeline was also heavily used in studying the efficacy of different labeling practices, like cancer targeted dyes binding to proteins over-expressed in cancer with possible clinical applications [66], fluorescence microspheres to study lugs [15] , to absorbing/fluorescencing proteins expressed in cancerous cells after viral transfection [173] or to label specific neurons of interest. Another use of our cryo-imaging, was to validate in-vivo imaging. While we already discussed how our pipeline generated knowledge for planar-epifluorescence measurements, its capability to also acquire both multispectral reflection and fluorescence volumetric data rendered it a great gold-standard for other (non-destructive) imaging modalities like Phase-contrast X-ray CT [177], Optoacoustic Tomographic Mesoscopy [31, 30], Rastar-Scanning optoacoustic Microscopy [133] or Fully body Multiscectral Optoactoustic Tomography [185]. After having set up both the instrumentation and the imaging protocols/pipelines, using the aforementioned projects/publications in this paragraph (that we co-authored), the system is currently running also in a "core-facility"-like mode with our technical assistants being able to independently generate quality datasets and figure for internal and external collaborations.

3.3.2 Translucent brains: Neurobehavioral studies of Zebrafish Larvae

Moving away from a clinical setup to pre-clinical studies and basic research, researchers have higher flexibility with their experimental design. Such examples include genetic modification of neurons to shine brighter light when they are activated and the use of transparent model organisms. In the next paragraphs we will provide a short introduction to the field of all-optical electrophysiology and try to answer why zebrafish larvae is a suitable animal model to study brain function with such methods. We will focus on the importance of both single snapshots three dimensional (3D) acquisitions and imaging of freely behaving organisms, which was our motivation for working on the systems presented in the last two publications of this dissertation.

While as a community we are far from understanding as a whole the function of brains[90], even discoveries in smaller scales (e.g. how a specific circuit works), can provide insights in both therapeutic approaches of related diseases and how to better designs biomimicking artificial neural networks. Most existing imaging modalities (bold fMRI[188], EEG and diffuse optical tomography[39], PET[154]) allow mainly secondary measurements (blood volume, metabolic activities) and as averages of big regions. A stretched analogy for that is an electronics engineer that tries to study a circuit using a thermal camera. Of course, putting electrodes is the brain is possible[91] but contrary to the few pins of simple circuits, thousands of neurons form millions of connections even in simple animal brains. So probing one or few of them at a time is at least painstaking and limits the sort of experiments. Furthermore, the tool that engineers use to back-engineer a circuit is not an oscilloscope, but a network analyzer, a device that apart from recording can give specific signals of interest as inputs. When scientists managed to develop the genetic machinery needed to create apart from optical sensors of neuronal activity also actuators (proteins that force neurons to fire when illuminated with light, a technique termed optogenetics[42, 43]) the field of **all-optical electrophysiology**[51] was born. New optical methods are developed to match the genetic tools, enabling both detecting photons across big volumes with high resolution and accordingly shaping light to provide sophisticated excitation patterns (even in closed loop approached). One of the main bottlenecks for such optical approaches is the existence of scattering in humans/mammals/insect brains. Scientists work towards adaptive optics techniques which allow shaping of the wavefront to overcome the effects of scattering, but there are organism like Zebrafish larvae that are transparent already.

One of the main advantages of **Zebrafish larvae** is that they are transparent[10] offering direct optical access to their whole brain (or other organs like the heart[158]). The size of the brain is another advantage, both in terms of optical imaging and computational neuroscience.

It is small enough to fit in the field of view of a microscope that provides almost cellular resolution (with scannings) and the number of neurons and their connections appears addressable with modern computational methods, contrary to e.g. a mouse brain where a full-functional connectomic analysis would be prohibiting for modern computers. Worms (c. elegance is commonly used) are also transparent and have fewer neurons, but (probably exactly because of this small number) they have a quite limited repertoire of behaviors contrary to Zebrafish. Even at the larvae stage (e.g. <7 days post fertilization), the larvae are developed enough to show complex sensory perception and behaviors[92], with the main exception of social behaviour which is developed later. It is up to this age of 7 days that working with larvae is also in terms of logistics, since it is easy to breed the parents that give a big number of offsprings which are easy to maintain and use for any of a huge catalog of biotechnology techniques (e.g. viral injections) to ensure the optimal sample before imaging. This logistic simplicity renders them optimal also for high-throughput studies, bridging the gap between in-situ (cell culture/ lab on a chip) and mouse experiments in the drug development pipelines in the future, and those they are most commonly use than other fish that remain transparent even at older ages (like Danionella translucida[150]). Apart from all the above that lead to a wide use of Zebrafish as a generic animal model, there are specialized biological studies that could benefit from either the similarity of zebrafish to human physiology or of their differences. In the first case we can find e.g. circadian rhythms studies[209] since Zebrafish are diurnal animals (contrary to mice which are nocturnals) and thus they might be a more suitable model for those, while in the second category belong the studies on regenerations. Contrary to humans, zebrafish are able to regenerate[143, 17] some of their tissues extremely efficiently. Understanding how this is done could lead to new therapies, in case of brain injuries or neurodegenerative diseases.

Zebrafish larvae appear to be an ideal model for system neuroscience[63] (despite some limitation e.g. lack of cortex), where multiple sensory inputs are processes by multiple brain circuits and based on their analysis signals are sent to motor neurons to enable a specific behavior. All that takes place with feedback loops. Being able to see the actual "signals" traveling through the nervous system and the resulting behavior to specific sensory (or even direct neuronal) stimulation will allow a much better understanding of the brain. We have identified and work on two main technical limitations of existing methods: (1) the need for co-current acquisitions of data across the whole brain in 3D (2) and acquisition of neuronal data from freely behaving animals.

Co-current volumetric acquisitions: The state-of-art microscopes used to probe the brain of Zebrafish[2, 193] work at around 10-Hz and in literature techniques exist to push this further[206]. They do so by rapidly scanning a sheet of light across z-planes, acquiring one image at each plane. The question that arose are: (a) do we need even faster acquisitions? (b) is the fact that each plane is acquired with few ms delay from the other a problem? For the majority of optical electrophysiology projects currently in place the answer is no. But we were intrigued by two fronts of new experimental designs and novel probes and thus we investigated technologies that might offer co-current acquisitions.

Genetically Expressed Calcium Indicators (GECIs) are proven to be extremely useful for visualizing neuronal activity. But their fluorescence changes are related to the influx of calcium inside the neurons and not the actual firing potentials. Thus they present a temporal average of the activity pattern, while they have inherently relatively slow dynamics[4, 181]. After the initial increase of the fluorescence signal it takes several dozens of milliseconds to return to default state even without firings. Thus they are, so far, the bottleneck in terms of capturing fast events (at least when light sheet microscopes are used). Not only new generations of GECI's with faster dynamic are being developed[33], but Voltage-sensitive dyes and fluorescent proteins[100] are being developed, that can respond with extreme temporal precision to the actual firing potential of the neurons. If those neurons are distributed in three

dimensions (a Zebrafish brain or a cultured brain-like organoid[95]) being able to acquire data from the whole volume is of extreme interest. However, such data should provide some sort of meaningful 3D information and not just be a projection of the whole volume. While we are not yet at a point that we can easily infer causation from the correlation of neuronal firings[160], just by following the signal traveling neuron by neuron and through all the feedback loops, being able to record co-currently signals across the whole brain with close to millisecond exposures might be a useful tool.

Even assuming that the fluorescence probes themselves are slow, there are scenarios where the co-current 3D acquisition is beneficial. In experimental paradigms with non-immobilized/non-anaesthetized fish or moving organs like the heart, the capture signals are a combination of the actual changes in intensity due to neuronal activity (which can be slow) and the movement of the fish which can be extremely rapid[25]. There are cases, like the heart imaging[120], that due to known priors (e.g. maximum possible movement of each cell) and ability to perform multiple acquisitions during almost identical movement (e.g. averaging across many pulsation cycles), combining data from scanning systems is possible using proper registrations and reconstruction methods, but it is not trivial. In other cases, like the one of freely swimming fish, this becomes almost impossible. Thus acquisition of slow phenomena but on fast moving (parts of/) animals could benefit from co-current volumetric imaging. Just observing in high temporal resolution 3D movements of fish or in higher resolution fins of fish while they move could push forward research on biomechanics as well.

Freely Behaving : While the need for co-current acquisition might be more apparent a few years from now, the importance of capturing behavioral output from the imaged brains which are exposed to naturalistic environment is already evident in literature[107]. In model organisms (like c.elange[191, 127]) where this was possible with the use of motorized stages, systems already exist, while for Zebrafish Virtual Reality setups[193, 172] were specific environments were project to the fish, that were modified based on its motor outputs (as those were recorded by electrodes since the animals was anesthetized). But such complex setup for zebrafish, although they allow the capability to break down and analyze in detail specific reflex-like responses, does not allow us to observe natural behavior. We will provide such examples -that were also our driving force for building our tracking microscope the way we did.

A significant amount of literature focuses on the different ways that animals, including zebrafish, are sensing the world. In many projects though the animals end up being a passive receiver of an input. They are embedded in agarose or restrained with other methods and are presented with a stimulation e.g. an odor. The researcher might be able to modify this stimulation (intensity/duration/... etc) and create a big dataset with responses to be analyzed. Often combined with either some behavioral output (e.g. monitor tail) or a purely behavioral experiment that run in parallel. Animals that are allowed to behave freely though are seldomly passive receivers of inputs. What we have already observed in one of our showcase studies for NeuBtracker, is that Zebrafish larvae when an repelling odor is presented in their arena they do not just avoid it. They actually visit the location of the high gradient of the odor and probe the smell for several miliseconds before taking decisions. Indeed the nose is a sensory organ that can be studied independently of the rest of the fish[62], but being able to study how the fish is actually using the sensory organ that it has at its disposal to actively sense the world is intriguing.

Another area of research of a tracking microscope that does not perturb the fish is the field of default network activity without external stimulation. Intuitively we can imagine an embedded Zebrafish like someone sitting in an MRI and asked to not think of something specific. But the reality is that restraining the fish (or even accelerating it in order to track it) or exposing it even to a non-homogeneous illumination of a microscope might be sensory inputs to the fish that do not allow it to reach the so-called default state. Properly modifying

the experiment (e.g providing enough acclimating time) and using controls (e.g. monitoring anxiety related hormones), might enable performing such studies on other instruments, but we still consider our implementation a fitting tool. By monitoring the activity of the fish we should be able to find multiple instances (even across several hours or even days) that the fish remains in such a state. Similar studies can be expanded also to sleep-related research.

Those research direction can already benefit from our instrumentation while future technical improvements (e.g. increasing resolution across all dimensions) on it might render the embedding preparation unnecessary. But until those improvements are invented/engineered, working on complementary dataset from both freely behaving and embedded fish is a way forward.

Having provided a quick introductions an the core-concept of optical imaging in terms of imaging and contrast mechanisms, the basic idea behind our instrumentation advances and the core research project they enable, we present in the next chapter the actual publications. Before each one a short introduction summarizing the core motivation-method-result of each project from an engineering view point is presented.

3.3.3 How Electrical and Computer Engineering enables and accelerates those Programs?

This introduction is mainly focused on providing a wide background on the biological projects that our novel instrumentation/imaging pipelines allowed. By reading the actual papers, the reader can identify a plethora of other aspects of these projects that require the application of electrical and computer engineering tools, or even the development of new ones. Even if a specific biomedical imaging project does not require the engineering of an imaging rig (as was the case in most of our projects), chances are that an engineering skill-set like back-of-the-envelope calculations about the expected signals, estimating the needed amount of animals/experiments to be able to perform a meaningful statistical analysis, and some degree of systems understanding to model the observed phenomena are required.

Specifically for our projects an additional computationally challenging step included the transformation of the raw acquired images and videos to quantities that us and our collaborators could understand and act upon. To do so we had to customise a series of algorithms from the field of computer vision, to allow the transformation of the images to common frameworks. When the images were brought to this common framework, visualisation and segmentation of the regions of interest were performed to tabulate the data and perform statistical tests.

Almost any application could benefit from fully automated high-throughput imaging systems (lower cost, increased accuracy etc). But automating the whole laboratory pipeline (using imaging and computer vision along with other automations), can also assist in improving imaging by enabling efficient screening and directed evolution approaches. Thus we foresee even further penetration of traditional engineering tools (e.g. robots) in the biological laboratory.
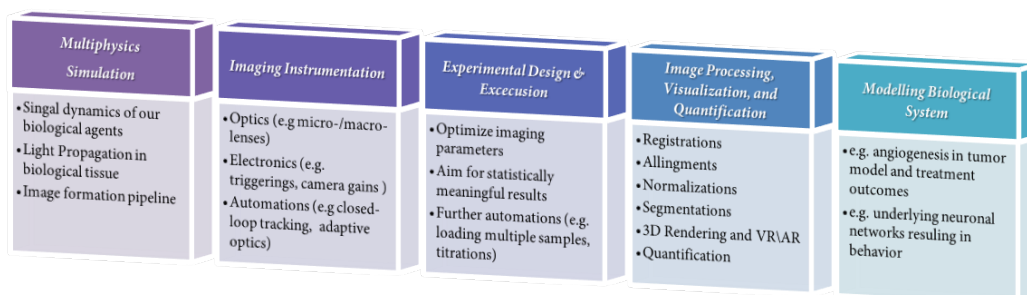
4 References

[1]   Jesse K Adams et al. "Single-frame 3D fluorescence microscopy with ultraminiature lensless FlatScope". en. In: *Sci Adv* 3.12 (Dec. 2017), e1701548.

[2]   Misha B Ahrens et al. "Whole-brain functional imaging at cellular resolution using light-sheet microscopy". en. In: *Nat. Methods* 10.5 (May 2013), pp. 413–420.

[3]   Joanna Aizenberg and Gordon Hendler. "Designing efficient microlens arrays: lessons from Nature". en. In: *J. Mater. Chem.* 14.14 (2004), pp. 2066–2072.

[4]   Jasper Akerboom et al. *Optimization of a GCaMP Calcium Indicator for Neural Activity Imaging.* 2012.

[5]   Jarmo T Alander et al. "A review of indocyanine green fluorescent imaging in surgery". en. In: *Int. J. Biomed. Imaging* 2012 (Apr. 2012), p. 940585.

[6]   Angelique Ale et al. "FMT-XCT: in vivo animal studies with hybrid fluorescence molecular tomography-X-ray computed tomography". en. In: *Nat. Methods* 9.6 (June 2012), pp. 615–620.

[7]   Maria Anastasopoulou et al. "Comprehensive phantom for interventional fluorescence molecular imaging". en. In: *J. Biomed. Opt.* 21.9 (Sept. 2016), p. 091309.

[8]   J Andrasko and B Rosén. "Sensitive identification of hemoglobin in bloodstains from different species by high performance liquid chromatography with combined UV and fluorescence detection". en. In: *J. Forensic Sci.* 39.4 (July 1994), pp. 1018–1025.

[9]   Jacqueline M Andreozzi et al. "Camera selection for real-time in vivo radiation treatment verification systems using Cherenkov imaging". en. In: *Med. Phys.* 42.2 (Feb. 2015), pp. 994–1004.

[10]   Paride Antinucci and Robert Hindges. "A crystal-clear zebrafish for in vivo imaging". en. In: *Sci. Rep.* 6 (July 2016), p. 29490.

[11]   Nick Antipa et al. "DiffuserCam: lensless single-exposure 3D imaging". en. In: *Optica, OPTICA* 5.1 (Jan. 2018), pp. 1–9.

[12]   S R Arridge and J C Hebden. "Optical imaging in medicine: II. Modelling and reconstruction". en. In: *Phys. Med. Biol.* 42.5 (May 1997), pp. 841–853.

[13]   Kavita Aswani, Tushare Jinadasa, and Claire M Brown. "Fluorescence Microscopy Light Sources". In: *Micros. Today* 20.04 (July 2012), pp. 22–28.

[14]   Adnan Bajwa et al. "Assessment of tissue perfusion in the lower limb: current methods and techniques under development". en. In: *Circ. Cardiovasc. Imaging* 7.5 (Sept. 2014), pp. 836–843.

[15]   Nirav Barapatre et al. "Quantitative detection of drug dose and spatial distribution in the lung revealed by Cryoslicing Imaging". en. In: *J. Pharm. Biomed. Anal.* 102 (Jan. 2015), pp. 129–136.

[16]   Sh Bazrafkan and K Kazemi. "Modeling time resolved light propagation inside a realistic human head model". en. In: *J Biomed Phys Eng* 4.2 (June 2014), pp. 49–60.

[17]   Catherina G Becker and Thomas Becker. "Adult zebrafish as a model for successful central nervous system regeneration". en. In: *Restor. Neurol. Neurosci.* 26.2-3 (2008), pp. 71–80.

[18]   Pascal Berto et al. "Programmable single-pixel-based broadband stimulated Raman scattering". en. In: *Opt. Lett.* 42.9 (May 2017), pp. 1696–1699.

[19]   C S Betz et al. "A comparative study of normal inspection, autofluorescence and 5-ALA-induced PPIX fluorescence for oral cancer diagnosis". In: *J. Cancer* (2002).

[20]   Thomas S Blacker and Michael R Duchen. "Investigating mitochondrial redox state using NADH and NADPH autofluorescence". en. In: *Free Radic. Biol. Med.* 100 (Nov. 2016), pp. 53–65.

[21]   Franklin Bretschneider et al. "Zebrafish can hear sound pressure and particle motion in a synthesized sound field". In: *Anim. Biol. Leiden Neth.* 63.2 (Jan. 2013), pp. 199–215.

[22]   Jim C Brooker et al. "Total colonic dye-spray increases the detection of diminutive adenomas during routine colonoscopy: a randomized controlled trial". en. In: *Gastrointest. Endosc.* 56.3 (Sept. 2002), pp. 333–338.

[23]   AEX Brown and B de Bivort. "The study of animal behaviour as a physical science". In: *bioRxiv* (2017).

[24]   Michael Broxton et al. "Wave optics theory and 3-D deconvolution for the light field microscope". en. In: *Opt. Express* 21.21 (Oct. 2013), pp. 25418–25439.

[25]   S A Budick and D M O'Malley. "Locomotor repertoire of the larval zebrafish: swimming, turning and prey capture". en. In: *J. Exp. Biol.* 203.Pt 17 (Sept. 2000), pp. 2565–2579.

[26]   Santiago Ramón y Cajal. *Studies on vertebrate neurogenesis.* Thomas, 1960, 432pgs.

[27]   Santiago Ramón y Cajal and Léon Azoulay. *Histologie du systeme nerveux de l'homme & des vertebres.* Consejo superior de investigaciones cientificas, Instituto Ramon Y Cajal, 1952.

[28]   P Carmeliet and R K Jain. "Angiogenesis in cancer and other diseases". en. In: *Nature* 407.6801 (Sept. 2000), pp. 249–257.

[29]   Mark A Changizi, Qiong Zhang, and Shinsuke Shimojo. "Bare skin, blood and the evolution of primate colour vision". en. In: *Biol. Lett.* 2.2 (June 2006), pp. 217–221.

[30]   Andrei Chekkoury et al. "High-Resolution Multispectral Optoacoustic Tomography of the Vascularization and Constitutive Hypoxemia of Cancerous Tumors". en. In: *Neoplasia* 18.8 (Aug. 2016), pp. 459–467.

[31]   Andrei Chekkoury et al. "Optical mesoscopy without the scatter: broadband multispectral optoacoustic mesoscopy". en. In: *Biomed. Opt. Express* 6.9 (Sept. 2015), pp. 3134–3148.

[32]   Fei Chen, Paul W Tillberg, and Edward S Boyden. "Optical imaging. Expansion microscopy". en. In: *Science* 347.6221 (Jan. 2015), pp. 543–548.

[33]   Tsai-Wen Chen et al. "Ultrasensitive fluorescent proteins for imaging neuronal activity". en. In: *Nature* 499.7458 (July 2013), pp. 295–300.

[34]   Zhuo Chen et al. "Protein microarrays with carbon nanotubes as multicolor Raman labels". en. In: *Nat. Biotechnol.* 26.11 (Nov. 2008), pp. 1285–1292.

[35]   Shih-Wei Chou et al. "A molecular basis for water motion detection by the mechanosensory lateral line of zebrafish". en. In: *Nat. Commun.* 8.1 (Dec. 2017), p. 2234.

[36]   D Clements, P McMaster, and E Elias. "Indocyanine green clearance in acute rejection after liver transplantation". en. In: *Transplantation* 46.3 (Sept. 1988), pp. 383–385.

[37]   Noy Cohen et al. "Enhancing the performance of the light field microscope using wavefront coding". en. In: *Opt. Express* 22.20 (Oct. 2014), pp. 24817–24839.

[38] Lin Cong et al. "Rapid whole brain imaging of neural activity in freely behaving larval zebrafish (Danio rerio)". en. In: *Elife* 6 (Sept. 2017), e28158.

[39] R J Cooper et al. "Transient haemodynamic events in neurologically compromised infants: a simultaneous EEG and diffuse optical imaging study". en. In: *Neuroimage* 55.4 (Apr. 2011), pp. 1610–1616.

[40] William J Croft. *Under the Microscope: A Brief History of Microscopy*. en. Vol. 5. World Scientific, 2006, p. 138.

[41] Delphine Débarre et al. "Imaging lipid bodies in cells and tissues using third-harmonic generation microscopy". en. In: *Nat. Methods* 3.1 (Jan. 2006), pp. 47–53.

[42] Karl Deisseroth. "Optogenetics". en. In: *Nat. Methods* 8.1 (Jan. 2011), pp. 26–29.

[43] Karl Deisseroth. "Optogenetics: 10 years of microbial opsins in neuroscience". en. In: *Nat. Neurosci.* 18.9 (Sept. 2015), pp. 1213–1225.

[44] Winfried Denk and Heinz Horstmann. "Serial block-face scanning electron microscopy to reconstruct three-dimensional tissue nanostructure". en. In: *PLoS Biol.* 2.11 (Nov. 2004), e329.

[45] Nikolas Dimitriadis et al. "Spectral and temporal multiplexing for multispectral fluorescence and reflectance imaging using two color sensors". en. In: *Opt. Express* 25.11 (May 2017), pp. 12812–12829.

[46] Alexander Doronin and Igor Meglinski. "Online object oriented Monte Carlo computational tool for the needs of biomedical optics". en. In: *Biomed. Opt. Express, BOE* 2.9 (Sept. 2011), pp. 2461–2469.

[47] W Drexler et al. "Ultrahigh-resolution ophthalmic optical coherence tomography". en. In: *Nat. Med.* 7.4 (Apr. 2001), pp. 502–507.

[48] Gaddum Duemani Reddy et al. "Three-dimensional random access multiphoton microscopy for functional imaging of neuronal activity". en. In: *Nat. Neurosci.* 11.6 (June 2008), pp. 713–720.

[49] Christophe Dupre and Rafael Yuste. "Non-overlapping Neural Networks in Hydra vulgaris". en. In: *Curr. Biol.* 27.8 (Apr. 2017), pp. 1085–1097.

[50] Jason M Eichenholz and John Dougherty. "Ultracompact fully integrated megapixel multispectral imager". In: *Integrated Optics: Devices, Materials, and Technologies XIII*. Vol. 7218. International Society for Optics and Photonics, Feb. 2009, p. 721814.

[51] Valentina Emiliani et al. "All-Optical Interrogation of Neural Circuits". en. In: *J. Neurosci.* 35.41 (Oct. 2015), pp. 13917–13926.

[52] Turan Erdogan. "Optical filters for wavelength selection in fluorescence instrumentation". en. In: *Curr. Protoc. Cytom.* Chapter 2 (Apr. 2011), Unit 2.4.

[53] Andre Esteva et al. "Dermatologist-level classification of skin cancer with deep neural networks". en. In: *Nature* 542.7639 (Feb. 2017), pp. 115–118.

[54] Sergio Fantini and Enrico Gratton. "Fluorescence photon-density waves in optically diffusive media". In: *Opt. Commun.* 173.1 (Jan. 2000), pp. 73–79.

[55] T J Farrell, M S Patterson, and M Essenpreis. "Influence of layered tissue architecture on estimates of tissue optical properties obtained from spatially resolved diffuse reflectometry". en. In: *Appl. Opt.* 37.10 (Apr. 1998), pp. 1958–1972.

[56] T J Farrell et al. "Modeling of photosensitizer fluorescence emission and photobleaching for photodynamic therapy dosimetry". en. In: *Appl. Opt.* 37.31 (Nov. 1998), pp. 7168–7183.

[57] Itia A Favre-Bulle et al. "Optical trapping of otoliths drives vestibular behaviours in larval zebrafish". en. In: *Nat. Commun.* 8.1 (Sept. 2017), p. 630.

[58] Marco Feuerstein et al. "Reconstruction of 3-D Histology Images by Simultaneous Deformable Registration". In: *Medical Image Computing and Computer-Assisted Intervention – MICCAI 2011*. Springer Berlin Heidelberg, 2011, pp. 582–589.

[59] Carl J Fisher et al. "ALA-PpIX mediated photodynamic therapy of malignant gliomas augmented by hypothermia". en. In: *PLoS One* 12.7 (July 2017), e0181654.

[60] Jonathan A N Fisher, Brian M Salzberg, and Arjun G Yodh. "Near infrared two-photon excitation cross-sections of voltage-sensitive dyes". en. In: *J. Neurosci. Methods* 148.1 (Oct. 2005), pp. 94–102.

[61] S T Flock et al. "Monte Carlo modeling of light propagation in highly scattering tissues. I. Model predictions and comparison with diffusion theory". In: *IEEE Transactions on Biomedical Engineering* 36.12 (Dec. 1989), pp. 1162–1168.

[62] Rainer W Friedrich. "Neuronal computations in the olfactory system of zebrafish". en. In: *Annu. Rev. Neurosci.* 36.1 (July 2013), pp. 383–402.

[63] Rainer W Friedrich, Gilad A Jacobson, and Peixin Zhu. "Circuit Neuroscience in Zebrafish". In: *Curr. Biol.* 20.8 (Apr. 2010), R371–R381.

[64] I Fukui et al. "In vivo staining test with methylene blue for bladder cancer". en. In: *J. Urol.* 130.2 (Aug. 1983), pp. 252–255.

[65] Diana Fernanda Galvis-Carreño, Yuri Hercilia Mejıa-Melgarejo, and Henry Arguello-Fuentes. "Efficient reconstruction of Raman spectroscopy imaging based on compressive sensing". In: *Dyna* 81.188 (2014), pp. 116–124.

[66] P Beatriz Garcia-Allende et al. "Towards clinically translatable NIR fluorescence molecular guidance for colonoscopy". en. In: *Biomed. Opt. Express* 5.1 (Dec. 2013), pp. 78–92.

[67] Pilar Beatriz Garcia-Allende et al. "Uniqueness in multi-spectral constant-wave epi-illumination imaging". In: ().

[68] Nahum Gat. "Imaging spectroscopy using tunable filters: a review". In: *Wavelet Applications VII*. Vol. 4056. International Society for Optics and Photonics, Apr. 2000, pp. 50–65.

[69] Jürgen Glatz et al. "Concurrent video-rate color and near-infrared fluorescence laparoscopy". en. In: *J. Biomed. Opt.* 18.10 (Oct. 2013), p. 101302.

[70] Christine Grienberger and Arthur Konnerth. "Imaging calcium in neurons". en. In: *Neuron* 73.5 (Mar. 2012), pp. 862–885.

[71] Dhruv Grover, Takeo Katsuki, and Ralph J Greenspan. "Flyception: imaging brain activity in freely walking fruit flies". en. In: *Nat. Methods* 13.7 (July 2016), pp. 569–572.

[72] David F Gruber et al. "Biofluorescence in Catsharks (Scyliorhinidae): Fundamental Description and Relevance for Elasmobranch Visual Ecology". en. In: *Sci. Rep.* 6 (Apr. 2016), p. 24751.

[73] Costas G Hadjipanayis, Georg Widhalm, and Walter Stummer. "What is the Surgical Benefit of Utilizing 5-Aminolevulinic Acid for Fluorescence-Guided Surgery of Malignant Gliomas?" en. In: *Neurosurgery* 77.5 (Nov. 2015), pp. 663–673.

[74] A G Hadjivassiliou et al. "Fluorometric study of serum in patients with chronic renal failure". en. In: *Clin. Nephrol.* 22.1 (July 1984), pp. 39–43.

[75]   D Hanahan and R A Weinberg. "The hallmarks of cancer". en. In: *Cell* 100.1 (Jan. 2000), pp. 57–70.

[76]   Douglas Hanahan and Robert A Weinberg. "Hallmarks of cancer: the next generation". en. In: *Cell* 144.5 (Mar. 2011), pp. 646–674.

[77]   Fritjof Helmchen and Winfried Denk. "Deep tissue two-photon microscopy". en. In: *Nat. Methods* 2.12 (Dec. 2005), pp. 932–940.

[78]   David Grant Colburn Hildebrand et al. "Whole-brain serial-section electron microscopy in larval zebrafish". en. In: *Nature* 545.7654 (May 2017), pp. 345–349.

[79]   Chihiro Hiramatsu et al. "Experimental evidence that primate trichromacy is well suited for detecting primate social colour signals". en. In: *Proc. Biol. Sci.* 284.1856 (June 2017).

[80]   Guosong Hong et al. "Through-skull fluorescence imaging of the brain in a new near-infrared window". en. In: *Nat. Photonics* 8.9 (Sept. 2014), pp. 723–730.

[81]   Guosong Hong et al. "Ultrafast fluorescence imaging in vivo with conjugated polymer fluorophores in the second near-infrared window". en. In: *Nat. Commun.* 5 (June 2014), p. 4206.

[82]   Pepijn van Horssen et al. "Improved detection of fluorescently labeled microspheres and vessel architecture with an imaging cryomicrotome". en. In: *Med. Biol. Eng. Comput.* 48.8 (Aug. 2010), pp. 735–744.

[83]   Nicholas G Horton et al. "In vivo three-photon microscopy of subcortical structures within an intact mouse brain". en. In: *Nat. Photonics* 7.3 (Mar. 2013).

[84]   Bo Huang, Mark Bates, and Xiaowei Zhuang. "Super-resolution fluorescence microscopy". en. In: *Annu. Rev. Biochem.* 78.1 (2009), pp. 993–1016.

[85]   D E Hyde et al. "A diffusion theory model of spatially resolved fluorescence from depth-dependent fluorophore concentrations". en. In: *Phys. Med. Biol.* 46.2 (Feb. 2001), pp. 369–383.

[86]   Frederic E Ives. "Parallax stereogram and process of making same". 725567. Apr. 1903.

[87]   Rakesh K Jain, Lance L Munn, and Dai Fukumura. "Dissecting tumour pathophysiology using intravital microscopy". en. In: *Nat. Rev. Cancer* 2.4 (Apr. 2002), pp. 266–276.

[88]   R Jalan et al. "A pilot study of indocyanine green clearance as an early predictor of graft function". en. In: *Transplantation* 58.2 (July 1994), pp. 196–200.

[89]   Na Ji. "Adaptive optical fluorescence microscopy". en. In: *Nat. Methods* 14.4 (Mar. 2017), pp. 374–380.

[90]   Eric Jonas and Konrad Paul Kording. "Could a Neuroscientist Understand a Microprocessor?" en. In: *PLoS Comput. Biol.* 13.1 (Jan. 2017), e1005268.

[91]   James J Jun et al. "Fully integrated silicon probes for high-density recording of neural activity". en. In: *Nature* 551.7679 (Nov. 2017), pp. 232–236.

[92]   Allan V Kalueff et al. "Towards a comprehensive catalog of zebrafish behavior 1.0 and beyond". en. In: *Zebrafish* 10.1 (Mar. 2013), pp. 70–86.

[93]   Doycho Karagyozov et al. "Recording neural activity in unrestrained animals with 3D tracking two photon microscopy". en. Nov. 2017.

[94]   M A Kay, J C Glorioso, and L Naldini. "Viral vectors for gene therapy: the art of turning infectious agents into vehicles of therapeutics". en. In: *Nat. Med.* 7.1 (Jan. 2001), pp. 33–40.

[95]   Iva Kelava and Madeline A Lancaster. "Dishing out mini-brains: Current progress and future prospects in brain organoid research". en. In: *Dev. Biol.* 420.2 (Dec. 2016), pp. 199–209.

[96]   S Keren et al. "Noninvasive molecular imaging of small living subjects using Raman spectroscopy". en. In: *Proc. Natl. Acad. Sci. U. S. A.* 105.15 (Apr. 2008), pp. 5844–5849.

[97]   A Kienle et al. "Why do veins appear blue? A new look at an old question". en. In: *Appl. Opt.* 35.7 (Mar. 1996), p. 1151.

[98]   Dal Hyung Kim et al. "Pan-neuronal calcium imaging with cellular resolution in freely swimming zebrafish". en. In: *Nat. Methods* 14.11 (Nov. 2017), pp. 1107–1114.

[99]   Moritz F Kircher. "How can we apply the use of surface-enhanced Raman scattering nanoparticles in tumor imaging?" en. In: *Nanomedicine* 12.3 (Feb. 2017), pp. 171–174.

[100]   Thomas Knöpfel, Yasir Gallero-Salas, and Chenchen Song. "Genetically encoded voltage indicators for large scale cortical imaging come of age". en. In: *Curr. Opin. Chem. Biol.* 27 (Aug. 2015), pp. 75–83.

[101]   Hisataka Kobayashi and Peter L Choyke. "Target-cancer-cell-specific activatable fluorescence imaging probes: rational design and in vivo applications". en. In: *Acc. Chem. Res.* 44.2 (Feb. 2011), pp. 83–90.

[102]   Masaki Kobayashi, Daisuke Kikuchi, and Hitoshi Okamura. "Imaging of ultraweak spontaneous photon emission from human body displaying diurnal rhythm". en. In: *PLoS One* 4.7 (July 2009), e6256.

[103]   Maximilian Koch et al. "Threshold Analysis and Biodistribution of Fluorescently Labeled Bevacizumab in Human Breast Cancer". en. In: *Cancer Res.* 77.3 (Feb. 2017), pp. 623–631.

[104]   F Koenig et al. "Laser induced autofluorescence diagnosis of bladder cancer". en. In: *J. Urol.* 156.5 (Nov. 1996), pp. 1597–1601.

[105]   Nobuyuki Kosaka et al. "Near infrared fluorescence-guided real-time endoscopic detection of peritoneal ovarian cancer nodules using intravenously injected indocyanine green". en. In: *Int. J. Cancer* 129.7 (Oct. 2011), pp. 1671–1677.

[106]   Christoph Krafft et al. "Raman and coherent anti-Stokes Raman scattering microspectroscopy for biomedical applications". en. In: *J. Biomed. Opt.* 17.4 (Apr. 2012), p. 040801.

[107]   John W Krakauer et al. "Neuroscience Needs Behavior: Correcting a Reductionist Bias". en. In: *Neuron* 93.3 (Feb. 2017), pp. 480–490.

[108]   Hyun Kwon, R Huancaya, and Robert Polski. "Modeling light propagation in skin for visualization of subcutaneous veins". In: *Proceedings of COMSOL* (2013).

[109]   Andrew M Leifer et al. "Optogenetic manipulation of neural activity in freely moving Caenorhabditis elegans". en. In: *Nat. Methods* 8.2 (Feb. 2011), pp. 147–152.

[110]   M Levoy, Z Zhang, and I McDowall. "Recording and controlling the 4D light field in a microscope using microlens arrays". en. In: *J. Microsc.* 235.2 (Aug. 2009), pp. 144–162.

[111]   M R Lewis, H A Sloviter, and P P Goland. "In vivo staining and retardation of growth of sarcomata in mice". en. In: *Anat. Rec.* 95 (June 1946), pp. 89–96.

[112]   Bu-Hong Li and Shu-Sen Xie. "Autofluorescence excitation-emission matrices for diagnosis of colonic cancer". en. In: *World J. Gastroenterol.* 11.25 (July 2005), pp. 3931–3934.

[113] Xing Lin et al. "Dual-coded compressive hyperspectral imaging". en. In: *Opt. Lett.* 39.7 (Apr. 2014), pp. 2044–2047.

[114] Zhuang Liu et al. "Multiplexed multicolor Raman imaging of live cells with isotopically modified single walled carbon nanotubes". en. In: *J. Am. Chem. Soc.* 130.41 (Oct. 2008), pp. 13540–13541.

[115] Guolan Lu and Baowei Fei. "Medical hyperspectral imaging: a review". en. In: *J. Biomed. Opt.* 19.1 (Jan. 2014), p. 10901.

[116] Bin Ma et al. "Use of Autostitch for automatic stitching of microscope images". en. In: *Micron* 38.5 (2007), pp. 492–499.

[117] H Maeda. "The enhanced permeability and retention (EPR) effect in tumor vasculature: the key role of tumor-selective macromolecular drug targeting". en. In: *Adv. Enzyme Regul.* 41 (2001), pp. 189–207.

[118] Kshitij Marwah et al. "Compressive Light Field Photography Using Overcomplete Dictionaries and Optimized Projections". In: *ACM Trans. Graph.* 32.4 (July 2013), 46:1–46:12.

[119] Y Mendelson. "Pulse oximetry: theory and applications for noninvasive monitoring". en. In: *Clin. Chem.* 38.9 (Sept. 1992), pp. 1601–1607.

[120] Michaela Mickoleit et al. "High-resolution reconstruction of the beating zebrafish heart". en. In: *Nat. Methods* 11.9 (Sept. 2014), pp. 919–922.

[121] P Mohajerani et al. "Optical and Optoacoustic Model-Based Tomography: Theory and current challenges for deep tissue imaging of optical contrast". In: *IEEE Signal Process. Mag.* 32.1 (Jan. 2015), pp. 88–100.

[122] Timothy J Mohun and Wolfgang J Weninger. "Generation of volume data by episcopic three-dimensional imaging of embryos". en. In: *Cold Spring Harb. Protoc.* 2012.6 (June 2012), pp. 681–682.

[123] Mostafa A Nashaat et al. "Pixying Behavior: A Versatile Real-Time andPost HocAutomated Optical Tracking Method for Freely Moving and Head Fixed Animals". en. In: *eNeuro* 4.1 (Jan. 2017).

[124] J R Nayler. "Clinical photography: a guide for the clinician". en. In: *J. Postgrad. Med.* 49.3 (July 2003), pp. 256–262.

[125] Andre Nel, Erkki Ruoslahti, and Huan Meng. "New Insights into "Permeability" as in the Enhanced Permeability and Retention Effect of Cancer Nanotherapeutics". en. In: *ACS Nano* 11.10 (Oct. 2017), pp. 9567–9569.

[126] Ren Ng et al. "Light field photography with a hand-held plenoptic camera". In: *Computer Science Technical Report CSTR* 2.11 (2005), pp. 1–11.

[127] Jeffrey P Nguyen et al. "Whole-brain calcium imaging with cellular resolution in freely behaving Caenorhabditis elegans". en. In: *Proc. Natl. Acad. Sci. U. S. A.* 113.8 (Feb. 2016), E1074–81.

[128] N Nguyen, P Milanfar, and G Golub. "A computationally efficient superresolution image reconstruction algorithm". en. In: *IEEE Trans. Image Process.* 10.4 (2001), pp. 573–583.

[129] Vasilis Ntziachristos, Christoph Bremer, and Ralph Weissleder. "Fluorescence imaging with near-infrared light: new technological advances that enable in vivo molecular imaging". en. In: *Eur. Radiol.* 13.1 (Jan. 2003), pp. 195–208.

[130] Vasilis Ntziachristos et al. "Fluorescence molecular tomography resolves protease activity in vivo". en. In: *Nat. Med.* 8.7 (July 2002), pp. 757–760.

[131]   Vasilis Ntziachristos et al. "Looking and listening to light: the evolution of whole-body photonic imaging". en. In: *Nat. Biotechnol.* 23.3 (Mar. 2005), pp. 313–320.

[132]   A L Oldenburg et al. "Molecular OCT Contrast Enhancement and Imaging". In: *Optical Coherence Tomography: Technology and Applications*. Ed. by Wolfgang Drexler and James G Fujimoto. Berlin, Heidelberg: Springer Berlin Heidelberg, 2008, pp. 713–756.

[133]   Murad Omar et al. "Pushing the optical imaging limits of cancer with multi-frequency-band raster-scan optoacoustic mesoscopy (RSOM)". en. In: *Neoplasia* 17.2 (Feb. 2015), pp. 208–214.

[134]   Kasper Paasch. "The history of optics : From ancient times to the middle ages The history of optics : From ancient times to the middle ages ." In: July (2017).

[135]   Ina Pavlova et al. "Understanding the biological basis of autofluorescence imaging for oral cancer detection: high-resolution fluorescence microscopy in viable tissue". en. In: *Clin. Cancer Res.* 14.8 (Apr. 2008), pp. 2396–2404.

[136]   Nicolas C Pégard et al. "Compressive light-field microscopy for 3D neural activity recording". en. In: *Optica, OPTICA* 3.5 (May 2016), pp. 517–524.

[137]   Joseph Peller et al. "Hyperspectral imaging based on compressive sensing to determine cancer margins in human pancreatic tissue ex vivo". In: *Optical Biopsy XV: Toward Real-Time Spectroscopic Imaging and Diagnosis*. Vol. 10060. International Society for Optics and Photonics, Feb. 2017, 100600J.

[138]   Verónica Pérez-Schuster et al. "Sustained Rhythmic Brain Activity Underlies Visual Motion Perception in Zebrafish". en. In: *Cell Rep.* 17.4 (Oct. 2016), pp. 1098–1112.

[139]   Christian Perwaß and Lennart Wietzke. "Single lens 3D-camera with extended depth-of-field". In: *Human Vision and Electronic Imaging XVII*. Vol. 8291. International Society for Optics and Photonics, Feb. 2012, p. 829108.

[140]   Wibool Piyawattanametha et al. "Fast-scanning two-photon fluorescence imaging based on a microelectromechanical systems two- dimensional scanning mirror". en. In: *Opt. Lett.* 31.13 (July 2006), pp. 2018–2020.

[141]   Brian W Pogue and Michael S Patterson. "Review of tissue simulating phantoms for optical spectroscopy, imaging and dosimetry". en. In: *J. Biomed. Opt.* 11.4 (July 2006), p. 041102.

[142]   Ruben Portugues et al. "Whole-field visual motion drives swimming in larval zebrafish via a stochastic process". en. In: *J. Exp. Biol.* 218.Pt 9 (May 2015), pp. 1433–1443.

[143]   Kenneth D Poss, Mark T Keating, and Alex Nechiporuk. "Tales of regeneration in zebrafish". en. In: *Dev. Dyn.* 226.2 (Feb. 2003), pp. 202–210.

[144]   Andrew D Pris et al. "Towards high-speed imaging of infrared photons with bio-inspired nanoarchitectures". In: *Nat. Photonics* 6 (Feb. 2012), p. 195.

[145]   *Professional Guide to Assessment*. en. Lippincott Williams & Wilkins, 2006.

[146]   Timothy Ragan et al. "Serial two-photon tomography for automated ex vivo mouse brain imaging". en. In: *Nat. Methods* 9.3 (Jan. 2012), pp. 255–258.

[147]   Daniel Razansky et al. "Multispectral opto-acoustic tomography of deep-seated fluorescent proteins in vivo". In: *Nat. Photonics* 3 (June 2009), p. 412.

[148]   Jay Reichman. "Handbook of optical filters for fluorescence microscopy". In: *Chroma Technology Corporation* (2000).

[149]   Nunu Ren et al. "GPU-based Monte Carlo simulation for light propagation in complex heterogeneous tissues". en. In: *Opt. Express* 18.7 (Mar. 2010), pp. 6811–6823.

[150] Tyson R Roberts. "Danionella translucida, a new genus and species of cyprinid fish from Burma, one of the smallest living vertebrates". In: *Environ. Biol. Fishes* 16.4 (Aug. 1986), pp. 231–241.

[151] Debashish Roy et al. "3D cryo-imaging: a very high-resolution view of the whole mouse". en. In: *Anat. Rec.* 292.3 (Mar. 2009), pp. 342–351.

[152] Markus Rudin and Ralph Weissleder. "Molecular imaging in drug discovery and development". en. In: *Nat. Rev. Drug Discov.* 2.2 (Feb. 2003), pp. 123–131.

[153] Jun Sakakibara, Junichiro Kita, and Naoyuki Osato. "Note: High-speed optical tracking of a flying insect". en. In: *Rev. Sci. Instrum.* 83.3 (Mar. 2012), p. 036103.

[154] Anne Saulin, Markus Savli, and Rupert Lanzenberger. "Serotonin and molecular neuroimaging in humans using PET". en. In: *Amino Acids* 42.6 (June 2012), pp. 2039–2057.

[155] Massimo Scanziani and Michael Häusser. "Electrophysiology in the age of light". en. In: *Nature* 461.7266 (Oct. 2009), pp. 930–939.

[156] Nico Scherf and Jan Huisken. "The smart and gentle microscope". en. In: *Nat. Biotechnol.* 33.8 (Aug. 2015), pp. 815–818.

[157] Lothar Schermelleh, Rainer Heintzmann, and Heinrich Leonhardt. "A guide to super-resolution fluorescence microscopy". en. In: *J. Cell Biol.* 190.2 (July 2010), pp. 165–175.

[158] Paul J Scherz et al. "High-speed imaging of developing heart valves reveals interplay of morphogenesis and function". en. In: *Development* 135.6 (Mar. 2008), pp. 1179–1187.

[159] Werner Scheuer et al. "Drug-based optical agents: infiltrating clinics at lower risk". en. In: *Sci. Transl. Med.* 4.134 (May 2012), 134ps11.

[160] Jonathan Schiefer et al. "From Correlation to Causation: Estimation of Effective Connectivity from Continuous Brain Signals based on Zero-Lag Covariance". In: (Aug. 2017), pp. 1–18. arXiv: 1708.02423 [q-bio.NC].

[161] J M Schmitt. "Optical coherence tomography (OCT): a review". In: *IEEE J. Sel. Top. Quantum Electron.* 5.4 (July 1999), pp. 1205–1215.

[162] Dean A Scribner et al. "Bio-inspired optics". In: *Infrared Technology and Applications XXIX*. Vol. 5074. International Society for Optics and Photonics, Oct. 2003, pp. 312–318.

[163] Kaoru Seiriki et al. "High-Speed and Scalable Whole-Brain Imaging in Rodents and Primates". en. In: *Neuron* 94.6 (June 2017), 1085–1100.e6.

[164] Joeky T Senders et al. "Agents for fluorescence-guided glioma surgery: a systematic review of preclinical and clinical results". en. In: *Acta Neurochir.* 159.1 (Jan. 2017), pp. 151–167.

[165] Eva M Sevick-Muraca and John C Rasmussen. "Molecular imaging with optics: primer and case for near-infrared fluorescence techniques in personalized medicine". en. In: *J. Biomed. Opt.* 13.4 (July 2008), p. 041303.

[166] George Seward. "Optical design of microscopes". In: spie.org, 2010.

[167] Ludovico Silvestri et al. "Clearing of fixed tissue: a review from a microscopist's perspective". en. In: *J. Biomed. Opt.* 21.8 (Aug. 2016), p. 081205.

[168] Robert D Simoni et al. "A Classic Instrument: The Beckman DU Spectrophotometer and Its Inventor, Arnold O. Beckman". In: *J. Biol. Chem.* 278.49 (Dec. 2003), e1–e1.

[169] D Smetters, A Majewska, and R Yuste. "Detecting action potentials in neuronal populations with calcium imaging". en. In: *Methods* 18.2 (June 1999), pp. 215–221.

[170] Andrew M Smith, Michael C Mancini, and Shuming Nie. "Bioimaging: second window for in vivo imaging". en. In: *Nat. Nanotechnol.* 4.11 (Nov. 2009), pp. 710–711.

[171] David Stork, Aydogan Ozcan, and Patrick R Gill. "Imaging Without Lenses". In: *American Scientist* (Dec. 2017).

[172] John R Stowers et al. "Virtual reality for freely moving animals". en. In: *Nat. Methods* 14.10 (Oct. 2017), pp. 995–1002.

[173] Jochen Stritzker et al. "Vaccinia virus-mediated melanin production allows MR and optoacoustic deep tissue imaging and laser-induced thermotherapy of cancer". en. In: *Proc. Natl. Acad. Sci. U. S. A.* 110.9 (Feb. 2013), pp. 3316–3320.

[174] Arminda Suli et al. "Rheotaxis in larval zebrafish is mediated by lateral line mechanosensory hair cells". en. In: *PLoS One* 7.2 (Feb. 2012), e29727.

[175] Panagiotis Symvoulidis et al. "Steady-state total diffuse reflectance with an exponential decaying source". en. In: *Opt. Lett.* 39.13 (July 2014), pp. 3919–3922.

[176] P Symvoulidis et al. "Serial sectioning and multispectral imaging system for versatile biomedical applications". In: *2014 IEEE 11th International Symposium on Biomedical Imaging (ISBI)*. Apr. 2014, pp. 890–893.

[177] A Tapfer et al. "Three-dimensional imaging of whole mouse models: comparing nondestructive X-ray phase-contrast micro-CT with cryotome-based planar epi-illumination imaging". en. In: *J. Microsc.* 253.1 (Jan. 2014), pp. 24–30.

[178] Adrian Taruttis and Vasilis Ntziachristos. "Advances in real-time multispectral optoacoustic imaging and its applications". In: *Nat. Photonics* 9 (Mar. 2015), p. 219.

[179] George Themelis, Jung Sun Yoo, and Vasilis Ntziachristos. "Multispectral imaging using multiple-bandpass filters". en. In: *Opt. Lett.* 33.9 (May 2008), pp. 1023–1025.

[180] Alan B Thompson and Eva M Sevick-Muraca. "Near-infrared fluorescence contrast-enhanced imaging with intensified charge-coupled device homodyne detection: measurement precision and accuracy". en. In: *J. Biomed. Opt.* 8.1 (Jan. 2003), pp. 111–120.

[181] Lin Tian et al. "Imaging neural activity in worms, flies and mice with improved GCaMP calcium indicators". In: *Nat. Methods* 6 (Nov. 2009), p. 875.

[182] Vassiliy Tsytsarev et al. "Imaging cortical electrical stimulation in vivo: fast intrinsic optical signal versus voltage-sensitive dyes". en. In: *Opt. Lett.* 33.9 (May 2008), pp. 1032–1034.

[183] Quirijn R J G Tummers et al. "The Value of Intraoperative Near-Infrared Fluorescence Imaging Based on Enhanced Permeability and Retention of Indocyanine Green: Feasibility and False-Positives in Ovarian Cancer". en. In: *PLoS One* 10.6 (June 2015), e0129766.

[184] Stratis Tzoumas and Vasilis Ntziachristos. "Spectral unmixing techniques for optoacoustic imaging of tissue pathophysiology". en. In: *Philos. Trans. A Math. Phys. Eng. Sci.* 375.2107 (Nov. 2017).

[185] Stratis Tzoumas et al. "Eigenspectra optoacoustic tomography achieves quantitative blood oxygenation imaging deep in tissues". en. In: *Nat. Commun.* 7 (June 2016), p. 12121.

[186] Yasuteru Urano et al. "Selective molecular imaging of viable cancer cells with pH-activatable fluorescence probes". en. In: *Nat. Med.* 15.1 (Jan. 2009), pp. 104–109.

[187] Vaibhav Vaish et al. "Using plane+ parallax for calibrating dense camera arrays". In: *Computer Vision and Pattern Recognition, 2004. CVPR 2004. Proceedings of the 2004 IEEE Computer Society Conference on*. Vol. 1. ieeexplore.ieee.org, 2004, pp. I–I.

[188] Martijn P Van Den Heuvel and Hilleke E Hulshoff Pol. "Exploring the brain network: a review on resting-state fMRI functional connectivity". In: *Eur. Neuropsychopharmacol.* 20.8 (2010), pp. 519–534.

[189] Spencer R Van Leeuwen and Gladimir V G Baranoski. "Identifying the optical phenomena responsible for the blue appearance of veins". In: *Light in Nature VI.* Vol. 10367. International Society for Optics and Photonics, Sept. 2017, 103670F.

[190] Ivo M Vellekoop. "Feedback-based wavefront shaping". en. In: *Opt. Express* 23.9 (May 2015), pp. 12189–12206.

[191] Vivek Venkatachalam et al. "Pan-neuronal imaging in roaming Caenorhabditis elegans". en. In: *Proc. Natl. Acad. Sci. U. S. A.* 113.8 (Feb. 2016), E1082–8.

[192] Laura Vinckenbosch et al. "Monte Carlo methods for light propagation in biological tissues". en. In: *Math. Biosci.* 269 (Nov. 2015), pp. 48–60.

[193] Nikita Vladimirov et al. "Light-sheet functional imaging in fictively behaving zebrafish". en. In: *Nat. Methods* 11.9 (Sept. 2014), pp. 883–884.

[194] Lihong V Wang. "Multiscale photoacoustic microscopy and computed tomography". en. In: *Nat. Photonics* 3.9 (Aug. 2009), pp. 503–509.

[195] Lihong Wang, Steven L Jacques, and Liqiong Zheng. "MCML—Monte Carlo modeling of light transport in multi-layered tissues". In: *Comput. Methods Programs Biomed.* 47.2 (1995), pp. 131–146.

[196] Judith Weber, Paul C Beard, and Sarah E Bohndiek. "Contrast agents for molecular photoacoustic imaging". en. In: *Nat. Methods* 13.8 (July 2016), pp. 639–650.

[197] R Weissleder. "A clearer vision for in vivo imaging". en. In: *Nat. Biotechnol.* 19.4 (Apr. 2001), pp. 316–317.

[198] R Weissleder and U Mahmood. "Molecular imaging". en. In: *Radiology* 219.2 (May 2001), pp. 316–333.

[199] J Welzel. "Optical coherence tomography in dermatology: a review". en. In: *Skin Res. Technol.* 7.1 (Feb. 2001), pp. 1–9.

[200] John D Whited and James M Grichnik. "Does This Patient Have a Mole or a Melanoma?" In: *JAMA* 279.9 (Mar. 1998), pp. 696–701.

[201] E A Widder. "Bioluminescence in the ocean: origins of biological, chemical, and ecological diversity". en. In: *Science* 328.5979 (May 2010), pp. 704–708.

[202] K C Wikler, R W Williams, and P Rakic. "Photoreceptor mosaic: number and distribution of rods and cones in the rhesus monkey retina". en. In: *J. Comp. Neurol.* 297.4 (July 1990), pp. 499–508.

[203] Terence T W Wong et al. "Label-free automated three-dimensional imaging of whole organs by microtomy-assisted photoacoustic microscopy". en. In: *Nat. Commun.* 8.1 (Nov. 2017), p. 1386.

[204] Zhiwei Xiong et al. "Snapshot hyperspectral light field imaging". In: *The IEEE Conference on Computer Vision and Pattern Recognition (CVPR).* Vol. 2. openaccess.thecvf.com, 2017.

[205] Emre Yaksi and Rainer W Friedrich. "Reconstruction of firing rate changes across neuronal populations by temporally deconvolved Ca2+ imaging". en. In: *Nat. Methods* 3.5 (May 2006), pp. 377–383.

[206] Zhe Yang et al. "Dual-slit confocal light sheet microscopy for in vivo whole-brain imaging of zebrafish". en. In: *Biomed. Opt. Express* 6.5 (May 2015), pp. 1797–1811.

4 References

[207]   H Zeng et al. "Spectroscopic and microscopic characteristics of human skin autofluo-
         rescence emission". en. In: *Photochem. Photobiol.* 61.6 (June 1995), pp. 639–645.

[208]   Cha Zhang and Tsuhan Chen. "Light field capturing with lensless cameras". In: *IEEE
         International Conference on Image Processing 2005*. Vol. 3. ieeexplore.ieee.org, 2005,
         pp. III–792–5.

[209]   Irina V Zhdanova. "Sleep and its regulation in zebrafish". en. In: *Rev. Neurosci.* 22.1
         (2011), pp. 27–36.

[210]   Warren R Zipfel, Rebecca M Williams, and Watt W Webb. "Nonlinear magic: mul-
         tiphoton microscopy in the biosciences". en. In: *Nat. Biotechnol.* 21.11 (Nov. 2003),
         pp. 1369–1377.

5 Resulting Publications as first author

The remaining of the Thesis consists of the write-ups of some parts of the projects as publications to peer-reviewed journals and conferences. To begin with, a brief summary of the work is given highlighting my individual contributions as a Doctoral Candidate at the Faculty of Electrical and Computer Engineering.

5.1 Steady-state total diffuse reflectance with an exponential decaying source

Despite the wide use of back-scattered reflection imaging of biological tissue, a theoretical formulation of the captured intensities is only minimally studied and validated. Collaborating with Prof. Ripoll we proposed and validated a formula for plane wave illumination (found in the majority of clinical applications) with an exponentially decay source.

As a first author of this publication I:

a) Implemented (with the help of Dr. Radrich) the multispectral imaging system consisting of a macroscopic zooming system and a 25-position filter-wheel and characterized it using reflection standard (McBeth Color Chart and Spectralon targets).

b) Programmed a front end for the automation of the acquisitions,including definition of imaging protocols (e.g definition of excitation and emission filters per image) and auto-calibration routines to ensure proper use of cameras dynamic range per photo.

c) Designed and performed together with Karin Jentoft (equal contribution in the publication) multiple sets of replications of the validation phantoms. Literature review lead allowed us to define a physiological range for optical properties and the needed amount of blood and intralipid in liquid phantoms to approximate human tissue.

d) Evaluated the result of the phantoms experiments with the implementation of the formula(driven by Karin Jentoft) and Monte Carlo Simulation (performed by Dr. Allende).

e) After literature review, proposed and tested the hypothesis that the pigment packaging effect was a source of possible (small) mismatch between the observed spectra and the theoretically predicted ones.

Having established the validity of this formula our research continued. Dr. Allende showcased in [167] that the formula can not be solved for absorption and scattering parameters, but there is unique solution for terms including their ratio that might have clinical values. Those experiments were also repeated with fluorochromes in the phantoms and helped us established that reflection measurements are insufficient to accurately correct fluorescence attenuation, since -as also the formula predicts- proportional increase of both absorption and scattering results in identical reflection information but different fluorescence counts. Finally the multispectral acquisition system was used in studies of oxygenation and cryo-slicing by Dr. Radrich.

Steady-state total diffuse reflectance with an exponential decaying source

Panagiotis Symvoulidis,[1,†] Karin M. Jentoft,[1,†] P. Beatriz Garcia-Allende,[1] Jürgen Glatz,[1]
Jorge Ripoll,[2] and Vasilis Ntziachristos[1,*]

[1]*Institute for Biological and Medical Imaging, Helmholtz Zentrum München and
Technische Universität München, 85764 Neuherberg, Germany*

[2]*Department of Bioengineering and Aerospace Engineering, Universidad Carlos III of Madrid, 28911 Madrid, Spain*
Corresponding author: symvoulidis@helmholtz-muenchen.de

The increasing preclinical and clinical utilization of digital cameras for photographic measurements of tissue conditions motivates the study of reflectance measurements obtained with planar illumination. We examine herein a formula that models the total diffuse reflectance measured from a semi-infinite medium using an exponentially decaying source, assuming continuous plane wave epi-illumination. The model is validated with experimental reflectance measurements from tissue mimicking phantoms. The need for adjusting the blood absorption spectrum due to pigment packaging is discussed along with the potential applications of the proposed formulation.   © 2014 Optical Society of America

OCIS codes: (170.3660) Light propagation in tissues; (110.4234) Multispectral and hyperspectral imaging; (170.6935) Tissue characterization.

http://dx.doi.org/10.1364/OL.39.003919

Optical endoscopy is a critical bio-optical method for the diagnosis and management of gastrointestinal conditions and the surgical treatment of various diseases including cancer. Recent interest in fluorescence molecular imaging (FMI) for detection in endoscopic [1] and surgical applications [1,2] further leads to an increasing use of epi-illumination optical imaging in clinical applications.

The optical contrast generated in color endoscopy is due to anatomical features and due to the variation of tissue optical properties. Conversely, in FMI, contrast is generated via the preferential accumulation of an extrinsically administered fluorescent agent to the site of disease. In this case, the fluorescence signals collected depend on the agent concentration in the diseased tissue, the depth of the diseased tissue from the imaged surface, and the tissue optical properties. The collection of color images to capture optical property variation and compensate for their influence on the fluorescence signal has been considered as a method to improve FMI accuracy [3–5]. Both in color endoscopy and in FMI, images are acquired using high-resolution digital cameras [6]. These cameras operate in planar mode, i.e., collecting images emitted back from tissue after tissue illumination with a planar light field.

Herein we sought an analytical formulation that models the dependence of epi-illumination measurements on the underlying tissue optical properties. Such a model is useful to better understand the collected images and provide a forward model for simulation purposes.

Different methods have been already proposed for describing the light collected from tissue in epi-illumination mode, including Monte Carlo simulations or analytical solutions. Monte Carlo approaches are versatile but tend to be computationally expensive and impractical for time-efficient calculations. Alternatively, a set of analytical solutions were proposed by Farrell *et al.* [7], but only for wave and point source illumination, which accounted for an exponentially decaying source (a contribution that

in radiative transport theory is termed the reduced intensity, equivalent to Beer's-law [8]). Those formulas has been extensively used in most spatially resolved reflectance measurements (either with a single fiber probe [9], a pair of source-detector probes [10] for single spectrum measurement, or with more pairs [11], or CCD camera pixels as detectors [12] in "imaging" applications) for the determination of optical properties or for elucidating responses from structured illumination patterns [13]. Due to the fact that, to the best of our knowledge, most fluorescence or reflectance measurements have been performed with the use of point sources, the plane wave solution of Farrell has thus received very little attention.

In this work, we employed an alternative expression of Farrell's plane wave formula that introduces plane wave illumination with an exponentially decaying source in order to account for homogeneous or planar illumination scenarios. Derived in the spatial frequency domain, this formulation includes the contribution of the reduced intensity to the diffuse intensity [8], and the absorption dependence on the diffusion coefficient [14]. This new formulation allows the inclusion of arbitrary source profiles without the need to resort to the extrapolated boundary condition, thus maintaining the exponentially decaying contribution [15]. In this way, the proposed expression is more versatile and can be used for application with arbitrary illumination distributions, once its validity is proven against Monte Carlo simulations and Farrell's derivation for the source profiles considered by the latter. Importantly we opted to validate its performance in the visible and to examine whether it could be employed for measurements in color endoscopy, i.e., using cameras in the visible light spectrum. This theoretical study was followed by experimental measurements from phantoms. In order to account for the reduced intensity contribution, we introduce an exponentially decaying source. Assuming illumination with a plane wave, the flux J_{det} that traverses outward from diffusive medium into a nonscattering medium is defined by the boundary condition at

the interface $z = 0$ as (see [16] for a detailed derivation)

$$J_{\text{det}}(z = 0) = \frac{U(z = 0)}{\alpha}, \qquad (1)$$

with α representing the boundary coefficient, which accounts for the difference in refractive indices (note that $\alpha = 2$ in the index-matched case), and U represents the average intensity (in Watts/cm^2) at the interface and accounts for the diffusive contribution. If we now take into account an exponentially decaying intensity due to the reduced intensity contribution inside the diffusive medium and consider the effect of the boundary condition shown above, we may obtain, after a straightforward but lengthy derivation (see [15], Chap. 7 and 8), an expression for the average intensity as

$$U(z = 0) = \frac{\text{NA}^2 S_0 \mu_s'}{2\sqrt{D\mu_a}} \frac{1}{\mu_s' + \mu_a + \sqrt{\mu_a/D}} \frac{2\alpha D}{\sqrt{D/\mu_a} + \alpha D}, \qquad (2)$$

where NA is the numerical aperture of the lens, S_0 is the power per area that reaches the diffusive medium (in Watts/cm^2), μ_a and μ_s' are the absorption and reduced scattering coefficients, respectively, and D is the diffusion coefficient, which we will define as

$$D = \frac{1}{3(\mu_s' + a\mu_a)}, \qquad (3)$$

with a representing a coefficient, which accounts for the absorption dependence of the diffusion coefficient following [17]. Typical values of a range from 0.2 to 0.5. Since S_0 represents the power that reaches the diffusive medium, we may account for the power lost to specular reflection and express S_0 in terms of the total power per area incident on the interface as

$$S_0 = (1 - R_{\text{air} \to n0}) S^{(\text{inc})}, \qquad (4)$$

where $R_{\text{air} \to n0} = (n_{\text{air}} - n0/n_{\text{air}} + n0)^2$ is the reflectance going from air into the diffusive medium of index of refraction n_0, and $S^{(\text{inc})}$ is the total power per area incident on the interface. Regrouping terms and introducing these relations, we may rewrite the expression for the detected flux as

$$J_{\text{det}}(z = 0) = \frac{(1 - R_{\text{air} \to n0}) S^{(\text{inc})} \mu_s' \sqrt{D\mu_a}}{\left((\mu_s' + \mu_a)\sqrt{D\mu_a} + \mu_a\right)\left(1 + \alpha\sqrt{D\mu_a}\right)}. \qquad (5)$$

Note that this expression assumes a numerical aperture of our detector of NA $= 1$. As expected, if the semi infinite diffusive medium is nonabsorbing (i.e., $\mu_a = 0$) the total flux reflected would be $J_{\text{det}}(z = 0) = (1 - R_{\text{air} \to n0}) S^{(\text{inc})}$.

We compared Eq. (5) and the Farrell formulation in [7] to a Monte Carlo simulation using the algorithm in [18,19]. In simulations, we assumed a model for steady-state light transport in multilayer tissue [20]. The comparisons assumed typical optical properties for tissue in the visible as previously described [21]. In
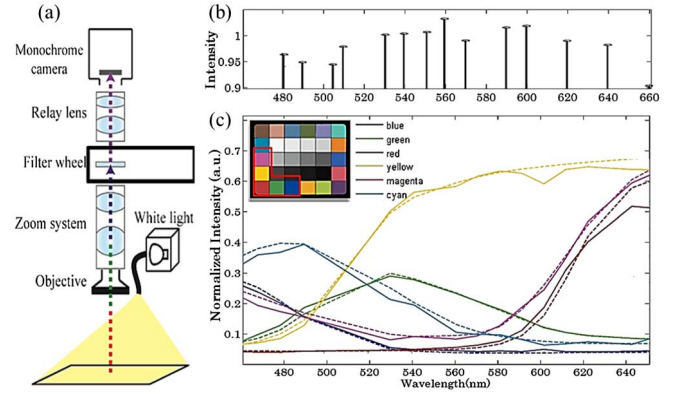

Fig. 1. (a) System schematic. (b) System response (mean measurement from diffuse standard before correction). (c) comparison of measured reflection intensity (solid lines) and documented spectra (dashed lines) of a Macbeth chart.

particular, the simulation was computed for absorption coefficient μ_a values in the range of 0.1–10 cm^{-1} and reduced scattering coefficient μ_s' values in the range of 4–16 cm^{-1}. We assumed that the spectral dependence of μ_a resembled that of blood for different levels of oxygenation varying from 0 to 100%. The spectral dependence of μ_s assumed Mie scattering, i.e., $\mu_s = a * \lambda^{-b}$, with $b \sim 2.3$. A value of $n_{\text{tissue}} = 1.33$ was used as the refractive index of tissue and g values corresponding to Intralipid 10%, according to Flock et al. were utilized [22]. The comparison revealed similar performance for the two analytical equations, resulting in a maximum root-mean-square (RMS) error of 0.69% across the entire visible wavelength range. The RMS error between the epi-illumination predictions offered between Eq. (5) and the Monte Carlo calculation was somewhat larger, resulting in ~2.76%, which nevertheless demonstrated good agreement.

Due to the agreement observed between analytical and numerical computation, we focused primarily on investigating the agreement between Eq. (5) and experimental measurements. Multispectral reflectance images of aqueous phantoms were acquired with the system shown in Fig. 1(a). The multispectral imaging system mainly consists of a monochromatic camera Luca R (Andor Technology plc, Belfast, UK) employing a 25-position filter-wheel manufactured by Cairn-Research (Kent, UK) and a custom-made casing. 10 nm narrowband filters from Chroma Technology Co. (Bellows Falls, USA) were employed for each waveband of interest [as shown in Fig. 1(b)]. Optical detection was through a Z16 APO A lens (Leica Microsystems GmbH, Wetzlar, Germany) with 1× objective, while white light illumination was provided by a halogen lamp (KL2500, Schott AG, Mainz, Germany). Image acquisition was automated with a custom-developed Labview program (National Instruments, USA), while MATLAB (Ver 2013a Mathworks, USA) was used for data preview and postprocessing.

System calibration was performed in order to compensate for wavelength-dependencies of the camera system. First, dark images were acquired with exposure times that were identical to the epi-illumination images collected. The dark images were subtracted from all the epi-illumination images collected to eliminate DC

offsets. Every epi-illumination image collected through one of the bandpass filters was divided by a corresponding epi-illumination image [mean values shown in Fig. 1(b)] obtained with the same filter, exposure time, and aperture from a diffuse reflectance standard (Ocean Optics, USA), under identical illumination conditions. This division was applied to compensate for filter and illumination specific gains and losses. Figure 1(c) shows the results of the spectral calibration.

The aqueous tissue mimicking phantoms measured consisted of rabbit blood (with the addition of anticlotting agent) with concentrations in the 0.5%–1.94% range using a 0.18% titration step and Intralipid (Sigma-Aldrich, USA) with concentrations in the 0%–5.8% range with a 0.6% titration step. The blood/intralipid solutions were placed in cylinders of ~2 cm radius and ~2.5 cm depth. Since the solution was exposed to air and was well mixed to be as homogeneous as possible before imaging, the hemoglobin is assumed to be fully oxygenated. To compare the experimental results with the output of the proposed formulation [Eq. (5)], we used the absorption spectrum of blood from Oregon Medical Laser Center database (http://omlc.ogi.edu/spectra/) and Intralipid's reduced scattering coefficient as documented in [22].

Figure 2 plots predictions of Eq. (5) against the experimental results collected. It is observed that Eq. (5) accurately predicts the experimental measurements with a mean error of 4.5%, smaller than 10% for all the optical property combinations and across all wavelengths (Fig. 2).

Although the mismatch observed between experimental measurements and theoretical predictions was small, a noticeable correlation with the spectral dependence of hemoglobin extinction coefficients was observed [as seen in Fig. 2(c)]. Accordingly, we investigated the possible sources of error, including a pipetting error and variance

of expected hemoglobin concentration in the blood. A reasonable explanation that matched our experimental result is in the discussion by Finley [23], regarding the alteration of reflectance spectra of samples containing red blood cells due to pigment packaging effects. Figure 3 compares the blood absorption spectrum as extracted by the fitting of our experimental data with the value given from the formula presented in [22] using the values reported by the authors. This led to significant improvement in matching between experimental measurements and theoretical predictions. Figure 3(b) shows the spectra obtained after incorporating this blood absorption spectrum correction factor (fixed for all the blood concentrations we used) in the formula. Correspondingly, an evenly distributed mean error of 3.9% (12% decrease of error compared with the 4.5% of the uncorrected data) across the whole physiological range of optical properties in the visible wavelengths was found (Fig. 3).

The corrected Eq. (5) demonstrates good agreement with experimental results, pointing to an accurate analytical approach for modeling color CCD camera measurements obtained in epi-illumination mode. The results further imply that despite the diffusion equation approximations, which are better matched in the NIR, the use of Eq. (5) can be efficiently applied in the visible.

Overall, Eq. (5) is a new theoretical formulation of diffuse reflectance, which, in contrast to solutions derived in the past, incorporates arbitrary exponentially decaying sources and describes noncontact planar wave imaging, as performed by clinical cameras. We investigated the

Fig. 2. (a), (b) Comparison of experimental measurements (stars) with theoretical spectral predictions (lines with circles for different blood (a) and Intralipid (b) concentrations. (c) Box plot of the mean error per wavelength for all concentrations (red points: outliers, whiskers: minimum/maximum excluding outliers, box: 25% quartiles; red line: mean value). (d) Mean error per concentration across wavelength (color change from blue to red corresponds to increasing blood concentration).
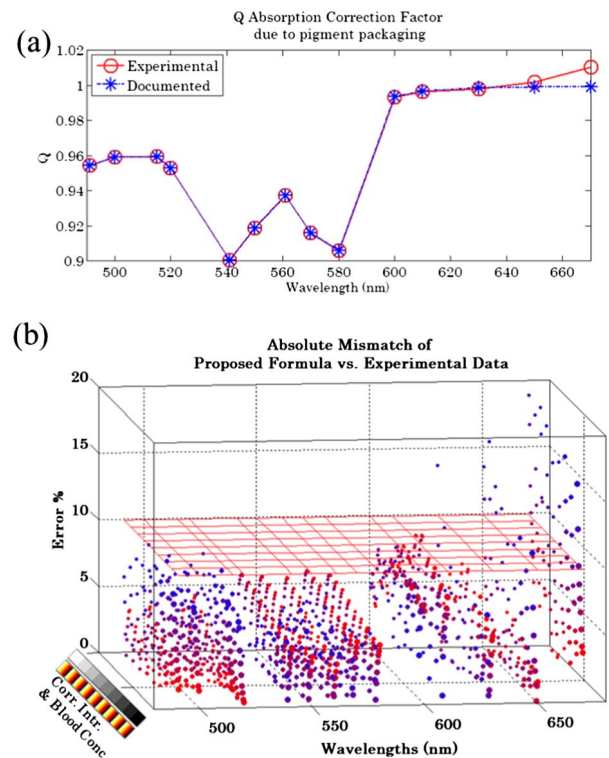

Fig. 3. (a) Comparison of documented and experimentally measured effect of pigment packaging. (b) Absolute error % for all measurements. Marker size: Intralipid conc., marker color (from blue to red): Increasing blood conc. The red horizontal plane thresholds the 10% error.

validity of this formula in modeling responses in the visible range and found it appropriate for predicting epi-illumination measurements for varying optical properties, especially when a correction factor that accounts for pigment packaging effects is incorporated. We further compared Eq. (5) with the existing models and document minor mismatches. Equation (5) therefore provides straightforward implementation for modeling plane wave measurements in the visible range in a quantitative manner and can be used to better interpret measurements obtained by clinical systems in the visible as well.

†These authors contributed equally to the work

References

1. P.-L. Hsiung, J. Hardy, S. Friedland, R. Soetikno, C. B. Du, A. P. Wu, P. Sahbaie, J. M. Crawford, A. W. Lowe, and C. H. Contag, Nat. Med. **14**, 454 (2008).
2. G. M. van Dam, G. Themelis, L. M. Crane, N. J. Harlaar, R. G. Pleijhuis, W. Kelder, A. Sarantopoulos, J. S. de Jong, H. J. Arts, and A. G. van der Zee, Nat. Med. **17**, 1315 (2011).
3. W. Scheuer, G. M. van Dam, M. Dobosz, M. Schwaiger, and V. Ntziachristos, Sci. Transl. Med. **4**, 134ps111 (2012).
4. V. Ntziachristos, G. Turner, J. Dunham, S. Windsor, A. Soubret, J. Ripoll, and H. A. Shih, J. Biomed. Opt. **10**, 064007 (2005).
5. R. S. Bradley and M. S. Thorniley, J. R. Soc. Interface **3**, 1 (2006).
6. P. A. Valdés, F. Leblond, A. Kim, B. T. Harris, B. C. Wilson, X. Fan, T. D. Tosteson, A. Hartov, S. Ji, and K. Erkmen, J. Neurosurg. **115**, 11 (2011).
7. G. Themelis, J. S. Yoo, K.-S. Soh, R. Schulz, and V. Ntziachristos, J. Biomed. Opt. **14**, 064012 (2009).
8. T. J. Farrell, M. S. Patterson, and B. Wilson, Med. Phys. **19**, 879 (1992).
9. A. Ishimaru, *Wave Propagation and Scattering in Random Media* (Academic, 1978).
10. G. Zonios, J. Bykowski, and N. Kollias, J. Invest. Derm. **117**, 1452 (2001).
11. F. Bevilacqua, A. J. Berger, A. E. Cerussi, D. Jakubowski, and B. J. Tromberg, Appl. Opt. **39**, 6498 (2000).
12. R. X. Xu, B. Qiang, J. J. Mao, and S. P. Povoski, Appl. Opt. **46**, 7442 (2007).
13. F. Fabbri, M. A. Franceschini, and S. Fantini, Appl. Opt. **42**, 3063 (2003).
14. D. J. Cuccia, F. Bevilacqua, A. J. Durkin, F. R. Ayers, and B. J. Tromberg, J. Biomed. Opt. **14**, 024012 (2009).
15. J. Ripoll, D. Yessayan, G. Zacharakis, and V. Ntziachristos, J. Opt. Soc. Am. A **22**, 546 (2005).
16. J. Ripoll, *Principles of Diffuse Light Propagation: Light Propagation in Tissues with Applications in Biology and Medicine* (World Scientific, 2012).
17. R. Aronson, J. Opt. Soc. Am. A **12**, 2532 (1995).
18. R. Aronson and N. Corngold, J. Opt. Soc. Am. A **16**, 1066 (1999).
19. L. Wang, S. L. Jacques, and L. Zheng, Comput. Methods Programs Biomed. **47**, 131 (1995).
20. L. Wang, S. L. Jacques, and L. Zheng, Comput. Methods Programs Biomed. **54**, 141 (1997).
21. E. Alerstam, T. Svensson, and S. Andersson-Engels, J. Biomed. Opt. **13**, 060504 (2008).
22. S. T. Flock, S. L. Jacques, B. C. Wilson, W. M. Star, and M. J. van Gemert, Lasers Surg. Med. **12**, 510 (1992).
23. J. C. Finlay and T. H. Foster, Opt. Lett. **29**, 965 (2004).

5.2 Serial sectioning and multispectral imaging system for versatile biomedical applications

While a prototype cryo-slicing imaging system existed in our lab and publication proved its usability, three main issues existed. The image acquisition software was hard-coded and modifications of the actual Labview code were required to change imaging protocols or even parameters inside the same protocol. Secondly, while the imaging equipment could be theoretically used outside the cryotome as a planar epi-fluorescence imaging system, neither the mechanical support nor the software were optimized for that. Finally, a user had to be present during the slicing to manually rotate a handwheel. While working on to address the first two issues on our existing cryotome, we managed to get access to another cryotome machine that allows cutting with the press of a button. After some modifications and using the updated software of the manual one, we created the fully automated version that was presented in this publication.

Specifically my contributions on the development of the fully automated cryo-slicer included:

a) The development of the fully automated acquisition pipeline based on Labview. It is similar to the one used for the publication presented in 2.1. With some additional features to match the volumetric character of the machine, like enumerating slice and ability to add comments per slice from the front end.

b) Establishing a reconstruction, analysis, and visualization pipeline based on Matlab (stack loading, normalization of exposure time etc) and Amira (Volumetric Renderings, ROIs analysis).

c) Designing mechanical support for both systems to enable the use of imaging equipment outside the cryo-chamber and acquiring (together with Carlos Cruz) showcase dataset presenting in this work.

d) Supervised our master's student Carlos Cruz Perez on modifying the electronics of the new cryotome machine to allow fully automated function using an arduino and relays. The help of Maximilian Koch must be acknowledged.

e) Designed the imaging system of the new cryotome based on a zooming lens (rather than photographic lens that the other system uses) and additional stages allowing higher throughput.

Both the fully automated machine (being continuously improved by Dr. Gorpas) and the manual slicing ones are still an integral part of our lab works. The manually automated one has reached a point of user-friendliness that allows for it to be run from our technical assistants or even external collaborators with just a short introduction, while the automated one can run in fully unattended mode. Thus both systems have been used in numerous studies both studying the biodistribution of probes and as validation tools for other imaging modalities. In one of them, together with Max Koch, we used the manual one that offers the user the possibility to keep thin slices as the base of validation pipeline including in-vivo imaging, cryoslicing, imaging of thin slices before and after staining, that was important both to confirm the findings of a clinical study and to acquire intuition about the effects of optical properties of fluorescence in an intraoperative framework. Maria Anastopoulou is currently working on the development of systems and methods to translate this intuition in an actual practical solution of the image reversion problem.

SERIAL SECTIONING AND MULTISPECTRAL IMAGING SYSTEM FOR VERSATILE BIOMEDICAL APPLICATIONS

Symvoulidis, P. [1,3], Cruz Pérez, C.[1], Schwaiger, M[2], Ntziachristos, V[1,3], Westmeyer, G.G. [1,2]

[1]Institute of Biological and Medical Imaging, Helmholtz Zentrum München
[2]Department of Nuclear Medicine & [3]Chair of Biological Imaging, Technische Universität München

ABSTRACT

Serial sectioning combined with microscopy provides high resolution volumetric data to complement *in-vivo* imaging modalities and aid *ex-vivo* diagnostics. We describe the design of a fully-automated cryomicrotome combined with a multispectral reflection and fluorescence imaging system that enables high-throughput analyses of biological specimens with a large field of view and cellular resolution while keeping the manufacturing and running costs low. We show the performance of the system for representative applications in high-resolution volumetric imaging of reporter animals and multispectral tissue analysis. Furthermore, we demonstrate the versatility of the economical imaging system in applications such as *in vivo* epifluorescence imaging, histology slide scanning, cell counting and gel electrophoresis documentation.

Index Terms— cryo-microtome serial tissue sectioning, epifluorescence imaging, cryoslicer imaging, multispectral imaging, 3D visualization

1. INTRODUCTION

Despite substantial advances in non-invasive optical imaging hardware (*e.g.* FMT-XCT [1], bioluminescence or optoacoustic systems [2]]) and contrast agents (*e.g.* near and far infrared fluorescence dyes and proteins [3]), complex light-tissue interactions pose a physical limitation to the penetration depth and resolution of intra-vital imaging that prevents cellular resolution in deeper layers of opaque biomedical specimens.

On the other hand, sequential sectioning combined with microscopy, a method that can provide 3D reconstructions of biomedical specimens at cellular resolution, is often prohibitively time-consuming and inaccurate in providing volumetric data. This is mainly because each tissue slice has to be manually transferred and prepared for planar imaging (*e.g.* by coverslipping) resulting in complex mechanical distortions.

It is only recently that a few commercial systems have become available that combine an automated serial sectioning device (vibratome [4], microtome [5] or cryotome [6]) with an optical imaging system (2-photon, reflection or epifluorescence microscopy respectively) to obtain volumetric data of biological samples. These integrated systems, however, are naturally limited in their flexibility and may not be affordable by the majority of biomedical laboratories that could greatly benefit from such a device.

In this work we present a custom-built, automated cryosectioning and imaging system engineered to be modular
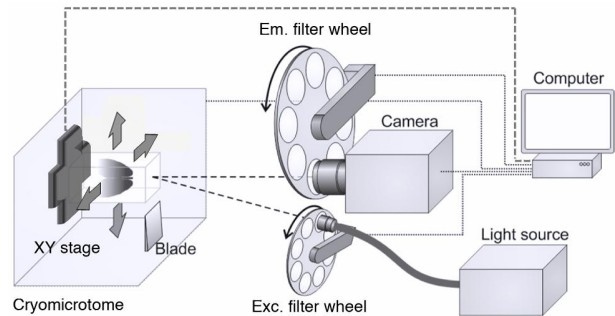

Figure 1. Schematic of the fully automated cryosectioning and imaging system. Serial sections are cut off from a frozen biological specimen mounted on an XY-motorized stage system. RGB images and fluorescent images are acquired from the planar surface of the tissue block by choosing appropriate optical filters on a motorized filter wheel. High resolution images can be obtained by sequential acquisition of multiple fields of view (FOVs) followed by automated image fusion. The scheme was adapted from [8].

and versatile while keeping the manufacturing and running costs low. We demonstrate some representative applications and provide examples of how efficient algorithms can achieve robust performance of this economical imaging system.

2. MATERIAL AND METHODS

2.1 System Components
The serial sectioning system is based on a CM3500 cryotome from Leica (Wetzlar, Germany). In order to accommodate the imaging system, minor mechanical modifications were made (addition of a supporting frame and housing for the imaging system).

An Arduino (Torino, Italy) microcontroller was inserted into the analog circuit to control the cutting process through automation software written in Labview (National Instruments, Austin, USA).

Additional stages and stands were fabricated for mounting the imaging system on an optical table and for manual sectioning on a CM1950 Leica microtome, a common machine available in many laboratories. A Leica Z16 Apo Macroscope was chosen as a lens system, allowing automated adjustments of zoom and focus and a large range of Fields of View (FOV) using either a 5x or 0.5x objective. We used a KL2500 light source (Schott, New York, USA) filtered through a FW102C motorized filter-wheel (Thorlabs, New Jersey, USA) and coupled to gooseneck fiber bundles. In the lens-camera path,
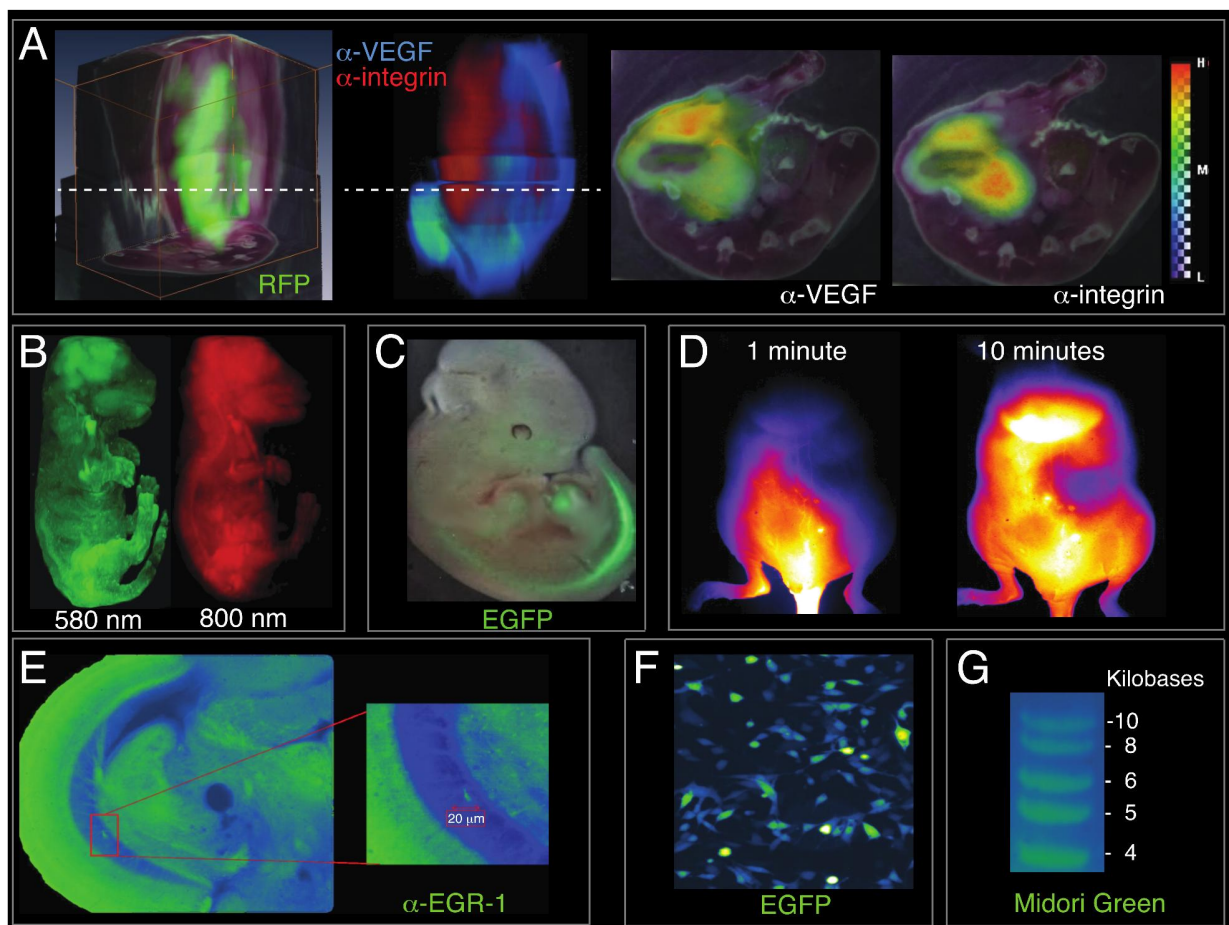
Figure 2. Multiscale and multispectral imaging (**A**) A corner cut of an RGB volume of a 4T1 tumor xenografted intramuscularly into a mouse, expressing RFP shown on a green color scale (left). A volumetric representation of fluorescently labeled probes specific for VEGF (blue) or integrin (red) measured at 680 and 750 nm respectively (middle). Fluorescent signal from the same fluorescent probes overlaid onto an RGB picture of the tissue section indicated by the broken lines. (**B**) Maximum Intensity Projections of 3D reflectance volumes of a mouse embryo imaged at 580 nm (peak of hemoglobin absorption) and 800 nm (NIR window). (**C**) Planar epifluorescent image of a mouse embryo expressing GFP in the spinal cord. (**D**) Biodistribution of the fluorescent dye ICG, 1 minute and 10 minutes after an *i.v.* injection into a mouse. (**E**) Coronal slice through an adult zebrafish brain stained with an anti-Egr1 antibody (secondary antibody labeled with AF488). The composite image was stitched together from16 automatically acquired FOVs of 0.3x0.3mm each. (**F**) Cultured HEK293 cells expressing EGFP imaged for expression analysis and cell counting. (**G**) Electrophoresis gel showing DNA ladder visualized with Midori Green.

we added an identical filter-wheel that allows the quick exchange of filters.

Images were obtained with a cooled CMOS 5.5M sensor (Neo sCMOS, Andor Technologies, CT) with up to 100 FPS and high quantum efficiency in the near-infrared range. An additional USB web-cam was used to monitor the cutting process. Motorized XY linear stages with 100 mm travel distance (Zaber, Vancouver, Canada) positioned the sample to allow raster scanning for higher resolutions and/or FOV.

The system is fully automated using custom software implemented in LabView (National Instruments, Austin, USA) to control the sectioning, positioning and multispectral imaging based on adjustable protocols and a user-friendly graphical interface. Integrated Matlab (Mathworks, MA, USA) scripts optimize image acquisition through auto-focus, automatic choice of exposure time, RGB color reconstruction of reflection images and stitching of multiple images in raster scanning mode. An image registration routine [7] implemented in ImageJ (version 1.48c, NIH, USA) was used to assemble higher resolution images in Figure 2E. Further image processing and visualization was performed in Amira (FEI Visualization Sciences Group, Burlington, USA).

The cost of the fully automated system with the NIR sensitive camera is ~40000 euros. The simpler system mounted onto a standard cryomicrotome for manual operation costs ~20000 euros.

All animal experiments were approved by the District Government of Upper Bavaria.

2.2. Basic operation and performance

The main application of the system is for automated serial cryosectioning and planar imaging. In a standard cryoslicing routine, the user positions the embedded sample(s) in the holder, chooses the cutting step size and number of slices, the imaging positions and an appropriate imaging protocol specifying the sequence of filters and exposure times to be used. The imaging system then automatically performs the sectioning and imaging and can be remotely controlled via a network application.

The estimated time for an imaging session is given by a formula of the form:

$$t = \left(\frac{SampleArea}{CameraFOV}\right) * \left(\frac{SampleLength}{SlicingStep}\right) *$$

$$(\textstyle\sum_{Channels} ExposureTime + MovementTime)$$

For example, an imaging scenario similar to that presented in Figure 3B and 3C with four zebrafish embedded in a rectangular block of 0.5 x 0.5 x 1 cm, imaged at an XY resolution of ~1.25 μm (0.25 cm FOV) and a Z resolution of 20 μm at 3 fluorescence wavelengths and RGB (~1 sec exposure each) would result in a dataset of 4 multispectral cubes (one for each Zebrafish) of 2000 x 2000 x 500 voxels each acquired over ~3 hours of automated image acquisition. Addition of high-powered light sources such as lasers can certainly decrease the acquisition time drastically. Even without any post-processing, the user can obtain a multispectral (reflection and fluorescence) volumetric reconstruction since misalignments of the slices are small. Redundancies in the data (*e.g.* spatial overlap between images acquired by raster scanning) can be exploited by post-processing algorithms, which improve registration of individual slices and compensate for noise.

3. RESULTS

In Figure 2 we show representative data obtained from the imaging system in sequential sectioning and epifluorescence mode as well as in stand-alone mode for alternative planar imaging applications. Figure 2A shows the volumetric reconstruction of multispectral images from an intramuscular xenograft of 4T1 tumor cells expressing RFP (left). These tumor cells are also targeted with fluorescent probes specific for VEGF and integrin whose distribution is shown as an overlay on a blue and red color map (middle) or on separate maps (right). Figure 2B shows 3D volume reconstructions of a mouse embryo obtained from intrinsic reflection contrast in the visible (580 nm) and NIR spectra (800 nm).

Figure 2C demonstrates the use of the imaging system as a stand-alone device mounted on an optical table for planar epifluorescence imaging of a transgenic mouse embryo with GFP fluorescence in the spinal cord. Figure 2D displays two frames of a kinetics study on the biodistribution of ICG injected intravenously into a healthy mouse.

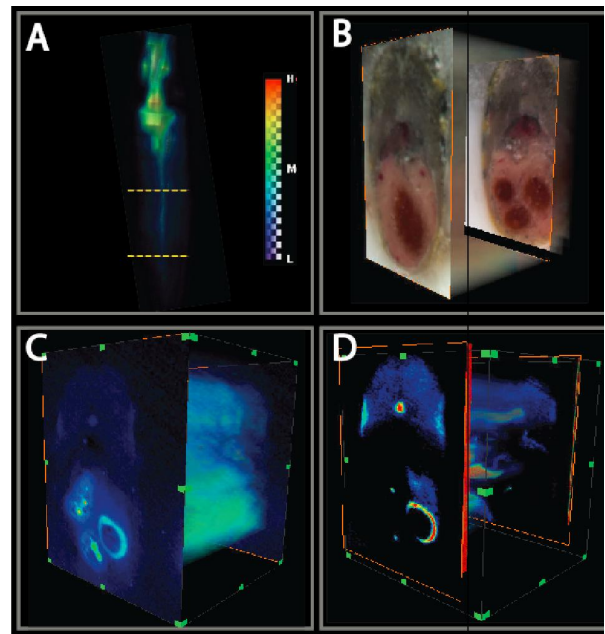The combination of the xy-stages, the lens system and the appropriate automation and image-stitching algorithms allows

Figure 3. Suppression of background fluorescence by multispectral imaging. (A) Maximum intensity projection of the corrected fluorescence signal from an adult zebrafish with pan-neuronal expression of GFP showing strong signal from the brain (top) as well as signal from the spinal cord (vertical lines). **(B)** Volumetric representation of the RGB images consisting of two axial orthoslices (positioned at the two broken lines in (A)) and maximum intensity projection between them. **(C)** Same volumetric representation as in (B) depicting the fluorescent images acquired with a single emission filter (510/10 nm). **(D)** Volumetric data as in (C) corrected for background fluorescence with data obtained from an additional emission filter (550/10 nm). The fluorescent signal from GFP-expressing neurons in the spinal cord (top) is enhanced whereas the signal from the gastrointestinal tract (bottom) is suppressed.

the system to also be used as a slide scanner for coverslipped tissue sections either in reflection (*i.e.* for H&E staining) or fluorescence mode. As an example, Figure 2D shows a coronal immunohistochemical slice through an adult zebrafish brain, stained with an antibody against EGR-1 and a secondary antibody fluorescently labeled with Alexa Fluor 488. These data show that a similar image quality can be obtained from the surface of a frozen tissue block and conventional cover glasses. In addition to the imaging results from tissue samples, we show exemplary alternative applications of the imaging system for cell counting and expression analysis (Figure 2F) as well as documentation of electrophoresis gels (Figure 2G).

Figure 3 illustrates how background fluorescence can be effectively reduced by multispectral imaging. The fluorescence signal from the spinal cord neurons of a zebrafish with pan-neuronal expression of GFP is masked by autofluorescence of the surrounding tissue (Figure 3C). In addition, strong background fluorescence is present in the gastrointestinal tract when imaged with a single emission filter (510/10 nm)

optimized for the GFP emission peak (Figure 3C). To reduce these unspecific signals, we acquired additional images with an emission filter (550/10 nm) outside of the peak emission of GFP but still capturing background fluorescent signals. Combining these two spectral images we were thus able to enhance the GFP-specific signal and reveal the GFP-expressing neurons in the spinal cord (Figure 3D, top center). This correction allowed for the selective detection of GFP expressing neurons throughout the entire zebrafish as shown by a maximum intensity projection in Figure 3A. If necessary, additional filter sets can be used to provide data for more accurate spectral fitting methods.

4. DISCUSSION

We have used our previous experience with a prototypical cryoslicing and imaging system [8] on various biomedical specimens and conditions to build an improved serial sectioning and multispectral imaging system. This device minimizes human resources for image acquisition and post-processing and provides an economical solution for a variety of biological imaging applications. The use of a cryomicrotome instead of a vibratome [4] allows for simple shock freezing and high-throughput sectioning of entire specimens (*e.g.* multiple fluorescent reporter mice) including hard tissues such as bone. The imaging system is modular such that individual parts can easily be modified to improve performance for a particular application (*e.g.* adding laser illumination to minimize exposure times). Furthermore, the automated slicing, focus and iris control enable detailed and systematic interrogation of light-tissue interaction, *e.g.* the out-of-plane or in-plane fluorescence light diffusion at different scales and multiple wavelengths.

5. CONCLUSIONS

Serial sectioning and epifluorescence microscopy is a powerful technology to complement non-invasive *in vivo* imaging methodology with cellular resolution images from deep and opaque biomedical specimens. To overcome the labor-intensive manual sectioning, coverslipping, imaging and image processing steps of a traditional workflow, we have built a modular and economical fully automated cryomicrotome-imaging system that delivers hands-off volumetric and multispectral imaging data. The system is assembled from off-the-shelf components integrated with user-friendly custom software that enables high-throughput imaging and volumetric reconstruction of multiple biomedical specimens at once. The imaging system can also be used for *in vivo* epifluorescence imaging or for planar imaging of histochemical tissue samples, cultured cells or electrophoresis gels. The modular and versatile imaging device thus provides an economical and streamlined solution for many imaging needs in biomedical laboratories.

6. ACKNOWLEDGMENTS

7. REFERENCES

[1] A. Ale, V. Ermolayev, E. Herzog, C. Cohrs, M. H. de Angelis, and V. Ntziachristos, "FMT-XCT: in vivo animal studies with hybrid fluorescence molecular tomography-X-ray computed tomography," *Nature Methods,* vol. 9, no. 6, pp. 615-620, Jun, 2012.

[2] D. Razansky, M. Distel, C. Vinegoni, R. Ma, N. Perrimon, R. W. Köster, and V. Ntziachristos, "Multispectral opto-acoustic tomography of deep-seated fluorescent proteins in vivo," *Nature Photonics,* vol. 3, no. 7, pp. 412-417, 2009.

[3] D. Shcherbo, E. M. Merzlyak, T. V. Chepurnykh, A. F. Fradkov, G. V. Ermakova, E. A. Solovieva, K. A. Lukyanov, E. A. Bogdanova, A. G. Zaraisky, and S. Lukyanov, "Bright far-red fluorescent protein for whole-body imaging," *Nature Methods,* vol. 4, no. 9, pp. 741-746, 2007.

[4] T. Ragan, L. R. Kadiri, K. U. Venkataraju, K. Bahlmann, J. Sutin, J. Taranda, I. Arganda-Carreras, Y. Kim, H. S. Seung, and P. Osten, "Serial two-photon tomography for automated ex vivo mouse brain imaging," *Nature Methods,* vol. 9, no. 3, pp. 255-258, 2012.

[5] W. J. Weninger, S. H. Geyer, T. J. Mohun, D. Rasskin-Gutman, T. Matsui, I. Ribeiro, L. d. F. Costa, J. C. Izpisua-Belmonte, and G. B. Müller, "High-resolution episcopic microscopy: a rapid technique for high detailed 3D analysis of gene activity in the context of tissue architecture and morphology," *Anatomy and Embryology,* vol. 211, no. 3, pp. 213-221, 2006.

[6] D. Wilson, D. Roy, G. Steyer, M. Gargesha, M. Stone, and E. McKinley, "Whole mouse cryo-imaging," *Proceedings of SPIE,* vol. 6916, pp. 69161I-69161I-9, 2008.

[7] S. Preibisch, S. Saalfeld, and P. Tomancak, "Globally optimal stitching of tiled 3D microscopic image acquisitions," *Bioinformatics,* vol. 25, no. 11, pp. 1463-1465, 2009.

[8] A. Sarantopoulos, G. Themelis, and V. Ntziachristos, "Imaging the bio-distribution of fluorescent probes using multispectral epi-illumination cryoslicing imaging," *Molecular Imaging and Biology,* vol. 13, no. 5, pp. 874-85, Oct, 2011.

5.3 Calcium neuroimaging in behaving zebrafish larvae using a turn-key light field camera

The specifications of a light field imaging sensor and one of fluorescence imaging seem to be contradictory. Light-field imaging requires sensors with numerous pixels (normally above >5 Megapixels), since the lateral resolution of the raw image is sacrificed to provide axial in the reconstructed volume. Fluorescence imaging sensors though use bigger pixels (than conventional commercial cameras) to increase sensitivity and thus a smaller number of them can fit on a sensor. In this work we partnered with a commercial light field company (Raytrix GmbH) to confirm that with their conventional cameras we could capture fluorescence light field at speeds faster than the state of art scanning (e.g. light sheet or multi-photons) systems.

My contribution to this publication includes:

a)   Back-of-the-envelope calculations based on preliminary data of similar biological experiments (performed by Dr. Lauri and C.C. Perez), to confirm the feasibility of the study. Comparison based on provided documentation of Raytrix implementation vs. alternatives (e.g. Lytro and custom made solution)

b)   Assistance in all the data acquisitions session (both at Kiel and Munich), the analysis and visualizations.

c)   Evaluation of the imaging performance of the systems used, based on phantoms with fluorescence microscophers.

d)   Assistance in the discussion between Dr. Lauri (our biotechnologists), Dr. Cappetta (performed most of the analysis) and the technical personnel from Raytrix (including Mr. Erdmann). Since the commercial software was offering only depth and shape renderings, we had to collaborate with Raytrix to achieve volumetric reconstructions.

e)   Observation of the fact that the high-dynamic range of the sensor used captured information from not only the brain (high intensity fluorescence signal) but also parasitic (bleed-through and ambient light reflections) signal from the tail of the animal. This co-current volumetric neurobehavioral imaging on a single sensor, resulted in Fig.2d.

During the data acquisition session for this publication, we experimented also with imaging freely swimming zebrafish larvae, by manually trying to repositioning them under the field of view when they were swimming away. This was a great motivation for our next publication with the (stage-free) tracking microscope. Additionally, while we achieved sufficient frame rates for calcium imaging, forseeing the future need for faster acquisition for voltage probes), we continue collaborating with both Raytrix and Prof. Lasser and Ms Anca Stefanoiu using the multi-focus microlens array on an imaging setup based on a commercial microscope and a scientific CMOS camera offering superior sensitivity. This has allowed us to acquired data at higher frames rates, suitable also for imaging heart dynamics in zebrafish larvae or beating zebrafish larvae.

Calcium neuroimaging in behaving zebrafish larvae using a turn-key light field camera

Carlos Cruz Perez
Antonella Lauri
Panagiotis Symvoulidis
Michele Cappetta
Arne Erdmann
Gil Gregor Westmeyer

SPIE.

Calcium neuroimaging in behaving zebrafish larvae using a turn-key light field camera

Carlos Cruz Perez,[a,b,†] Antonella Lauri,[a,b,c,†] Panagiotis Symvoulidis,[a,b,c,†] Michele Cappetta,[a,b,c] Arne Erdmann,[d] and Gil Gregor Westmeyer[a,b,c,e,*]
[a]Helmholtz Zentrum München, Institute of Biological and Medical Imaging, Ingolstädter Landstrasse 1, 85764 Neuherberg, Germany
[b]Helmholtz Zentrum München, Institute of Developmental Genetics, Ingolstädter Landstrasse 1, 85764 Neuherberg, Germany
[c]Technische Universität München, Department of Nuclear Medicine, Ismaningerstrasse 22, 81675 Munich, Germany
[d]Raytrix, Schauenburgerstrasse 116, 24118 Kiel, Germany
[e]Technische Universität München, School of Medicine, Ismaningerstrasse 22, 81675 Munich, Germany

Abstract. Reconstructing a three-dimensional scene from multiple simultaneously acquired perspectives (the light field) is an elegant scanless imaging concept that can exceed the temporal resolution of currently available scanning-based imaging methods for capturing fast cellular processes. We tested the performance of commercially available light field cameras on a fluorescent microscopy setup for monitoring calcium activity in the brain of awake and behaving reporter zebrafish larvae. The plenoptic imaging system could volumetrically resolve diverse neuronal response profiles throughout the zebrafish brain upon stimulation with an aversive odorant. Behavioral responses of the reporter fish could be captured simultaneously together with depth-resolved neuronal activity. Overall, our assessment showed that with some optimizations for fluorescence microscopy applications, commercial light field cameras have the potential of becoming an attractive alternative to custom-built systems to accelerate molecular imaging research on cellular dynamics. © *The Authors. Published by SPIE under a Creative Commons Attribution 3.0 Unported License. Distribution or reproduction of this work in whole or in part requires full attribution of the original publication, including its DOI.* [DOI: 10.1117/1.JBO.20.9.096009]

1 Introduction

Neuronal activity occurs on a millisecond time scale across cell circuits distributed over the entire nervous system. Capturing these spatiotemporal patterns at adequate sampling rates to uncover the underlying principles of neuronal information processing is a grand technical challenge for systems neuroscience. Recently, it became possible in transparent reporter zebrafish larvae expressing genetically encoded fluorescent calcium indicators (GECIs)[1,2] to detect calcium transients noninvasively in the whole nervous system. In this vertebrate model organism, imaging can thus deliver information about a close correlate of neuronal activation, calcium fluxes, at much higher spatial resolution than is achievable with electrophysiological point recordings. To exceed the speed of confocal or multiphoton laser scanning methods,[3] light sheet microscopy methods have recently been developed[4–6] that image an entire plane through the object of interest at once, such that about $\sim 10^5$ neurons in an entire zebrafish larval brain can be scanned at a frequency of about 1 Hz.[4] Volumetric acquisition can be accelerated even further by light field imaging, an elegant method that avoids having to scan the object but instead reconstructs it volumetrically from multiple views acquired simultaneously from many different angles. This imaging method has recently been adapted for microscopy by using arrays of microlenses projecting to

subregions of sufficiently sensitive and large image sensors.[7,8] Light field microscopy (also known as plenoptic microscopy) could thus, in principle, capture the majority of fluorescent neurons in the brain of a reporter zebrafish in a single acquisition without the need for interpolation to correct for time delays. Neuroimaging of reporter zebrafish would benefit directly from such a gain in imaging speed. For instance, state-of-the-art fast light sheet microscopy, operating at about one volume per second, still misses a substantial fraction of calcium fluctuations detected by sensors such as GCaMP5G (rise times of ~ 0.2 s and decay rates of ~ 0.7 s[1,4]). For faster fluorescent sensors, such as genetically encoded voltage sensors,[9] even higher frame rates[10] would be required for adequate sampling. Furthermore, fast volumetric imaging could simultaneously extract information from fluorescent molecular sensors together with "biomechanical" data from freely moving zebrafish larvae exhibiting unrestrained behavior; this may complement virtual environment approaches that investigate neural activity during fictive behavior in immobilized zebrafish larvae.[11] Lately, technical advances have been made in acquisition and reconstruction of light field microscopy data[12–14] and three light field microscopes have been custom-built in different laboratories specifically to image neuronal activity in immobilized *Caenorhabditis elegans* worms and zebrafish larvae.[8,14,15] Despite the generous provision of open access documentation on light field microscopy hardware and open source software,[16,17] an "off-the shelf" light field camera system would certainly help to disseminate this comparably straightforward and compact imaging technology for widespread biological use. In this work, we thus investigated the performance of commercially available multifocus plenoptic

---

*Address all correspondence to: Gil Gregor Westmeyer, E-mail: gil.westmeyer@tum.de

†Authors contributed equally.

cameras[18] (Raytrix GmbH) for fluorescence neuroimaging of zebrafish larvae.

2 Results and Discussion

For initial testing of the commercial light field camera for microscopy, we imaged the distribution of melanin containing pigments in the head region of wild-type zebrafish larvae (6 days post fertilization) using a custom-assembled microscopy setup [Fig. 1(a)]. The larvae were embedded in 0.8% low-melting agarose and imaged under white light illumination (10× objective from Nikon, 0.25 NA, FOV of ~1.9 mm × 1.3 mm, R9μ plenoptic camera; all animal experiments were conducted in accordance with the guidelines approved by the government of Upper Bavaria). As can be seen in Fig. 1, the head melanophores

of the larva and the eyes offered high contrast [Fig. 1(b)] and their localization along the dorsoventral axis was correctly captured by the depth map calculated from the light field images exploiting information from microlenses with different focal lengths [Fig. 1(c)]. We subsequently tested the performance of the plenoptic camera for fluorescence microscopy by imaging green fluorescent beads of 1 μm in diameter (FluoSpheres carboxylate, Life Technologies, Carlsbad, California) embedded in an agar phantom. The sample excitation and fluorescence detection was achieved via a 488-nm OBIS laser (Coherent), a dichroic mirror (510 nm, Chroma Technology Corp.), a 20× objective (UMPlanFl N 20×, 0.5 NA, FOV 650 μm × 440 mm) a 535/40 nm emission filter (Chroma), and a R12μ plenoptic camera. Figure 1(d) shows the projection of single microspheres onto the image sensor, obtained via the microlens array
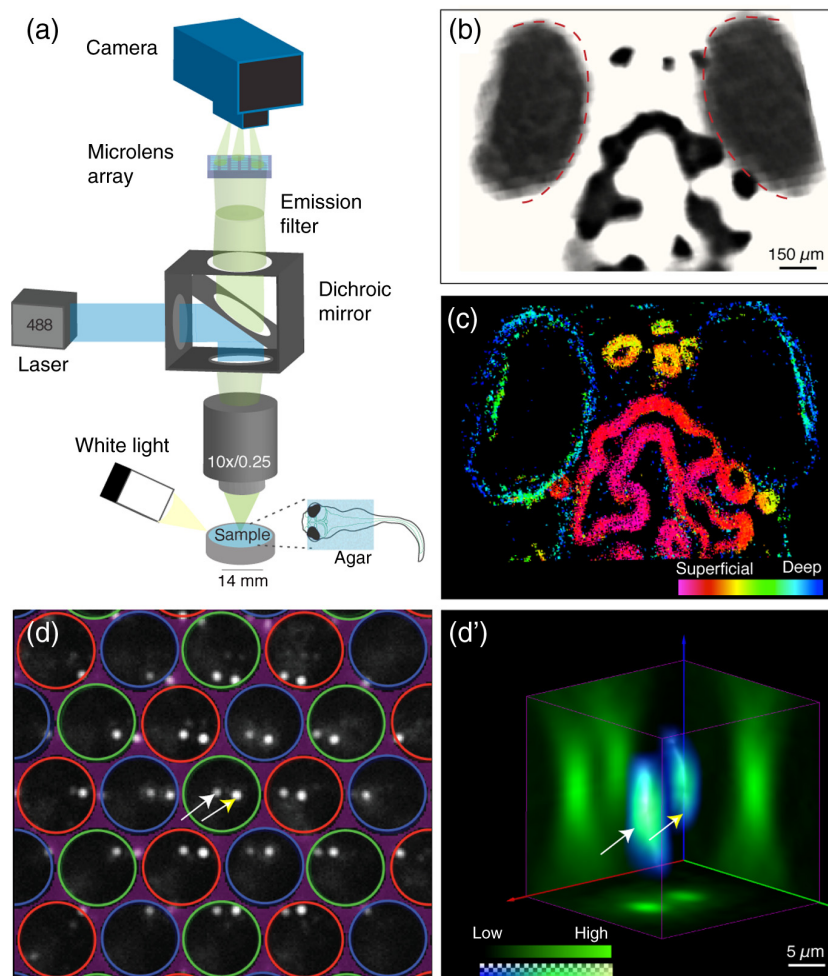
Fig. 1 Light field microscopy setup and volumetric imaging in bright field and fluorescence: (a) Fluorescent light from the specimen is guided via a dichroic mirror and emission filter to a microlens array projecting it to different subregions of the plenoptic camera's image sensor (reflectance images from white light illumination are captured without filters). (b) Reconstructed light field data obtained from a wild-type larva showing strong contrast from naturally present pigments in the eyes (red dashed outlines) and in the head region; (c) Corresponding depth information calculated from the light field data with most superficial structures shown in magenta and deeper structures in blue; (d) Raw grayscale image showing two fluorescence beads (1 μm in diameter, white and yellow arrows) embedded in an agar phantom projected onto the image sensor via microlenses with different focal lengths (red/green/blue circles label microlenses with close/medium/far focal lengths); and (d') Three-dimensional visualization of the same two volumetrically reconstructed fluorescent spheres (white and yellow arrows).
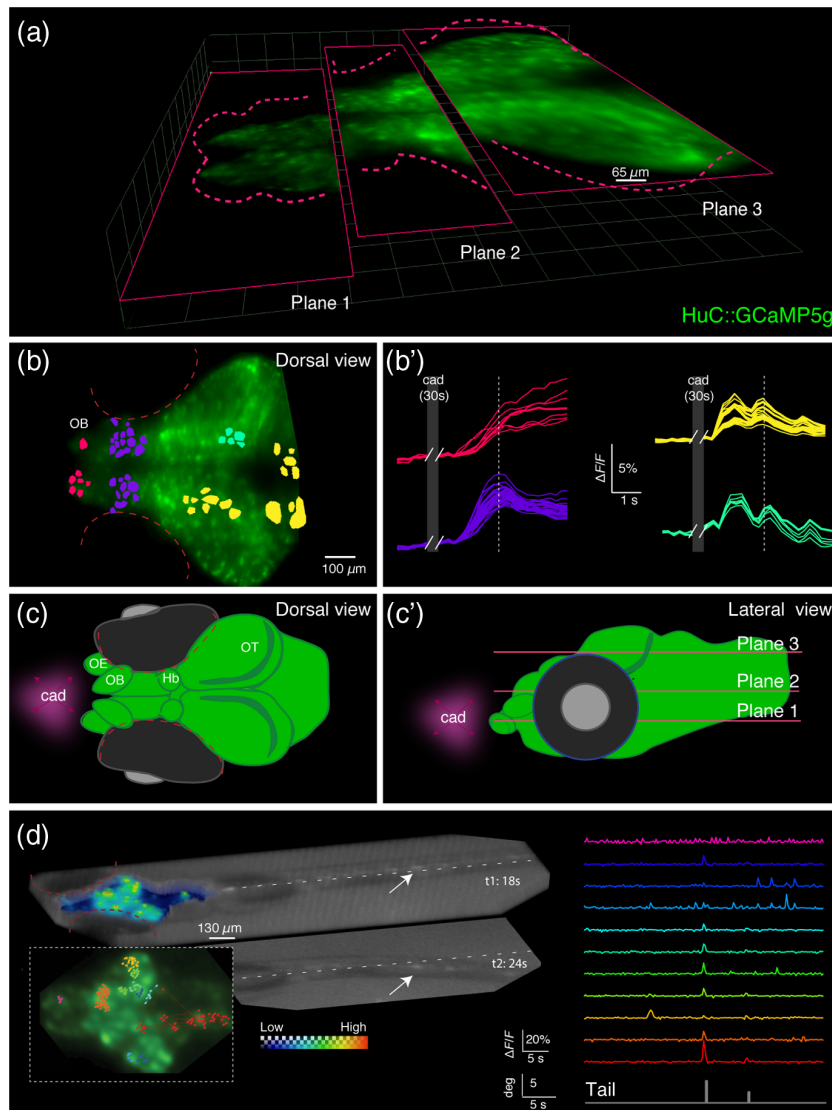
Fig. 2 Spatiotemporal patterns of neuronal responses to an aversive odor captured by light field microscopy: (a) Three transverse planes selected from the volumetric reconstruction of a single frame captured by the plenoptic camera showing fluorescence signals from the brain of a calcium reporter zebrafish larva (7-day-old HuC:GCaMP5g) during stimulation with the aversive odorant cadaverine; (b–b') Corresponding top-down maximum intensity projection with a colored overlay of regions of interest (ROIs) automatically selected for their substantial fluorescent signal changes in response to cadaverine. The color indicates the clusters of ROIs with high correlation between their corresponding temporal signal profiles shown in (b'). Delivery of cadaverine occurred during the omitted time points (dark gray area labeled "cad"). The white broken lines indicate the peak fluorescence signal of the deep purple trace as a reference to appreciate the earlier responses in the yellow and green traces; (c–c') Schematic drawings of the larval brain seen from dorsal (c) and lateral views (c') also indicating the site where the odorant cadaverine (cad) was presented. OE: olfactory epithelium, OB: olfactory bulb, OT: optic tectum, and Hb: habenula. (d) Rendered imaging volume showing simultaneous imaging of neuronal activity (high counts from fluorescence shown on color scale) and tail movements (low counts shown on grayscale) in response to cadaverine stimulation [deflection of the tail's axis from the dashed white line is shown for a second time point (t2)]. Clustered ROIs are shown on a top-down maximum intensity projection in the inset on the lower left and color-coded signal time courses are shown on the right. Tail deflections coincident with some neuronal activations are represented as gray bars.

consisting of microlenses with different focal lengths assembled in a hexagonal configuration.[18] The corresponding volumetric reconstruction is shown in Fig. 1(d') yielding a lateral resolution of 6 μm and an axial resolution of 16 μm (estimated by the averaged point spread function without additional postprocessing).

We were next interested to assess whether the light field microscopy setup could detect dynamic changes of neuronal activity in transgenic reporter zebrafish larvae with neuronal expression of a calcium indicator (HuC:GCaMP5g, identical optical setup as described above). To this end, we restrained

zebrafish larvae in 0.8% low-melting agarose not covering the nose. We stimulated the larvae with the odorant cadaverine (Cad, 10-μM solution), a diamine generated by decarboxylation of the amino acid lysine during decomposition of flesh, which is known to evoke olfactory-related neural activity and avoidance responses in zebrafish larvae.[19,20] Figure 2 shows three image planes through the volumetrically reconstructed light field dataset [Fig. 2(a)], as well as a top-down maximum intensity projection [Fig. 2(b)] showing robust fluorescent signal. Regions of interest (ROIs) could be automatically selected based on thresholding voxel signal changes in response to cadaverine and clustered with respect to the correlation (correlation coefficient larger than 0.8) of their respective baseline-corrected time courses [color coded in Fig. 2(b')]. Clusters of activity could be found in the olfactory bulb (OB) and habenula (Hb), the latter considered to be involved in relaying odor-evoked behavioral responses,[19,20] as well as in some neurons of the optic tectum (OT) [Figs. 2(b)–2(c)]. Whereas calcium signal amplitudes increased in the OB after cadaverine delivery [the delivery period is labeled "cad" on the gray area in Fig. 2(b)] during the observed time window, they partially decreased after peaking a few seconds after delivery of cadaverine (white broken lines in all traces); signal trajectories in the OT showed the first response peak occurring ∽1 s earlier than in the OB followed by multiple weaker calcium waves.

Next, we explored whether we could simultaneously capture neuronal activity while recording behavioral responses to the aversive odorant using the light field microscopy setup. To this aim, we embedded *HuC:GCaMP5g* larvae in agarose such that the tail was free to move and chose a 5× objective to obtain a field of view covering the entire larva. After cadaverine delivery, evoked neuronal calcium fluxes were recorded while concurrent tail movements were detected that are indicative of avoidance responses[21] [Fig. 2(d)]. Cluster analysis on automatically detected ROIs on this dataset interestingly showed activation in areas of the hindbrain that were in synchrony with the tail movements [gray bars underneath the signal time courses in Fig. 2(d)].

In summary, using a commercially available plenoptic camera (Raytrix GmbH) mounted on a custom-built microscope, we were able to volumetrically resolve calcium-dependent fluorescent signal changes elicited by the aversive odorant cadaverine in the brains of behaving zebrafish larvae. The capability of light field microscopy to acquire an entire volume in a single shot enabled us to detect diverse temporal response profiles from neuronal structures at different depths throughout the larval brain that motivate future detailed investigations. The current turn-key plenoptic camera could be successfully used to extract meaningful volumetric information about calcium signaling in distinct brain regions of reporter fish. However, both the spatial and temporal resolutions of the imaging system could be strongly improved by combining custom-designed multilens arrays and optimized reconstruction algorithms with scientific sCMOS image sensors that should provide an about four times higher sensitivity. These hardware improvements could be effectively complemented by the use of reporter fish expressing GECIs localized to the cell nucleus (as opposed to the entire cell), thereby aiding volumetric extraction of cellular calcium transients from the nonisotropic voxels obtained from current light field microscopy setups. As light field imaging is an elegant solution for fast molecular bioimaging applications, it is to be hoped that plenoptic cameras could be further optimized for fast fluorescence microscopy and be made more widely available to the biomedical research community.

Acknowledgments

References

1. J. Akerboom et al., "Optimization of a GCaMP calcium indicator for neural activity imaging," *J. Neurosci.* **32**(40), 13819–13840 (2012).
2. J. Akerboom et al., "Genetically encoded calcium indicators for multicolor neural activity imaging and combination with optogenetics," *Front. Mol. Neurosci.* **6**, 2 (2013).
3. D. Dombeck and D. Tank, "Two-photon imaging of neural activity in awake mobile mice," *Cold Spring Harbor Protoc.* **2014**(7), 726–736 (2014).
4. M. B. Ahrens et al., "Whole-brain functional imaging at cellular resolution using light-sheet microscopy," *Nat. Methods* **10**(5), 413–420 (2013).
5. P. J. Keller et al., "Reconstruction of zebrafish early light sheet microscopy," *Science* **322**(5904), 1065–1069 (2008).
6. F. O. Fahrbach et al., "Rapid 3D light-sheet microscopy with a tunable lens," *Opt. Express* **21**(18), 21010–21026 (2013).
7. M. Levoy and P. Hanrahan, "Light field rendering," in *Proc. 23rd Annual Conf. Computer Graphics and Interactive Techniques—SIGGRAPH, Association for Computing Machinery (ACM)* (1996).
8. R. Prevedel et al., "Simultaneous whole-animal 3D imaging of neuronal activity using light-field microscopy," *Nat. Med.* **11**, 727–732 (2014).
9. Y. Gong, J. Z. Li, and M. J. Schnitzer, "Enhanced archaerhodopsin fluorescent protein voltage indicators," *PLoS One* **8**(6), e66959 (2013).
10. F. St-Pierre et al., "High-fidelity optical reporting of neuronal electrical activity with an ultrafast fluorescent voltage sensor," *Nat. Neurosci.* **17**(6), 884–889 (2014).
11. N. Vladimirov et al., "Light-sheet functional imaging in fictively behaving zebrafish," *Nat. Methods* **11**(9), 883–884 (2014).
12. N. Cohen et al., "Enhancing the performance of the light field microscope using wavefront coding," *Opt. Express* **22**(20), 24817–24839 (2014).
13. M. Broxton et al., "Wave optics theory and 3-D deconvolution for the light field microscope," *Opt. Express* **21**(21), 25418–25439 (2013).
14. I. Iglesias and J. Ripoll, "Plenoptic projection fluorescence tomography," *Opt. Express* **22**(19), 23215–23225 (2014).
15. L. Grosenick et al., "Elastic source selection for in vivo imaging of neuronal ensembles," in *2009 IEEE International Symposium on Biomedical Imaging: From Nano to Macro*, pp. 1263–1266 (2009).
16. A. Vaziri et al., "Lightfield microscopy for high-speed, three-dimensional, simultaneous imaging of neural dynamics," in *Simultaneous whole-animal 3D imaging of neuronal activity using light-field microscopy*, Prevedel et al., Eds., Nature Methods 11, pp. 727–730, http://www.lightfieldscope.org/ (2014).
17. M. Levoy et al., "Stanford Light Field Microscope Project," http://graphics.stanford.edu/projects/lfmicroscope/ (8 2015).
18. C. Perwaß, L. Wietzke, and R. Gmbh, "Single lens 3D-camera with extended depth-of-field" Human Vision and Electronic Imaging XVII, Vol. 8291 (2012).

19. A. Hussain et al., "High-affinity olfactory receptor for the death-associated odor cadaverine," *Proc. Natl. Acad. Sci. U. S. A.* **110**(48), 19579–19584 (2013).
20. S. Krishnan et al., "The right dorsal habenula limits attraction to an odor in zebrafish," *Curr. Biol.* **24**(11), 1167–1175 (2014).
21. A. V. Kalueff et al., "Towards a comprehensive catalog of zebrafish," *Zebrafish* **10**(1), 70–86 (2013).

Carlos Cruz Pérez received his Diploma in Telecommunication Engineering from Technical University of Madrid in 2013. He then joined the Institutes of Biological and Medical Imaging (IBMI) and Developmental Genetics (IDG) at Helmholtz Zentrum München to work on optical systems for neuroimaging.

Antonella Lauri received her MS degree in medical biotechnology from the University of Naples "Federico II," Italy, in 2008. In 2013, she obtained her PhD (and Doctor of Science) from Heidelberg University and EMBL (European Molecular Biology Laboratory, Germany), applying different molecular and imaging methods to solve evolutionary and developmental questions. In 2013, she joined the Institutes of Biological and Medical Imaging and Developmental Genetics at Helmholtz Zentrum Muenchen, where she focuses on fish neuroimaging.

Panagiotis Symvoulidis received his Diploma in electrical and computer engineering from Technical University of Athens (NTUA), where he focused his studies on signal processing and electronics

for biomedical engineering application. Subsequently, he moved to the Technische Universitaet Muenchen, where he worked toward his PhD under the supervision of Prof. V. Ntziachristos on the systems and algorithms for fluorescence and multispectral tissue imaging in the diffusive regime. Recently, he joined Prof. Westmeyer's laboratory at Helmholtz Zentrum Muenchen, developing equipment and methods for neuroimaging studies.

Michele Cappetta has studied at the "University of the studies of Trieste" (Italy) where he obtained a Bachelor in physics in 2006 and his MS degree in astrophysics in 2008. In 2013 he concluded his PhD in physics at the Ludwig Maximilian University Munich conducting a research project on extrasolar planets at the Max-Planck-Institute for Extraterrestrial Physics in Munich. He became a member of IBMI and IDG the Helmholtz Zentrum Muenchen in 2014.

Gil Gregor Westmeyer completed his dissertation in medicine from Ludwig Maximilian University Munich. He conducted his postdoctoral training in Alan Jasanoff's laboratory at MIT before starting a laboratory at Helmholtz Center Munich (IBMI/IDG) and joining the medical faculty of Technische Universitaet Muenchen. The Westmeyer laboratory is developing next-generation molecular imaging and control technology to enable closed-loop cell circuit control with spatiotemporal precision and deep-tissue penetration for neuroscientific applications.

Arne Erdmann: Biography is not available.

5.4 NeuBtracker - imaging neurobehavioral dynamics in freely behaving fish

In this publication we designed and implemented a novel tracking microscope for zebrafish larvae, while also showcasing a series of applications that it enables. Additionally we ensured that the systems can not only be replicated (by sharing designs, automation and analysis code), but further expanded to meet special needs of individual labs. Thus in the publication we present data from at least two different implementations of the system along with a series of plug-ins, like additional tracking lasers for photostimulation, stages for high-throughput imaging etc

While since over the three years that this project lasts, due to personnel changes among others, I had to at least partially participate in most of the roles (e.g. including fish mating etc), my most importan contributions were that I:

a) Based on an idea from Dr. Koch and drawing of the optical setup from Dr. Jia, designed the system on CAD software, ordered the needed parts and assembled the first version of the system. With the help of Dr. Chmyrov upgraded the system incorporating a Zooming System.

b) Wrote the automation software that controls the image acquisitions including the control of all the cameras, tracking (based on algorithms from Dr. Cappetta and Ms Stefanoiu). We choose Matlab rather than Labview to allow easier replication of the system, due to higher modularity and bigger number of users.

c) Performed the characterization of the system, including both imaging of phantoms and timing response with additional input-output cards.

d) Performed all biological experiments (some with the assistance from Dr. Lauri and Prof. Westmeyer).

e) Assisted (Dr. Cappeta and Dr. Stefanoiou) the development of the analysis pipeline, including the registration and extraction of fluorescence signals. And performed the analysis of many of the datasets.

f) Assisted the final presentation of the result in a manuscript form (including text, figures, supplementary video and supporting website Neubtracker.com)

There is a series of follow-up steps on this projects, both in terms of biological experiments and improving the system. As a first step we are working on an optimizing validation system, including the light-field one and a light-sheet illumination microscope. Regarding the actual system we aim at increasing the performance of the tracking, making it more robust (e.g. experimenting with convolutional networks on existing datasets), and running it on an embedded system rather than the actual PC. Additional automations (e.g. water refreshing systems) can be added to the system to allow longer recording, which would be important for both circadian rhythm studies, and achieving recording of default (resting state) brain activity in instance that the fish is acclimate in the arena and does not move.

NeuBtracker—imaging neurobehavioral dynamics in freely behaving fish

Panagiotis Symvoulidis[1–3], Antonella Lauri[1–3],
Anca Stefanoiu[4], Michele Cappetta[1–3], Steffen Schneider[3],
Hongbo Jia[5], Anja Stelzl[1,2], Maximilian Koch[1],
Carlos Cruz Perez[1,2], Ahne Myklatun[1–3],
Sabine Renninger[6], Andriy Chmyrov[1,7],
Tobias Lasser[4], Wolfgang Wurst[2], Vasilis Ntziachristos[1,7]
& Gil G Westmeyer[1–3]

A long-standing objective in neuroscience has been to image distributed neuronal activity in freely behaving animals. Here we introduce NeuBtracker, a tracking microscope for simultaneous imaging of neuronal activity and behavior of freely swimming fluorescent reporter fish. We showcase the value of NeuBtracker for screening neurostimulants with respect to their combined neuronal and behavioral effects and for determining spontaneous and stimulus-induced spatiotemporal patterns of neuronal activation during naturalistic behavior.

An important goal in neuroscientific research is to record spatio-temporal patterns of brain activity in freely moving animals in order to reveal neuronal correlates of unperturbed perception and unrestrained behavior. However, a combination of physical restraint, pharmacological sedation and paralysis of the animal is typically necessary to enable neuroimaging. Whereas head-mounted optical imaging devices have been developed for rodents to achieve real-time neuroimaging of selected cell populations in freely moving animals[1], the accessible fields of view (FOVs) are usually much smaller than what can be achieved in transparent fish.

Advances in genetically encoded fluorescent sensors[2] and fast imaging instrumentation have established zebrafish (*Danio rerio*) as a powerful genetic vertebrate model organism for imaging-based neuroscience[3]. Virtual reality approaches in restrained zebrafish larvae[4–6], fluorescent imaging of unrestrained fish within a stationary FOV[7], and bioluminescent point measurements in freely behaving larvae[8] have been reported. There is also considerable interest in quantifying the versatile behavioral repertoire of zebrafish[9,10] in the context of high-throughput pharmacological screens[11].

Here we introduce an open-source and modular platform for neurobehavioral interrogation (NeuBtracker) that enables simultaneous and noninvasive monitoring of brain activity and behavioral parameters in freely swimming zebrafish larvae.

Fluorescent imaging solutions for nonvertebrate organisms such as *Caenorhabditis elegans* have been developed that utilize motorized stages to keep the animal in the FOV[12]. However, to achieve neuroimaging of swimming zebrafish larvae, this approach would necessitate moving a water-filled arena with such acceleration that confounding mechanosensory stimulation of the animals could occur. Furthermore, compared with *Drosophila*, from whose brain fluorescent data were obtained with a conventional photographic lens after surgical removal of the head cuticle[13], the transparency of zebrafish larvae affords tracking fluorescently labeled cells throughout the body, and this makes adjustable FOVs desirable. Zebrafish larvae also swim at different depths depending on their developmental stage and behavioral context.

To meet these specifications, we have built NeuBtracker to (i) operate without moving stages, objectives or excitation light beams; (ii) provide adjustable magnification; and (iii) allow for dynamic refocusing (**Fig. 1a,b**; **Supplementary Figs. 1–3**; **Supplementary Video 1**). NeuBtracker has two imaging channels—one is static to observe the behavior of the fish and locate its position, the other one tracks the freely swimming larva to provide magnified fluorescent images. Tracking of the fish is controlled by a custom-written acquisition software that receives the 1× image from an IR-sensitive camera as input, locates the fish's head, and moves galvanometric mirrors to the position that keeps the FOV of the fluorescent camera on the fish (**Supplementary Fig. 4–6**). A postprocessing algorithm coregisters the acquired images to enable analysis of the spatiotemporal patterns of calcium fluxes (**Supplementary Figs. 4** and **7**). For fluorescence excitation, we used an ~3.3-W LED centered at 460 nm to provide homogeneous illumination across the whole arena (**Supplementary Fig. 3h,i**) rather than guiding the excitation light through the tracking mirrors, which might result in confounding visual or thermal stimuli during imaging[14,15]. Magnification is obtained either by using lenses with a fixed focal length ('MicroFixed' configuration) or a zoom lens ('MacroZoom' configuration), which can achieve a resolution of up to 150 line pairs per mm (lp/mm) for FOVs ranging from the whole body of a larva to zoom-ins on only the larval brain (**Fig. 1a,b** and **Supplementary Fig. 1**). Furthermore, we inserted an electrically tunable lens (ETL) to enable fast refocusing with submicrometer steps up to a focal length of 10 mm (**Supplementary Fig. 8**).

NeuBtracker allowed us to simultaneously image the behavior and neuronal activity of freely swimming larvae expressing fluorescent calcium indicators. In fish with strong pan-neuronal expression of GCaMP6s, we found voxel time courses in the hindbrain that were significantly correlated ($P < 10^{-5}$,

[1]Institute of Biological and Medical Imaging, Helmholtz Zentrum München, Munich, Germany. [2]Institute of Developmental Genetics, Helmholtz Zentrum München, Munich, Germany. [3]Department of Nuclear Medicine, Technical University of Munich, Munich, Germany. [4]Computer Aided Medical Procedures, Technical University of Munich, Munich, Germany. [5]Institute of Neuroscience, Technical University of Munich, Munich, Germany. [6]Champalimaud Centre for the Unknown, Lisbon, Portugal. [7]Chair for Biological Imaging, Technical University of Munich, Munich, Germany. Correspondence should be addressed to G.G.W. (gil.westmeyer@tum.de).

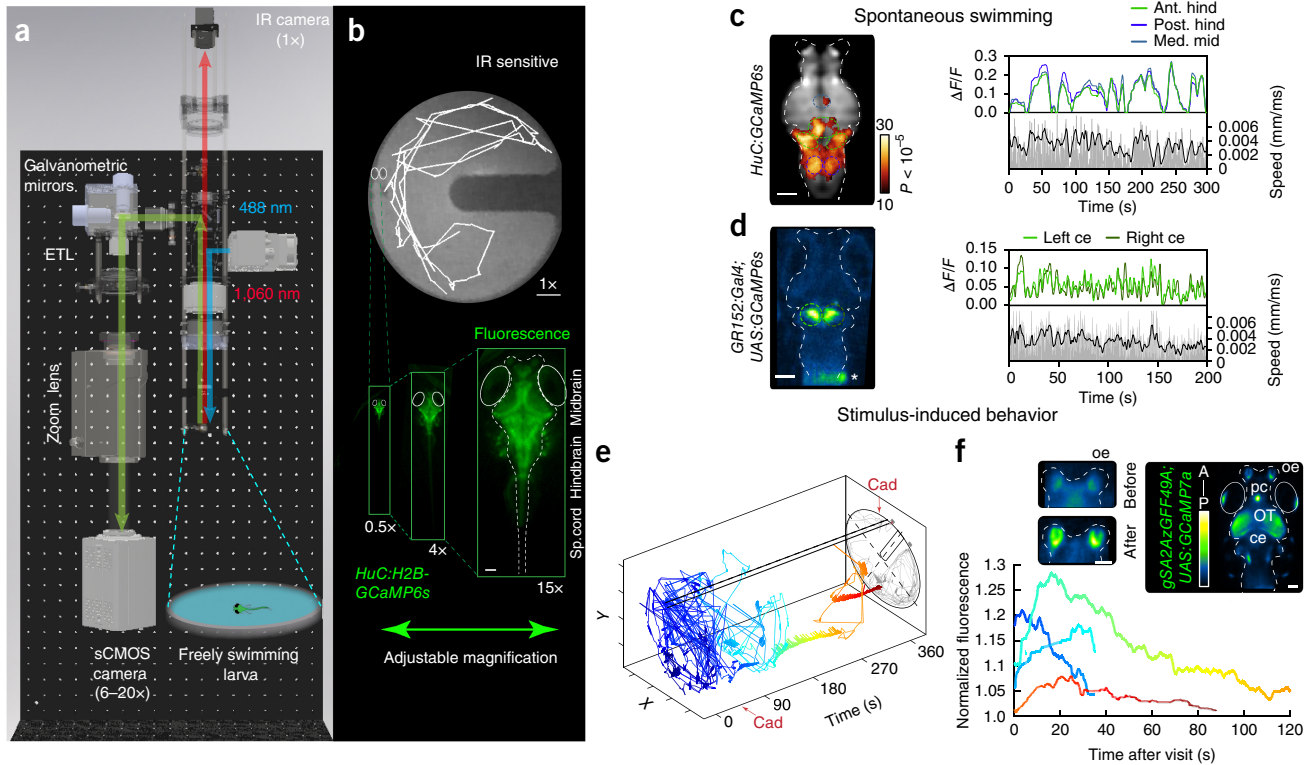**Figure 1** | Design and performance of NeuBtracker. (**a**) Rendering of the system showing the infrared (IR) channel (red arrow) for transillumination imaging as well as the fluorescence detection path (blue/green) that can be scanned across the arena with adjustable magnification and focusing via an electrically tunable lens (ETL). (**b**) Example of a swimming trajectory as well as fluorescent images obtained at different magnifications either capturing the whole arena (0.5×), covering the entire body (~4×) or just the brain (~15×) of a larva with pan-neuronal expression of GCaMP6s (tg(*HuC: H2B-GCaMP6s*)), 7 d postfertilization (dpf). Scale bar on the arena, 1 mm; scale bar for the fluorescent image, 100 μm. (**c**) Neurobehavioral imaging data from a spontaneously swimming zebrafish larva with pan-neuronal expression of GCaMP6s (tg(*HuC:GCaMP6s*)). Linear regression analysis revealed areas of the anterior and posterior hindbrain (ant. and post. hind) that were correlated with the swimming speed of the larva (coefficient map thresholded at a *P* value of 0.01, Bonferroni corrected to $P = 10^{-5}$) overlaid on the time-averaged image (displayed on grayscale). Right, corresponding fluorescent signal time courses color coded for the ROIs drawn on the map (med. mid., medial midbrain). (**d**) Fluorescent signal changes ($\Delta F/F$) during spontaneous swimming of a larva with GCaMP6s expression in the granule cells of the cerebellum (tg(*GR152:Gal4;UAS:GCaMP6s*)). * denotes non-neuronal autofluorescence. (**e**) Swimming trajectory of a larva with predominant expression of GCaMP7a in the optic tectum (OT) and anterior brain regions including the olfactory epithelium (oe) (tg(*gSA2AzGFF49A;UAS:GCaMP7a*)) before and after local administration of the odorant cadaverine (Cad, red arrows) into the left compartment of the test arena. (**f**) Fluorescent signal traces (normalized to the baseline signal) in the olfactory epithelium (oe) after multiple visits to the cadaverine port (color coded for time as in **e**). The insets show zoom-ins to oe before and after addition of Cad. Scale bars, 100 μm.

---

t-test on regression coefficient) with swimming speed during spontaneous swimming (**Fig. 1c** and **Supplementary Fig. 9a,b**; maximum correlation in the hindbrain, R = 0.48). This activation pattern partially overlaps with patterns observed in recent studies, in which fictive swimming was elicited in paralyzed larvae by presenting moving visual gratings[5,6]. Furthermore, we could detect calcium activity correlated with swimming speed in a zebrafish line with GCaMP6s expression in cerebellar granule cells (**Fig. 1d** and **Supplementary Fig. 9c**; correlation in the cerebellar region of interest (ROI), R = 0.45).

To analyze stimulus-induced neurobehavioral responses, we applied the odorant cadaverine[16] into one of two reservoirs of a custom-built arena such that it could diffuse on one side of a central divider (**Fig. 1e** and **Supplementary Fig. 10a,b**). We simultaneously tracked the swimming trajectory and the neuronal activity of larvae exhibiting prominent expression of GCaMP7a in the optic tectum and anterior brain regions[7] and observed repeated activations of the fish's olfactory epithelium after multiple visits to the cadaverine port (**Fig. 1e,f** and control experiments shown in **Supplementary Fig. 11**).

We then used NeuBtracker for studying neurobehavioral effects upon delivery of neuroactive compounds to complement high-throughput drug screens based only on behavioral readouts with simultaneous observation of brain activity[11]. We imaged two groups of tg(*HuC:GCaMP6s*) larvae stimulated with either 4-aminopyridine (4-AP) or vehicle control. The first group received 4-AP directly at 150 s from the start of the recording (t1), while the second group obtained water at t1 and then 4-AP at 300 s (t2). In the time period after drug administration, we observed an increase in the fluorescent signal change of more than 50% in some brain regions (**Fig. 2a**). In line with this, we detected an increase in average swimming velocity and more frequent swimming bursts after application of 4-AP (**Fig. 2b**). These data demonstrate how NeuBtracker can be used to screen neuroactive drugs in neurobehavioral screening assays, the throughput of which can be increased by using motorized stages and multiwell plates (**Supplementary Fig. 10f,g**).

Next, we sought to establish long-term recordings under IR illumination with optional intermittent periods of fluorescence imaging. When we imaged zebrafish with preferential expression of
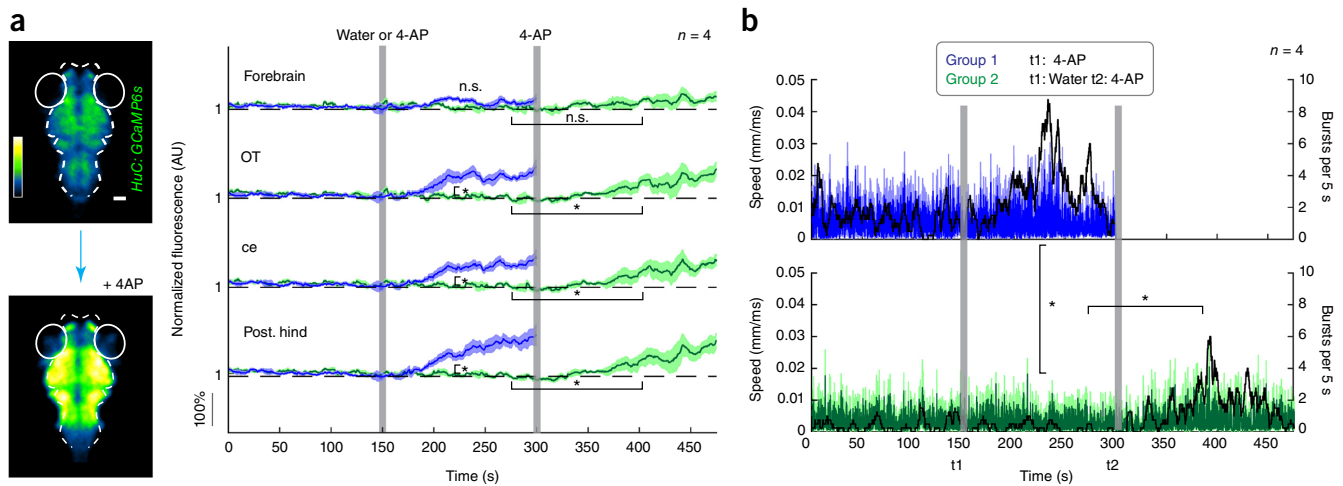
Figure 2 | Neurobehavioral responses to the neurostimulant 4-AP. (**a**) Left, representative fluorescent images from freely swimming zebrafish larvae expressing GCaMP6s (tg(*HuC:GCaMP6s*)), 5 dpf recorded on NeuBtracker before (top) and after (bottom) stimulation with the neuroactive drug 4-aminopyridine (4-AP). Scale bars, 100 μm. Right, fluorescent signal changes in different brain regions shown for two groups of fish (normalized to the baseline and averaged over animals, plotted with s.e.m.). After 150 s (t1), larvae in group 1 (*n* = 4, blue traces) were stimulated with 4-AP (~1,200 μM) added to the water of the arena which led to a significant increase in the GCaMP6s signal in the optic tectum (OT), cerebellum (ce), posterior hindbrain (post. hind) but not forebrain as compared to a vehicle control group of larvae (group 2, *n* = 4, green traces) that received only fish water at t1 (*t*-test, *P* values = 0.018, 0.032, 0.046 and 0.105 for the listed ROIs, respectively, see vertical brackets). Group 2 received 4-AP (~1,200 μM) at a later timepoint t2, which led to a significant increase of the fluorescent signal in OT, ce, and post. hind when compared to the preinjection period (paired *t*-test, *P* values = 0.03, 0.03, 0.04 for the respective ROIs; see horizontal brackets). No significant increase was observed in the forebrain (paired *t*-test, *P* value = 0.07). (**b**) The mean swimming speed (plotted with s.e.m. in lighter colors) of the two different groups (left *y*-axis) of fish was significantly increased compared to the vehicle control group (*t*-test, *P* value = 0.045). Group 2 also showed an increase in swimming speed after addition of 4-AP (paired *t*-test, *P* value = 0.049). The median counts of swimming bursts (instances of swimming speeds faster than 0.05 mm/ms counted over 5-s time windows) are shown as black solid lines (right *y*-axis).

GCaMP7a in light-responsive brain regions[7], we not only found a substantial increase in locomotor activity during periods when the blue LED was off, but also captured an elevated and subsequently decaying fluorescent signal in the pineal complex (pc) when the blue LED was turned on. The fluorescent signal time courses in pc recorded by NeuBtracker from a freely swimming larva during several dark–light cycles exhibited an exponential decay when averaged over cycles (**Fig. 3a**) or over animals (**Supplementary Fig. 12a**), which was not observed in the optic tectum (OT). Behavioral analysis showed that the distance traveled was substantially different between the illumination conditions (**Fig. 3b,c**). We confirmed the exponential signal decay in pc in an immobilized larva using a custom-built selective plane illumination microscope (SPIM) (**Fig. 3d**) and verified strong expression of GCaMP within cells of pc (known to possess nonvisual photoreceptors) by two-photon microscopy (**Supplementary Fig. 12b**). In addition, we confirmed the activation of pc through changes in the light conditions by neuronal-activity-dependent immunohistochemistry against phosphorylated ERK[17] (**Supplementary Fig. 12c**). We also directly compared the pc activity from a freely swimming and an immobilized larva on NeuBtracker to demonstrate that the same information could be obtained during tracking (**Supplementary Fig. 12d**).

The 2D galvanometric mirror system of NeuBtracker can also be used to project light patterns into the arena to provide, e.g., photostimulation. In order to demonstrate this feature, we coupled a 405-nm laser via the galvanometric mirrors and repeatedly steered the laser spot toward the head of the fish to elicit aversive responses at higher laser intensities (90-mW laser focused on a 200-μm area) or contralateral tectal responses using lower laser power (**Supplementary Fig. 13**).

In summary, we introduced a modular and open-source neurobehavioral imaging system that enables simultaneous neuroimaging and behavioral monitoring of unrestrained, natural behaviors in different lines of zebrafish expressing calcium indicators. We took care to minimize uncontrolled stimulation of the animals by employing tracking via galvanometric mirrors and providing homogeneous illumination of the entire arena.

NeuBtracker may be augmented with concurrent multiplanar and volumetric detection (such as multifocus or light-field microscopy[18]), which could be combined with planar or patterned excitation techniques[19] for optical sectioning. In addition, coupling of lasers with the mirror-tracking system could enable focused illumination at defined coordinates to serve as visual stimuli or possibly trigger spectrally compatible optogenetic tools to eventually even obtain closed-loop control[20] of neuronal activity during neuroimaging of unrestrained behavior.

METHODS

Methods, including statements of data availability and any associated accession codes and references, are available in the online version of the paper.

Note: Any Supplementary Information and Source Data files are available in the online version of the paper.
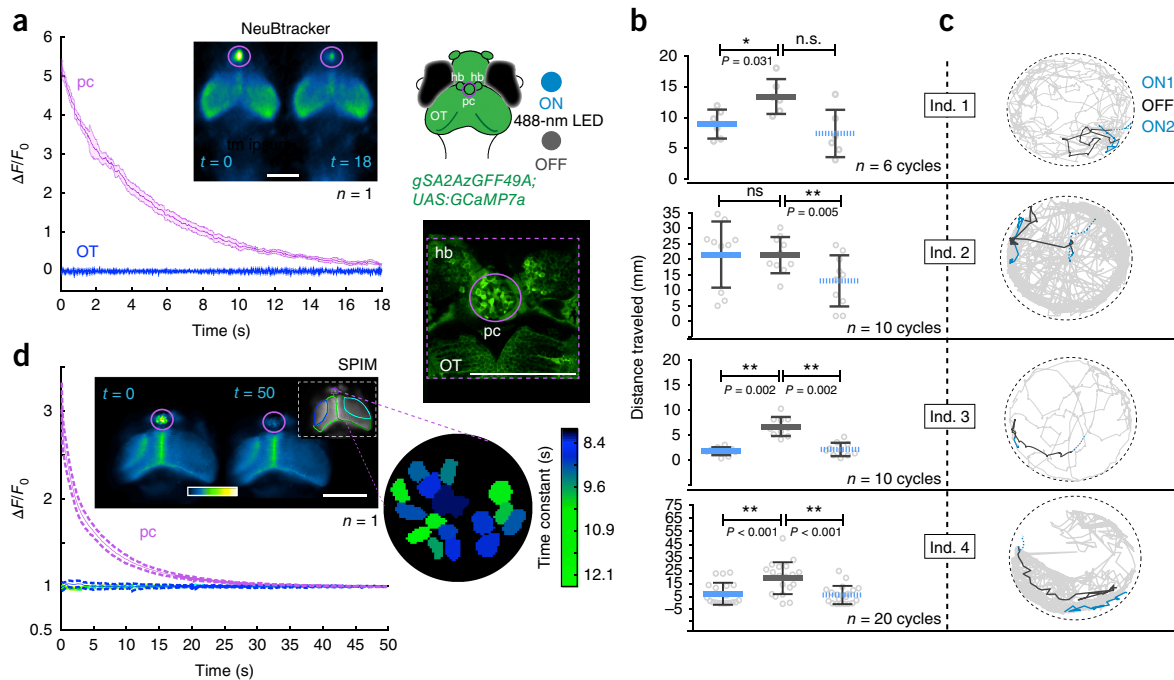
Figure 3 | Neurobehavioral responses of the pineal complex (pc) to dark–light cycles in freely swimming larvae. (**a**) Fluorescence signal changes obtained with NeuBtracker from pc and optic tectum (OT) in a larva expressing the calcium indicator GCaMP7a (tg(*gSA2AzGFF49A;UAS:GCaMP7a*), 6 dpf). The signal was averaged over ten dark–light cycles and is plotted with s.e.m. Right, schematic drawing and two-photon microscopy image of the anterior larval zebrafish brain showing pc, habenulae (hb) and OT. The symbols indicate the color coding of the stimulation paradigm consisting of alternating periods of illumination with the LED ON (blue) or OFF (gray). (**b**) Plot of the median and the interquartile range of the locomotor activity (distance traveled) across different cycles (50 s light ON, 10 s OFF and 50 s ON again) for four individuals (*P* values were derived from a two-tailed Wilcoxon signed-rank test). (**c**) Plot of swimming trajectories color coded for the illumination condition for four animals. (**d**) Fluorescent signal time courses (averaged over three cycles, shown with s.e.m.) in pc (purple ROI) detected by SPIM in the same transgenic larvae immobilized in 1% low melting agarose. Additional signal trajectories are shown from ROIs in OT (color coding indicated in the inset). The zoom-in on the right shows a magnified view of pc with fitted time constant overlaid in color on top of the respective ROI. Scale bars, 200 μm (**a**, **d**).

AUTHOR CONTRIBUTIONS
P.S. designed and implemented NeuBtracker with important contributions from H.J., M.K. and A.C.; programmed control software; conducted neurobehavioral imaging experiments including SPIM; analyzed data; and wrote the manuscript. A.L. designed and implemented neurobehavioral and two-photon experiments, conducted p-ERK imaging experiments, analyzed data, created illustrations and wrote the manuscript. A.S. and T.L. implemented image registration routines and improved tracking algorithm and analyzed data together with S.S. M.C. carried out the first implementation of tracking algorithm and performed original image and signal processing. C.C.P. carried out the initial implementation of SPIM. A.M. conducted photoaversion experiments on immobilized fish. A.S. was responsible for animal husbandry and provided support for neurobehavioral imaging. S.R. generated tg(*HuC:GCaMP6s*). W.W. and V.N. supported the project and provided feedback on the manuscript. G.G.W. conceived and supervised the work, analyzed data and wrote the manuscript.

COMPETING FINANCIAL INTERESTS
The authors declare no competing financial interests.

Reprints and permissions information is available online at http://www.nature.com/reprints/index.html. **Publisher's note:** Springer Nature remains neutral with regard to jurisdictional claims in published maps and institutional affiliations.

1. Kim, C.K. *et al. Nat. Methods* **13**, 325–328 (2016).
2. Looger, L.L. & Griesbeck, O. *Curr. Opin. Neurobiol.* **22**, 18–23 (2012).
3. Ahrens, M.B. & Engert, F. *Curr. Opin. Neurobiol.* **32**, 78–86 (2015).
4. Portugues, R., Feierstein, C.E., Engert, F. & Orger, M.B. *Neuron* **81**, 1328–1343 (2014).
5. Vladimirov, N. *et al. Nat. Methods* **11**, 883–884 (2014).
6. Ahrens, M.B. *et al. Nature* **485**, 471–477 (2012).
7. Muto, A., Ohkura, M., Abe, G., Nakai, J. & Kawakami, K. *Curr. Biol.* **23**, 307–311 (2013).
8. Naumann, E.A., Kampff, A.R., Prober, D.A., Schier, A.F. & Engert, F. *Nat. Neurosci.* **13**, 513–520 (2010).
9. Kalueff, A.V. *et al. Zebrafish* **10**, 70–86 (2013).
10. Orger, M.B. & de Polavieja, G.G. *Annu. Rev. Neurosci.* **40**, 125–147 (2017).
11. Bruni, G. *et al. Nat. Chem. Biol.* **12**, 559–566 (2016).
12. Nguyen, J.P. *et al. Proc. Natl. Acad. Sci. USA* **113**, E1074–E1081 (2016).
13. Grover, D., Katsuki, T. & Greenspan, R.J. *Nat. Methods* **13**, 569–572 (2016).
14. Haesemeyer, M., Robson, D.N.N., Li, J.M.M., Schier, A.F.F. & Engert, F. *Cell Syst.* **1**, 338–348 (2015).
15. Guggiana-Nilo, D.A. & Engert, F. *Front. Behav. Neurosci.* **10**, 160 (2016).
16. Hussain, A. *et al. Proc. Natl. Acad. Sci. USA* **110**, 19579–19584 (2013).
17. Randlett, O. *et al. Nat. Methods* **12**, 1039–1046 (2015).
18. Prevedel, R. *et al. Nat. Methods* **11**, 727–730 (2014).
19. Mertz, J. *Nat. Methods* **8**, 811–819 (2011).
20. Grosenick, L., Marshel, J.H. & Deisseroth, K. *Neuron* **86**, 106–139 (2015).

ONLINE METHODS

Details on NeuBtracker in MacroZoom configuration. We exclusively used commercially available off-the-shelf components for construction of the open-source NeuBtracker system (see the full list of components in **Supplementary Table 1** as well as schematics and photos of the design in **Supplementary Fig. 1**).

Objective. The FOV around the swimming arena (15 × 15 mm) was imaged by a 1× Nikon Objective from Stereo Microscope (HR Plan Apo WD 54).

Illumination. Excitation light was provided by a ~3.3 Watt LED (UHP-T-LED-460) coupled directly behind the objective using a dichroic (T495lpxr-UF1, Chroma) to illuminate the whole arena homogeneously and minimize thermal gradients that might have affected fish behavior[14,15,21]. A dichroic (T770lpxr, Chroma) was placed in a second filter cube to generate two images for the 1× and magnified paths; the relatively high residual transmission in the 530–560 nm range also allowed acquisition of both fluorescence and IR images from the low-magnification camera.

1× detection. The first image was projected by a 5:1 relay system (based on a pair of 150/30 mm achromatic doublets, Thorlabs) on the CCD of an IR-sensitive camera (MQ013RG-E2, Ximea), which was used for both the online tracking and behavioral recordings.

Beam steering. An *xy*-galvanometric mirror pair (GVS312/M, Thorlabs) was placed between a scan lens (constructed using a Plössl-type configuration with two 100 mm achromatic doublets placed back to back (effective focal length, 50 mm) and a tube lens (achromatic doublet *f* = 150, Thorlabs)). This ensemble projects the region of interest in the center of the FOV of a zoom lens system. The mirrors can be both moved manually and driven by the automatic tracking routine (see below).

Tunable lens. Close to the intermediate focus point of the scanning lens, an electrically focus-tunable lens (EL-10-30, Optotune) was placed to enable focusing at different *z*-planes.

Magnifications. The centered and focused images were captured by a zoom lens system (Z16, Leica with a 0.5× Objective), which enabled variable magnification in the range of 0.5× to 15×.

Fluorescence detection. A scientific CMOS (sCMOS) camera (Zyla5.5, Andor) was used to capture the fluorescence signals through an ET525/50m (Chroma) emission filter with exposure times as short as 5 ms. The sensitivity of the camera is also sufficient for using a fluorescent plastic slide (Chroma) as a light source and capturing transillumination imaging at >50 FPS (**Supplementary Fig. 2**), which enables high-resolution behavioral and anatomical imaging.

Details on NeuBtracker in MicroFixed configuration. To evaluate the modularity of the imaging platform, a second version of NeuBtracker ('MicroFixed') was assembled in which a series of modifications were tested. A Nikon 1× Microscopy Objective lens (CFI P-Achromat UW 1×/0.04/3.20) and a 200 mm tube lens (ITL 200 Thorlabs) were used to form the first images using the same LED source as in the 'MacroZoom' configuration that was coupled in the infinity space between the lenses. Infrared illumination (IR) was provided by a ring housing 12 LEDs (ELD-1060-525) centered at 1,060 nm, a wavelength that is invisible to the fish[22], and the beam splitter was replaced by a dichroic mirror (T770lpxr,

Chroma). The single 30 mm achromatic doublet worked both as a scanning lens and as the first lens of a 4-f Keplerian telescope. The modified 4-f system between the scan lens and the tube lens (200 mm in this version) also served as a magnifier and resulted in an ~7× magnification (200/30 = 6.6). Based on this configuration of the platform, a series of add-ons were tested, including the coupling of a 405 nm laser for tracked photostimulation and an *x*-stage for screening multiwell plates. The use of the microscope objective and a fixed magnification resulted in an overall lower sensitivity and resolution, a slightly smaller FOV (10 × 10 mm), and a more restricted working distance (1 cm). Nonetheless, the imaging data delivered comparable biological information in direct comparison to the MacroZoom configuration (**Fig. 3a** and **Supplementary Fig. 13a**).

Acquisition control software and automation of experimental procedures. A modular architecture based on Matlab (v.2014-2016, Mathworks) was used to ensure compatibility with various cameras, galvanometric mirrors and other controllable items (ETL, stimulation devices) while enabling fast prototyping with easy additions of pre-existing or custom-built routines in the acquisition pipeline. Two graphic user interfaces (GUIs) controlled five additional Matlab workers (W1-5), which were running asynchronously on a single PC (i7-3770, 32GB RAM) exchanging most recent data using a RAM-disk (**Supplementary Fig. 4**; open-source code available as **Supplementary Software** and on http://www.neubtracker.org).

Graphical user interface 1 'control panel'. Apart from the initialization of the system, GUI1 provides overall system control ('start/stop, tracking/recording'), panels for previewing intermediate results (e.g., 'tracking input') and other options for manually inserting comments on the whole experiment and/or current timepoint.

Graphical user interface 2, 'the previewer'. GUI2 shows the most recent 1× and fluorescence images with sliders enabling window/level. The same GUI is also used to preview tracking output and the *xy*-location of the galvanometric mirrors and enables the 'click-to-aim' manual tracking override by clicking on the desired target position in the whole FOV image. The same panel can also be used for viewing previously acquired data sets (in their raw form).

W1 and 2 camera control. These workers acquire continuously from the 1× IR-sensitive and the fluorescence channel and save the data along with metadata to a disk in binary format.

W3 tracking and aiming. W3 detects the center of mass of the fish from the IR channel. Once the coordinates are determined, they are transformed (based on a fixed transformation matrix built during a calibration step) into a pair of voltage values. If the center of mass exceeds a predefined distance from the center of FOV, these voltage command signals are sent via an IO card (NI USB-9263) to the galvanometric mirrors that move the FOV of the fluorescent channel (**Supplementary Figs. 4–6**). Manual overrides of the automated tracking are possible by either defining the desired coordinates of the FOV via a mouse click or by moving the FOV with a joystick.

W4 autofocus. This worker calculates a focus measure (Brenner's method provided the best trade-off between speed and robustness from different methods tested[23]) and if necessary adjusts the focal length of the ETL by acquiring a few images in adjacent focal planes

and fitting a second-degree polynomial to estimate the optimal focus (**Supplementary Fig. 8**).

W5 data logistics. this worker is responsible for cleaning the acquisition folder on the RAM-Disk by deleting not-recorded images (of the preview phases or between experiments) and archiving recorder frames during long acquisitions.

The Matlab-based acquisition framework enables the control of additional devices from the main platform (e.g., initializing stimulation schedules via an Arduino Microcontroller, Psytoolbox streaming to a projector positioned under the sample, control of translational stages for moving between samples located in multiwell arenas). The GUI allows for saving metadata during the experiment indexed to specific timepoints.

Data processing pipeline. Each single output data set of NeuBtracker is composed of two collections of images: one acquired by the fluorescence channel and one obtained from the 1× channel. This section describes the process of data analysis of the fluorescence images.

Quality check. An automated quality inspection of the fluorescence images (**Supplementary Fig. 4** and **Supplementary Video 1**) is performed in two stages. In the first stage, a fast and robust feature detection algorithm (SURF) is run on each single frame. The number of features detected is the first parameter considered in order to confirm the presence of the brain in the FOV in each frame. Any frame with less than five features detected is censored from subsequent analyses. In the second stage, the individual frames are grouped into batches. In each batch, an image with a high number of features is selected as a key frame, which is a good indicator for the presence of the brain in the FOV. All other frames in the batch are matched to the key frame using a similarity transform. Frames that yield no match to the key frame are censored, as well as frames that have a similarity transform with nonunit scaling (thresholded at ±0.1). The transformed frames in the batches are used as initialization for the subsequent registration routine.

Registration. To initialize the registration process, the key frame in each batch and the estimated transform computed from the feature matching (see quality check) are used. The frames in each batch are then cropped around the estimated position of the fish (see quality check) to reduce the file size. The registration then proceeds in three steps. First, for each batch the frames are registered to the key frame using an intensity-based registration algorithm maximizing the mutual information similarity measure, applying a rigid transformation model (see **Supplementary Figs. 4** and **7**; **Supplementary Video 1**). In a second step, a global template image is selected from the key frames. All frames of the image series are then rigidly registered to the global template by applying the same registration algorithm again, propagating the previous transformations. As a final step for fine tuning the registration result, all frames are again registered with respect to the global template. This is performed by optimizing the cross-correlation of the images in the Fourier domain and applying a transformation model using only translations.

Signal analysis. Fluorescence signals were normalized using different estimates of low-frequency trends as indicated in each figure legend.

Transgenic lines for neurobehavioral experiments. All animal experiments were conducted in accordance with the guidelines approved by the government of Upper Bavaria. 24 h embryos were collected from the parents and reared with a 14:10 light: dark cycle according to a standard protocol at 28 °C[24]. Positive fish expressing calcium indicators (tg*(gSA2AzGFF49A;UAS: GCaMP7a)*[7], tg*(HuC:GcaMP6s)*, tg*(HuC:H2BGcaMP6s)*, tg*(gSA2AzGFF152B;UAS:GCaMP6s)*[25,26] herein referred to as *GR152:Gal4*) and GFP controls tg*(HuC:Gal4;UAS:eGFP)* and tg*(OMP4;UAS:GCaMP1.6;mnGFF7:GFP)*[27], were selected between 72–96 hpf. The tg*(HuC:Gal4;UAS:eGFP)* were treated with PTU (N-Phenylthiourea ≥98%, Sigma-Aldrich) to inhibit melanin production. Imaging on NeuBtracker is noninvasive, and animals can be reimaged at different timepoints with NeuBtracker, SPIM or confocal microscopy.

Test arenas. We used NeuBtracker with a FOV of 15 × 15 mm and a working distance between objective and sample of ~10 cm. Any plastic dish (e.g., P35G-007-C, Matek) with transparent bottom, heights of 2 mm–1 cm and a diameter <1.5 cm can be used as an arena. To enable long-term recordings and controlled application of substances (e.g., odors), we designed custom-made circular arenas of 9 mm in diameter (see **Supplementary Fig. 10**) that contain two symmetric holes <10 µm connected to two ~25 µL compartments into which substances can be directly pipetted via external injection ports. We observed that a syringe pump running at 0.3 mL/h was able to adequately compensate water evaporation during experiments lasting more than 1 h. To ensure minimal contamination between experiments, the bottom of the custom-made arenas consists of a glass coverslip that can be changed between experiments. Versions with separators in the middle of the arena can be used either to generate local gradients of compounds injected through the ports or to enforce more complex swimming trajectories. Those designs can be implemented by CNC milling using different materials (such as anodized aluminum, which was used in the experiments with cadaverine). The addition of an *xy*-stage with a 3D printed coverslip holder enables the use of multiwell plates, while the large working distance provides enough space for future automation[28].

Pharmacological neurostimulation experiments. After 10 s of acclimation, larvae tg*(HuC:GCaMP6s)* (5 dpf) were imaged at a baseline while freely exploring the NeuBtracker arena before 10 µL of a 1,200 µM 4-AP solution (4-Aminopyridine, Sigma-Aldrich) was added at 150 s (t1) to one group of fish, while another group received only fish water at 150 s and 10 µL of 1,200 µM 4-AP at 300 s (t2). The exact injection timepoints were recorded on the 1× camera to temporally align each experimental run. Fish were randomly assigned to the experimental groups; data were processed with knowledge of the group assignment (no blinding).

Photostimulation experiments. Single zebrafish larvae tg (*gSA2AzGFF49A; UAS:GCaMP7a)* (6 dpf) were left free to explore a circular arena (9 mm) on NeuBtracker (containing ~100 µL of fish water). After a few seconds of acclimation, an automated tracker control routine was initiated that switched the 488 nm LED illumination OFF and ON (5 s OFF and 20 s ON (**Fig. 3a**) or 10 s OFF and 50 s ON (**Supplementary Fig. 13a**)) for several cycles to test for responses of the pineal complex known to contain photoreceptors[29]. Sample sizes were chosen based on preliminary experiments that showed robust activations of the

pineal complex in this stimulation paradigm. As the dynamics of neuronal activation in response to the OFF–ON were studied within each subject, no randomized assignment to experimental groups was made; data processing was performed with knowledge of the stimulation schedule (no blinding). For validation experiments, a custom-built single-plane illumination (SPIM) setup was used, which combines both a fast galvo-scanner light sheet[30] and an ETL[31] for the z-scanning of the optical path. The larvae were embedded in 1% low melting agarose in a custom-made chamber and illuminated by a light sheet (~10 μm thick) generated by a 488 nm laser (Obis, Coherent). One plane was imaged at 10 Hz. The same OFF–ON sequence used with NeuBtracker was applied for the stimulation using a beam blocker. Activation of the pineal complex was confirmed by immunodetection of phosphorylated ERK[17] on a different group of larvae of the same age and strain using the same dark–light cycles protocol as was used for the NeuBtracker (pERK antibody (Cell Signaling, 4370) and tERK antibody (Cell Signaling, 4696) with secondary anti-mouse AF 488 AB from Abcam ab150113 and anti-rabbit DyLight 594 from ThermoFisher Scientific, Cat # 35560).

Statistical analysis. *Spontaneous swimming.* To obtain the statistical map shown in **Figure 1c**, a linear regression between the relative change in the fluorescence signal and the swimming speed was computed for each voxel and coefficients displayed for P values < 10^{-5} (corresponds to $P < 0.01$, Bonferroni corrected for 1,000 voxels, two-sided t-test on the linear regression coefficient). For the scatter plots in **Supplementary Figure 9**, we used the same model on the signal time courses averaged over the indicated ROIs. For cluster analysis (**Supplementary Fig. 9**), the time trace for each pixel in the image was transformed using a principal component analysis, followed by fitting a Gaussian Mixture Model (GMM) with Expectation Maximization (EM) on the first 100 components explaining more than 90% of the variance.

Olfactory stimulation with cadaverine. The representative result shown in **Figure 1e** is complemented with control experiments shown in **Supplementary Figure 11**. The behavioral analysis was conducted by EthoVision XT software and custom-written Matlab routines and statistics were computed in GraphPad Prism 6 (two-tailed Wilcoxon matched-pairs signed rank test, $n = 8$ with P values for the different metrics reported in the legend of **Supplementary Fig. 11d**).

Pharmacological stimulation with 4-AP. Differences in fluorescent signal changes as well as differences in swimming speed (shown with s.e.m. between and within experimental groups were analyzed with unpaired or paired t-tests respectively, $n = 4$, with P values for the different comparisons indicated in the legend of **Fig. 2**).

Photostimulation of pc. The fluorescent signal time courses are shown averaged over ten cycles in one animal (**Fig. 3a,e**, with s.e.m.) or over four animals (**Supplementary Fig. 12a**). Control experiments are shown in **Figure 12b–d**. The corresponding behavioral data in **Figure 3c** were analyzed for each animal by a two-tailed Wilcoxon signed-rank test with the P values for each individual indicated in the figure legend.

Code availability. Additional detailed documentation of the optomechanical design along with assembly files, 3D files of the arena and the complete Matlab code (under a creative commons license) for automation and analysis can be found at http://www.neubtracker.org/.

Data availability statement. The data supporting the findings of this study are available from the corresponding author upon reasonable request.

A summary of the experimental design, statistical parameters and zebrafish lines used in this study can be found in the **Life Sciences Reporting Summary**.

21. Chen, X. & Engert, F. *Front. Syst. Neurosci.* **8**, 39 (2014).
22. Shcherbakov, D. *et al. PLoS One* **8**, e64429 (2013).
23. Pertuz, S., Puig, D. & Garcia, M.A. *Pattern Recognit.* **46**, 1415–1432 (2013).
24. Kimmel, C.B., Ballard, W.W., Kimmel, S.R., Ullmann, B. & Schilling, T.F. *Dev. Dyn.* **203**, 253–310 (1995).
25. Takeuchi, M. *et al. Dev. Biol.* **397**, 1–17 (2015).
26. Knogler, L.D., Markov, D.A., Dragomir, E.I., Štih, V. & Portugues, R. *Curr. Biol.* **27**, 1288–1302 (2017).
27. DeMaria, S. *et al. J. Neurosci.* **33**, 15235–15247 (2013).
28. Pardo-Martin, C. *et al. Nat. Methods* **7**, 634–636 (2010).
29. Li, X. *et al. PLoS One* **7**, e40508 (2012).
30. Keller, P.J., Schmidt, A.D., Wittbrodt, J. & Stelzer, E.H.K. *Science* **322**, 1065–1069 (2008).
31. Fahrbach, F.O., Voigt, F.F., Schmid, B., Helmchen, F. & Huisken, J. *Opt. Express* **21**, 21010–21026 (2013).

nature research

Corresponding author(s):   Gil G. Westmeyer

☐ Initial submission   ☐ Revised version   ☒ Final submission

Life Sciences Reporting Summary

Nature Research wishes to improve the reproducibility of the work that we publish. This form is intended for publication with all accepted life science papers and provides structure for consistency and transparency in reporting. Every life science submission will use this form; some list items might not apply to an individual manuscript, but all fields must be completed for clarity.

For further information on the points included in this form, see Reporting Life Sciences Research. For further information on Nature Research policies, including our data availability policy, see Authors & Referees and the Editorial Policy Checklist.

▸ Experimental design

1. **Sample size**

   Describe how sample size was determined.

   > The sample size was estimated from reported literature and pilot experiments.

2. **Data exclusions**

   Describe any data exclusions.

   > Imaging frames of insufficient quality (based on the algorithm and criteria presented in the text and in Supplementary Figures 4,6,7) were excluded from subsequent analyses.

3. **Replication**

   Describe whether the experimental findings were reliably reproduced.

   > Experimental findings were replicated several times in different animals and for most experiments also across different imaging conditions.

4. **Randomization**

   Describe how samples/organisms/participants were allocated into experimental groups.

   > In each experiment the larvae for each group (e.g. late vs. early delivery of 4-AP) were selected randomly from the same population. When different lines (e.g. GFP) were used as controls, those were mated on the same date and grown up under identical conditions.

5. **Blinding**

   Describe whether the investigators were blinded to group allocation during data collection and/or analysis.

   > No blinding of investigators to group allocation took place but the data acquisition and analysis pipeline was identical for all experimental groups and the analyses did not involve human scoring.

   Note: all studies involving animals and/or human research participants must disclose whether blinding and randomization were used.

6. **Statistical parameters**

   For all figures and tables that use statistical methods, confirm that the following items are present in relevant figure legends (or in the Methods section if additional space is needed).

n/a	Confirmed	
☐	☒	The exact sample size (n) for each experimental group/condition, given as a discrete number and unit of measurement (animals, litters, cultures, etc.)
☐	☒	A description of how samples were collected, noting whether measurements were taken from distinct samples or whether the same sample was measured repeatedly
☒	☐	A statement indicating how many times each experiment was replicated
☐	☒	The statistical test(s) used and whether they are one- or two-sided (note: only common tests should be described solely by name; more complex techniques should be described in the Methods section)
☐	☒	A description of any assumptions or corrections, such as an adjustment for multiple comparisons
☐	☒	The test results (e.g. P values) given as exact values whenever possible and with confidence intervals noted
☐	☒	A clear description of statistics including central tendency (e.g. median, mean) and variation (e.g. standard deviation, interquartile range)
☐	☒	Clearly defined error bars

   See the web collection on statistics for biologists for further resources and guidance.

▶ Software

Policy information about availability of computer code

7. Software

Describe the software used to analyze the data in this study.

> We used custom routines written in Matlab which are available in the zip file provided as Supplementary Information on NeuBtracker.org. For preliminary visualization of the data, Fiji was used (Schindelin, J.; Arganda-Carreras, I. & Frise, E. et al. (2012), "Fiji: an open-source platform for biological-image analysis", Nature methods 9(7): 676-682, PMID 22743772) as well as AFNI (Cox, R. W. AFNI: software for analysis and visualization of functional magnetic resonance neuroimages. Comput. Biomed. Res. 29, 162–173 (1996).)

For manuscripts utilizing custom algorithms or software that are central to the paper but not yet described in the published literature, software must be made available to editors and reviewers upon request. We strongly encourage code deposition in a community repository (e.g. GitHub). *Nature Methods* guidance for providing algorithms and software for publication provides further information on this topic.

▶ Materials and reagents

Policy information about availability of materials

8. Materials availability

Indicate whether there are restrictions on availability of unique materials or if these materials are only available for distribution by a for-profit company.

> -

9. Antibodies

Describe the antibodies used and how they were validated for use in the system under study (i.e. assay and species).

> -

10. Eukaryotic cell lines

a. State the source of each eukaryotic cell line used.

> -

b. Describe the method of cell line authentication used.

> -

c. Report whether the cell lines were tested for mycoplasma contamination.

> -

d. If any of the cell lines used are listed in the database of commonly misidentified cell lines maintained by ICLAC, provide a scientific rationale for their use.

> -

▶ Animals and human research participants

Policy information about studies involving animals; when reporting animal research, follow the ARRIVE guidelines

11. Description of research animals

Provide details on animals and/or animal-derived materials used in the study.

> tg(HuC:GCaMP6s)
> tg(HuC:H2B-GCaMP6s)
> tg(GR152:Gal4;UAS:GCaMP6s) [tg(gSA2AzGFF152B) referred to as GR152:Gal4]
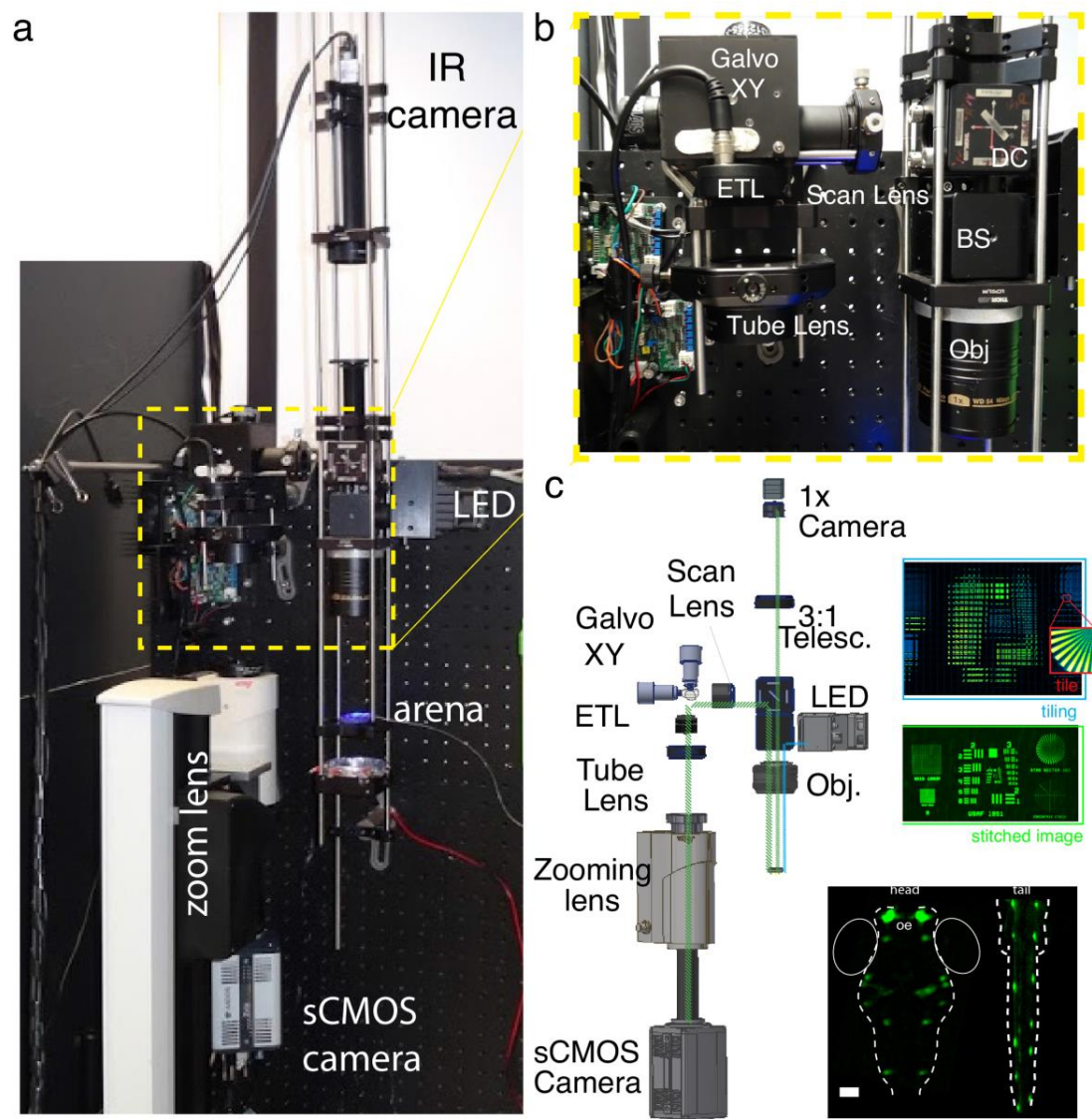> tg(gSA2AzGFF49A;UAS:GCaMP7a)
>
> tg(OMP4; GCaMP1.6 x mnGFF7; UAS:eGFP)
> tg(HuC:Gal4;UAS:GCaMP6s)
> tg(HuC:Gal4;UAS:eGFP)

Policy information about studies involving human research participants

12. Description of human research participants

Describe the covariate-relevant population characteristics of the human research participants.

> -

Supplementary Figure 1

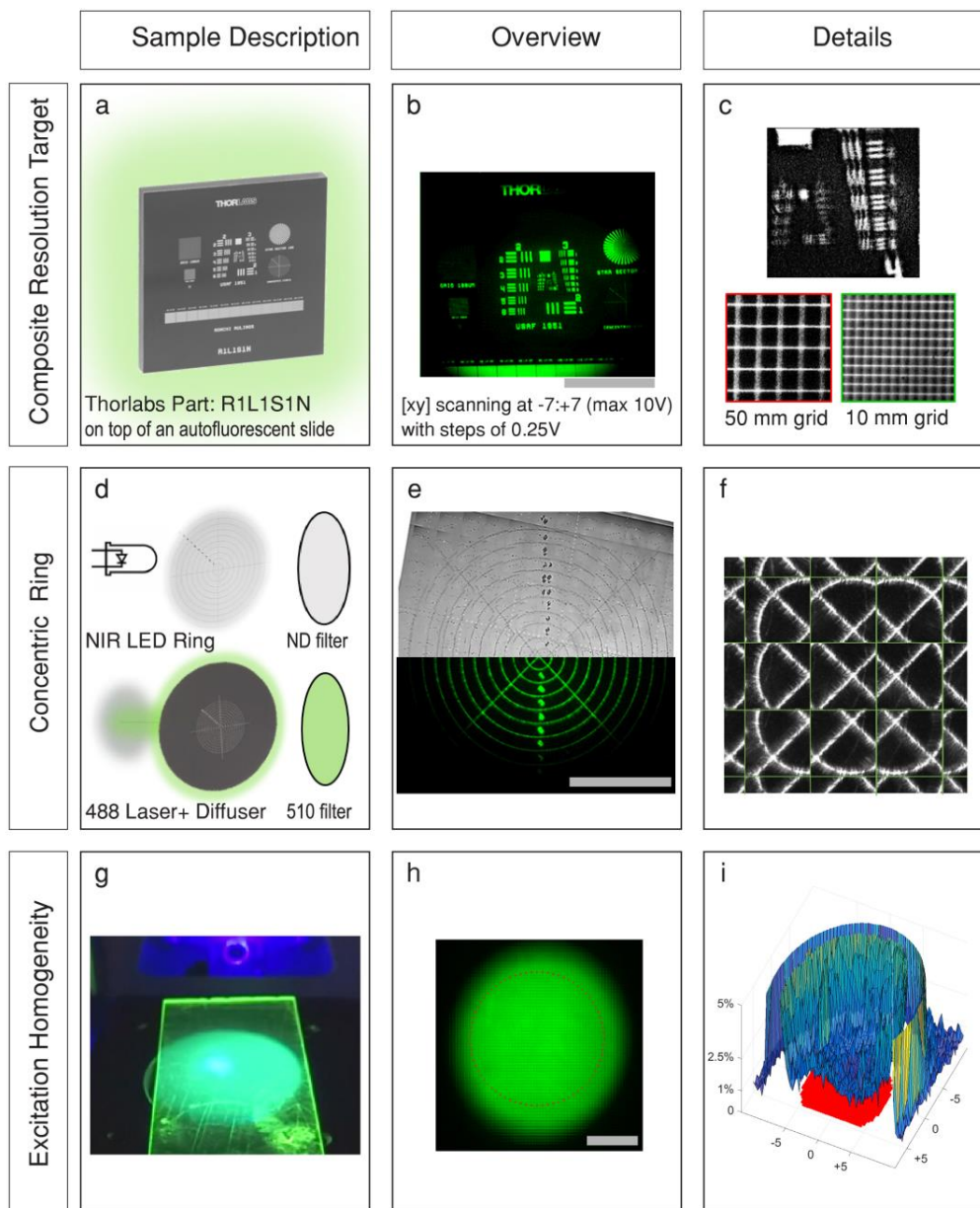Overview of NeuB*tracker* in MacroZoom configuration.

(**a**) Photograph of the system in its MacroZoom configuration (**b**) Zoom-in on the core system with labeling of the core parts; galvanometric mirrors (Galvo xy) for tracking, the electrically focus-tunable lens (ETL) for focusing, as well as the objectives used for excitation and detection by the two imaging channels (Beam splitter (BS) and dichroic mirror (DC)) (**c**) Drawing of the main components and the optical path to supplement the schematic in Figure 1. The inset on the upper right shows galvanometric scanning of a transparent composite resolution chart (with a fluorescent plastic slide placed underneath, 1951-USAF part: 3.7 x 3.7 mm) via the 15-fold magnified fluorescent channel. Individual tiles were acquired with overlap to allow for image stitching as shown below. The image on the lower right shows cellular features resolvable in a reporter line with sparse labeling of neurons throughout the anterior-posterior axis tg(*OMP4; GCaMP1.6 x mnGFF7; UAS:eGFP*). The scale bars represent 100 µm. All parts of NeuB*tracker* are compiled in a parts list that can be found in **Supplementary Table 1** and together with 3D CAD assemblies on neubtracker.org.
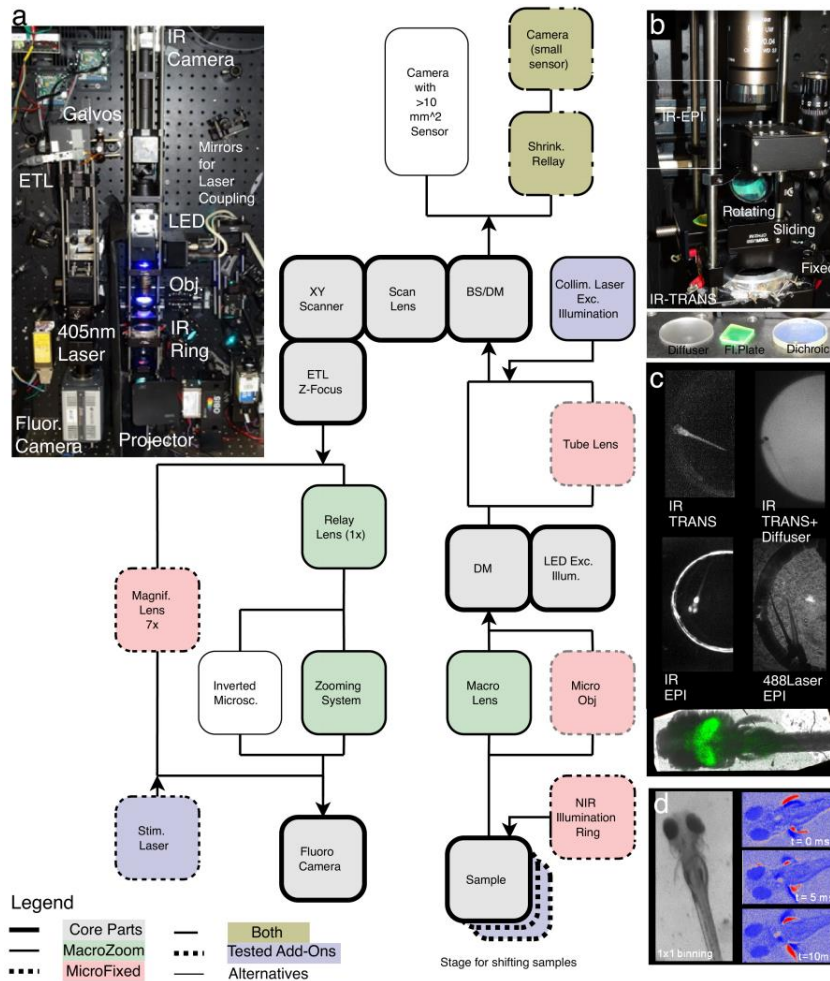
Supplementary Figure 2

Overview of the modular configurations of NeuB*tracker* as an imaging and interrogation platform

(**a**) Schematic of the combinations of the components used in the two configurations reported in this manuscript ('MacroZoom' and 'MicroFixed') and possible add-ons. The insets (upper left corner) gives a photographic overview of the alternative MicroFixed configuration which uses a microscope objective and fixed magnification. Several additional features were also tested such as coupling of additional lasers (either illuminating the whole arena or providing localized photostimulation via the galvanometric mirrors), or the use of motorized stages for high-throughput screening applications. (**b-d**) Different types of image contrasts that can be obtained by alternative configurations of NeuB*tracker*. As an example, the IR-illumination ring can either be positioned on top of the sample (IR-EPI inlet in (**b**)) or underneath it (IR-TRANS) to achieve epi- or transillumination. Furthermore, the addition of extra optical elements to the path can be achieved conveniently. A diffuser can be added for a projector to be placed under the sample (**c**- upper right). In this case, the noise level of the fluorescence channel is increased due to the bleed-through of backscattered excitation photons ((**d**)-middle right, images from MicroFixed configuration). By using a rotating holder, a dichroic can be positioned to deflect the excitation light after it passes through the sample. This results in images such as shown in **c** -top right. The presence of a sliding holder (or potentially a filter-wheel), enabled us to create the overlay in (bottom of **c**) were the same sensor captured fluorescence (green overlay) and directly afterwards, a brightfield image (gray) using an autofluorescent plastic plate as a 510 nm light source to create transillumination contrast utilizing the high dynamic range of the camera sensor. (**d**) To showcase the features that can be differentiated in the 7x magnified fluorescence channel of NeuB*tracker* MicroFixed, we show how the 7x channel may also be used to obtain anatomical details in reflection images with fast temporal sampling (5 ms exposure time) when an autofluorescent plastic slide (Chroma) is placed underneath the arena. The three frames on the right show movements of the fins and the heart displayed on a difference map (red for positive, blue for negative intensities with respect to the previous frame)

	Sample Description	Overview	Details

Composite Resolution Target

a — Thorlabs Part: R1L1S1N on top of an autofluorescent slide

b — [xy] scanning at -7:+7 (max 10V) with steps of 0.25V

c — 50 mm grid 10 mm grid

Concentric Ring

d — NIR LED Ring ND filter / 488 Laser+ Diffuser 510 filter

e

f

Excitation Homogeneity

g

h

i — 5% / 2.5% / 1% / 0 ; -5 / 0 / +5 ; -5 / 0 / +5

Supplementary Figure 3

Calibration of NeuB*tracker* components

(**a-c**) A composite resolution target (**a**) was placed on top of an autofluorescent plastic slide and scanned on the MicroFixed configuration by translating the FOV of the 7x fluorescent channel to generate (**b**) a stitched image of the entire resolution target at high resolution. Individual tiles are shown in (**c**) (**d-f**) Both positive and negative resolution targets consisting of concentric rings are placed in the sample holder to ensure proper registration of the FOVs of the two cameras. (**g-i**) Profile of the fluorescence excitation analyzed by using an autofluorescent plastic slide. The red circle in (**h**) indicates the diameter of the arena. (**i**) Corresponding plot of the standard deviation/mean for all xy-galvo positions to quantify the homogeneity throughout the arena (indicated by the red area).
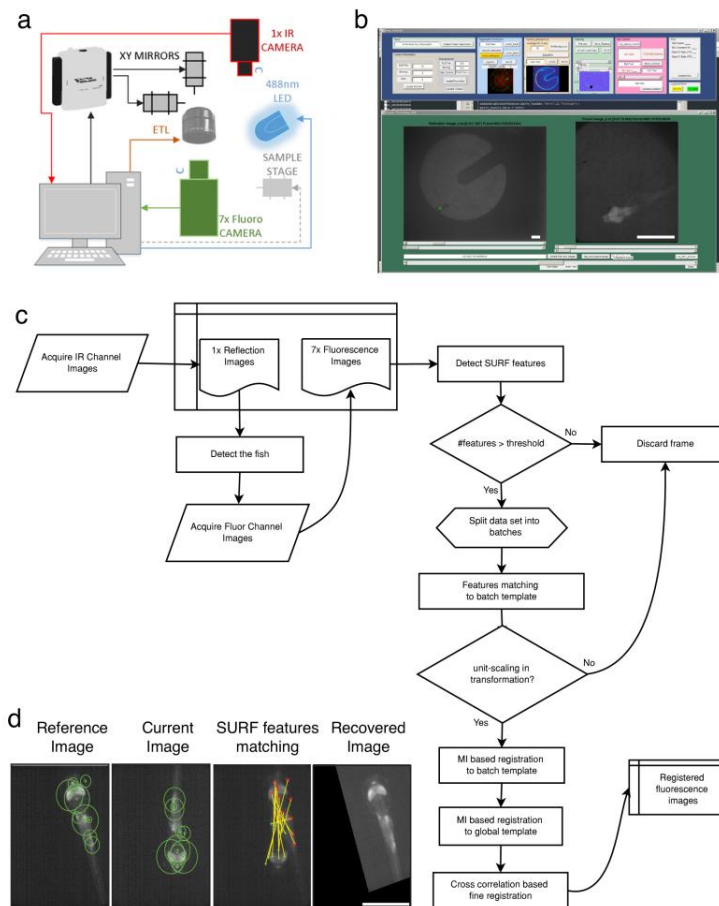
Supplementary Figure 4

Image acquisition automation and data processing pipeline

Image acquisition automation and data processing pipeline (**a**) Simplified schematic showing the main connections to and from the console running the control software. (**b**) Screenshot acquired during one of the acquisitions, showing the GUI of the control software displaying both of the imaging channels (left: 1x behavioral tracking, right: magnified real-time view of the fluorescent imaging). (**c**) Flowchart of the data acquisition and processing pipeline with (d) examples from the feature matching of the SURF registration. Scalebars represents 1 mm.
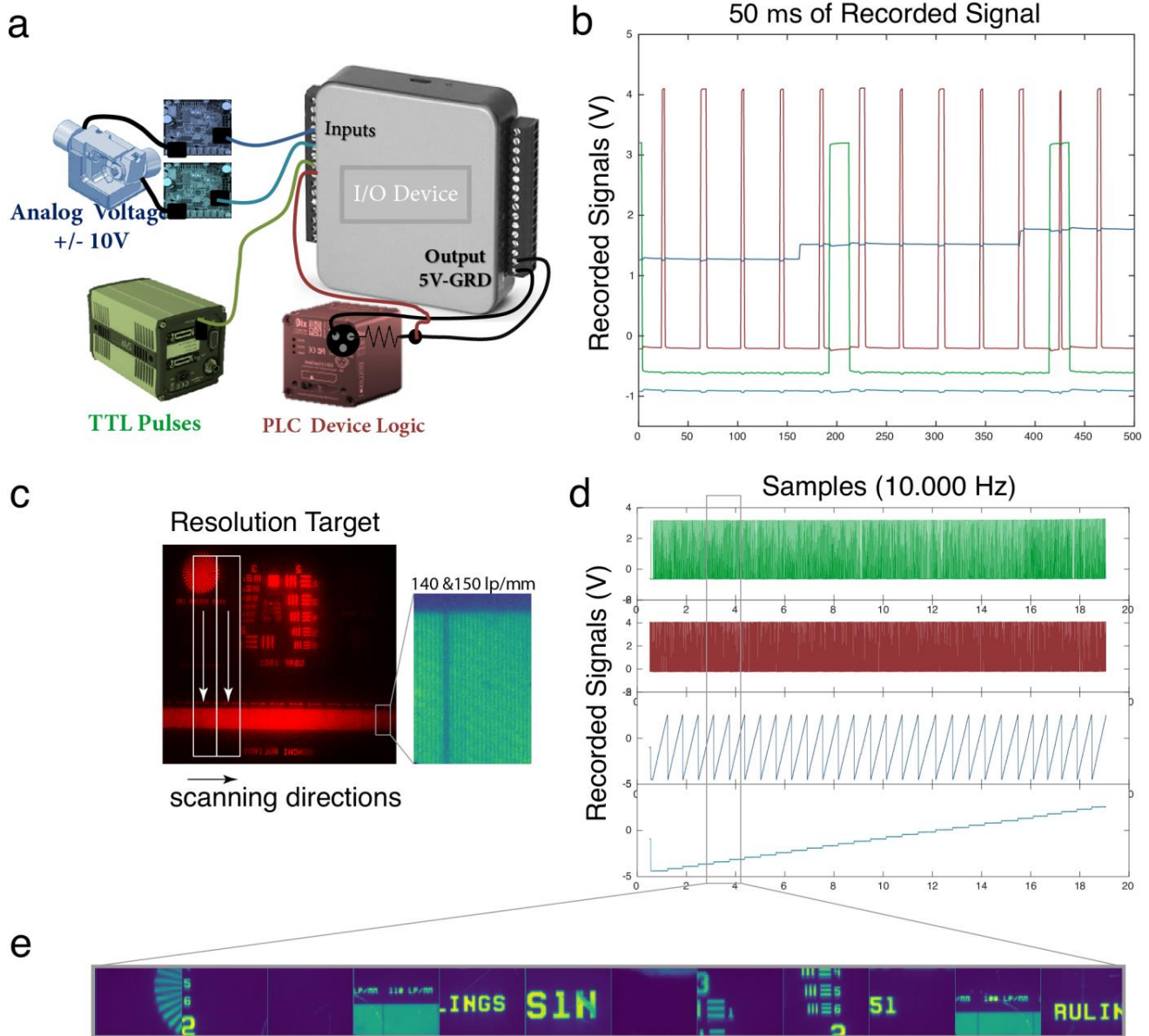
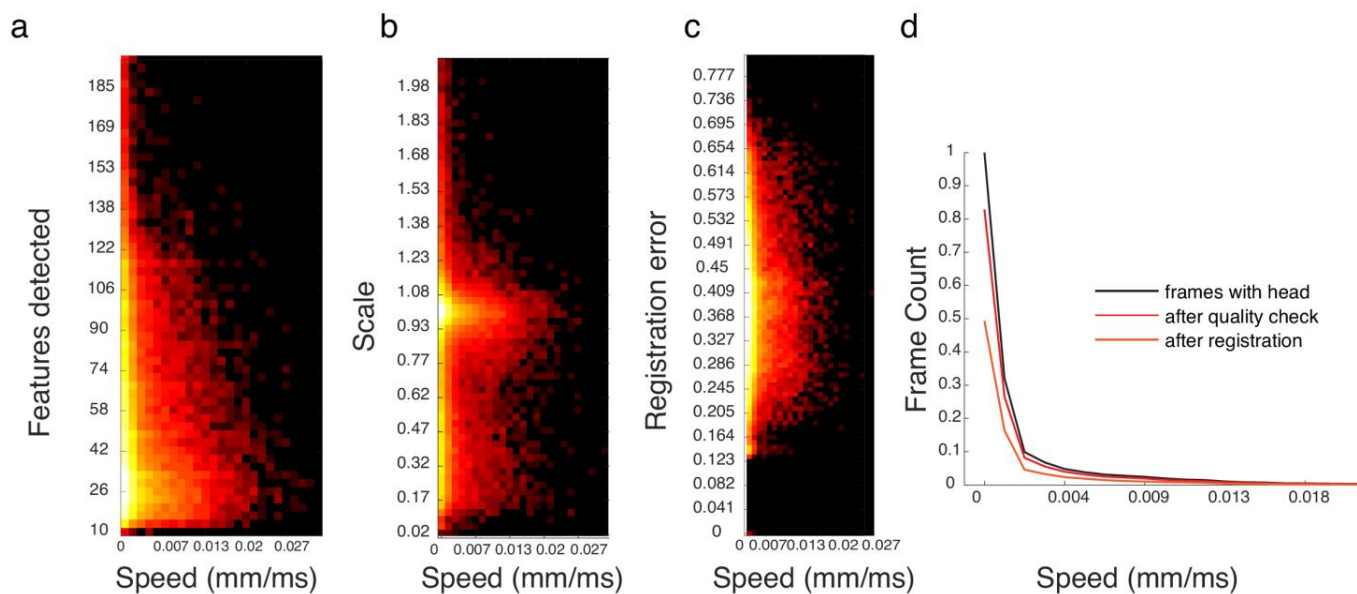**Supplementary Figure 5**

Synchronization of hardware components

(**a**) In addition to the timestamps obtained by the computer clock, we have recorded signals directly from the components of the system using different types of output (galvanometric mirrors: analog voltage, fluorescence camera: TTL pulses, 1x IR camera: PLC logic requiring additional input voltage). (**b**) Example raw signals from a 50 μs time window during which the 1x IR camera acquired at 200 Hz and magnified fluorescence images were obtained at 50 Hz (the beginning of the respective exposure times correspond to the high values in the red/green lines respectively). The blue and cyan signals are the control voltages to the galvanometric mirrors. (**c**) Image of the resolution target acquired for illustration by the 1x camera. (**d**) Example signals from the galvanometric mirrors from a raster scan of the resolution target shown in (**c**) resulting in 12 consecutive images shown as a montage in (**e**).
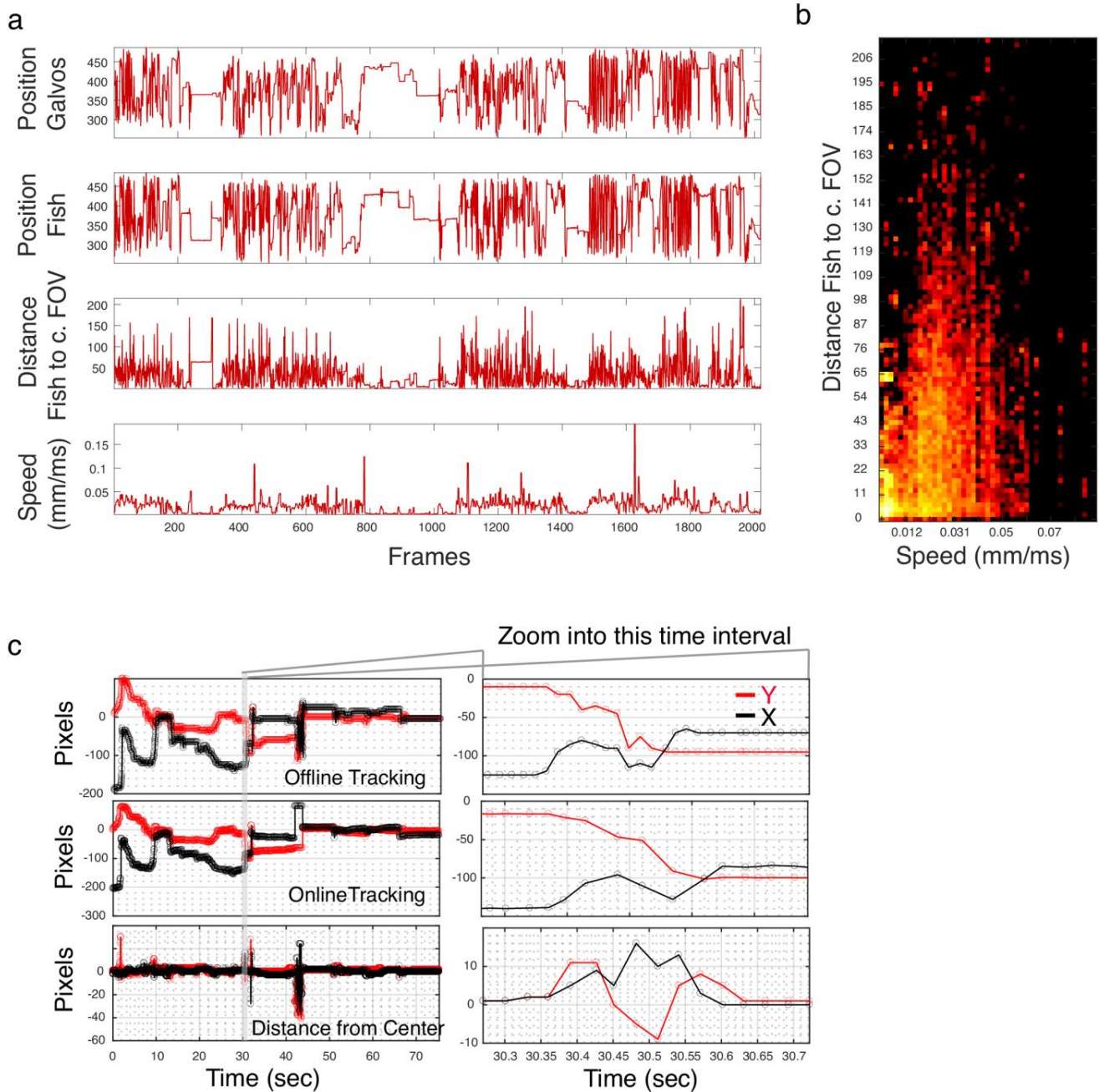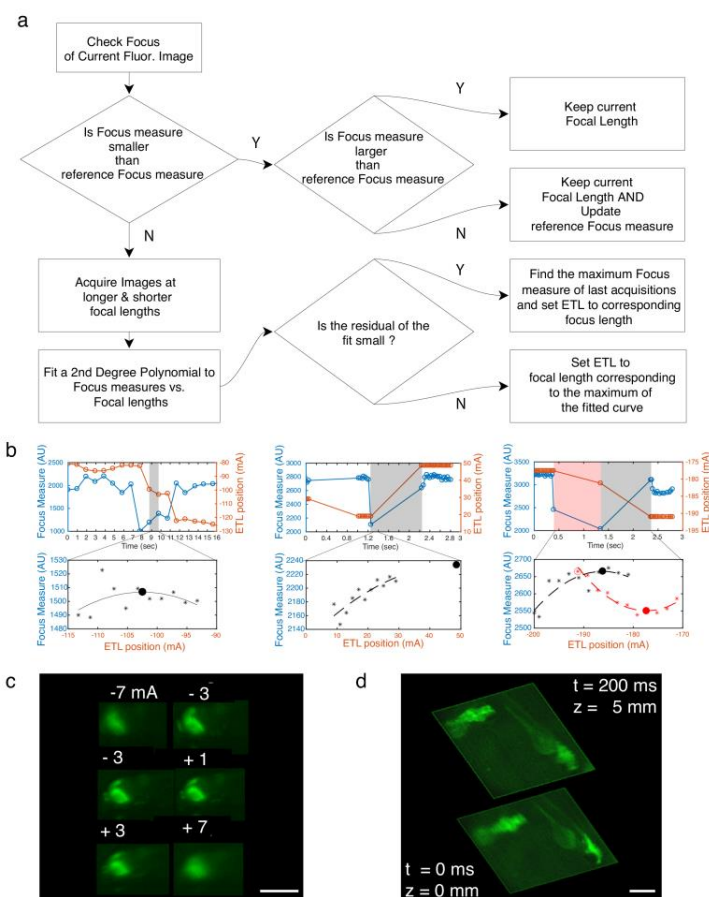
Supplementary Figure 6

Tracking accuracy

(**a**) Performance metrics of the tracking routine from an example dataset plotting the position of the galvanometric mirrors together with the position of the fish, the distance of the head of the fish to the center of the FOV and the swimming speed. (**b**) Heat map of aggregate data (used in Fig. 2a) showing the distance of the head of the fish to the center of the FOV as a function of swimming speed to illustrate how the tracking algorithm minimizes the movements of the galvanometric mirrors. (**c**) Comparison of the performance of online tracking *vs.* offline tracking as measured by the deviation of the distance of the head of the fish to the center of the FOV. The offline tracking has access to the entire image series and can apply better denoising and segmentation (based on background subtraction and spatial filtering in the frequency domain).

a   b   c   d

Supplementary Figure 7

Image quality assessment and performance of registration routine

The heat maps show several measures of the data shown in Figure 2 as a function of swimming speed: (**a**) the features detected by the initial quality check; frames with less than 5 features were discarded (**b**) the scaling factor of the similarity transformation obtained from the registration; this parameter was used to censor frames which deviated by more than 0.1 from unit scale (**c**) the registration error (ssd) from the final registration step of the remaining frames. (**d**) The histogram shows the imaging frames that survived the quality check and the subsequent selections based on registration quality.

Supplementary Figure 8

Flowchart and performance of autofocus routine using the ETL

(**a**) The electrically focus-tunable lens (ETL) can be controlled from the acquisition GUI for calibration of the system and optimizing the focus for each experimental run, reporter line and developmental stage used. It can also be run via an autofocus routine to enable, *e.g.*, refocusing for long-term recordings or screens. The routine operates by computing a focus measure of each acquired frame. If this measure is lower than a threshold, additional focus measures are obtained from images acquired by varying the focal length of the ETL in both directions. A 2nd-degree polynomial is fitted to the obtained focus measures *vs.* the focal lengths that were acquired. If the residuals of the fit are small, the ETL is set to the focal length that resulted in the largest focus measure. If the residuals are large, the maximum of the fitted curve is used to set the ETL to the corresponding focal length. (**b**) To systematically demonstrate the performance of the autofocus algorithm, we moved an arena containing a larva tg(*HuC:H2B-GCaMP6s*) out of focus and let the focus routine adjust the focal length of the ETL to recover focus. In the panels beneath the flowchart, three representative cases are shown. The left panel shows the case in which a drop of the focus measure occurred after a downward movement of the stage at 7 seconds (cyan, left y-axis). The control currents (-80 to -130 mA) that were sent to the ETL to change focal length and regain focus are plotted in orange (right y-axis). The bottom graph displays the focus measure against the ETL position for 10 acquisitions acquired at different focal lengths. The large black dot shows the estimation of the optimal focal length that was then used to recover focus. The middle graph shows a case in which the estimated optimal focal length (large black dot) falls outside the range of measurement that were taken; still, focus was recovered by setting the ETL to the predicted focal length. The right panel shows an instance in which the arena movement was continuing. This resulted in the focal measures from the acquisitions shown in red together with the fitted function and the estimated focal length. Since the first term of the fitted polynomial (shown in red) was negative, the routine selected the maximum focal measure it found among its acquired images (as opposed to the estimate) to set the focal length of the ETL. (**c**) Fine-focusing of the ETL (mA control currents correspond to submicron steps in the focal length) on a larval brain. (d) To showcase the focal length range of the ETL, fish swimming in different depths in a 10 mm deep arena were brought in focus. The bottom frame focuses on the right fish located close to the surface (fish is tilted). The top frame was acquired 200 ms later and focused on the left fish swimming at a greater depth.
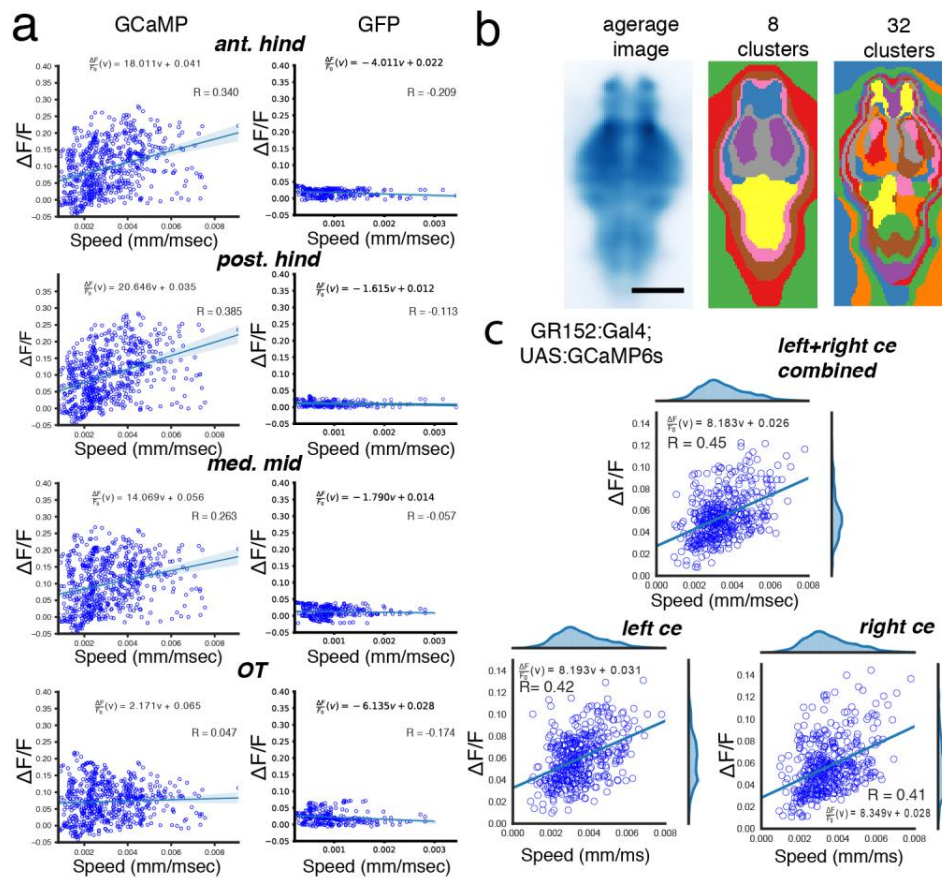
Supplementary Figure 9

Additional analysis of neuronal activity during spontaneous swimming

(**a**) Correlation plot of the fluorescent signal changes against the swimming speed in the anterior hindbrain (ant. hind), posterior hindbrain (post. hind), the medial midbrain (med. mid), and the optic tectum (OT) from the ROIs shown in Figure 1c. As compared to the other brain regions, OT showed lower correlations with speed. The plots in the right column show the same analysis for an animal with panneuronal expression of GFP instead of GCaMP6s (tg(HuC:Gal4;UAS:GFP x Ath5:Gal4) in which no correlated regions (more than 4 connected voxels) were found at the same threshold (p<10[-5]). **b**) Cluster analysis complementing the regression analysis shown in Figure 1c also identified highly correlated signal changes in the the anterior and posterior hindbrain regions (*e.g.,* yellow cluster when searching for maximally 8 clusters). (**c**) Correlation plots *vs.* swimming speed of the fluorescent signal detected in the left and right cerebellum (ce) (and both sides combined) from a fish with selective expression of GCaMP6s in only the granule cells of the cerebellum (tg(*gSA2AzGFF152B;UAS:GCaMP6s)* corresponding to the experiment shown in Figure 1d.
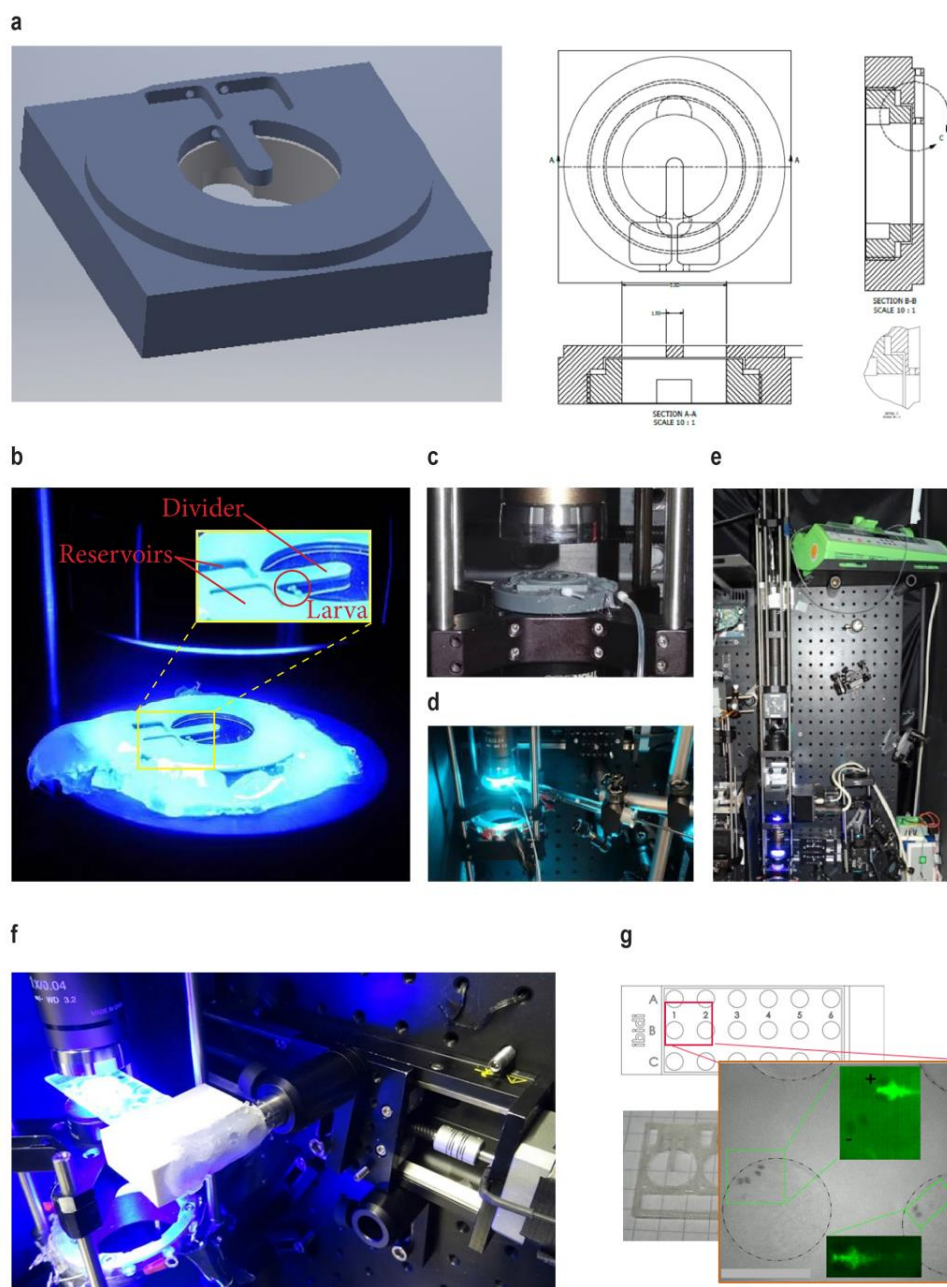
Supplementary Figure 10

Different designs of the NeuB*tracker* arena

(**a**) The default arena design consists of two CNS-milled plastic (or metal) parts, holding between them a glass coverslip of 9 mm in diameter (1 mm height) that can be easily exchanged between experiments. Shown here is a version used in the experiments of Figures 1-3 that has a central divider separating the arena in two compartments into which compounds can be delivered via diffusion from two quadratic reservoirs (**b**) The picture shows the illuminated arena. (**c-e**) The system allows for long-term recording over several hours in which case the water level (75-100 µL) can be kept constant by compensating for evaporation. This can be easily achieved via a syringe pump (green) as shown in the photograph. (**f**) A 150 mm travel path x-stage is incorporated into the system to move a (**g**) commercial multiwell-slides with 18 holes (5 mm diameter each) positioned by a custom-made 3D printed holder. We showcase the use of this configuration for sorting zebrafish based on their expression level of GCaMP5g (+ and – in the upper fluorescent image).
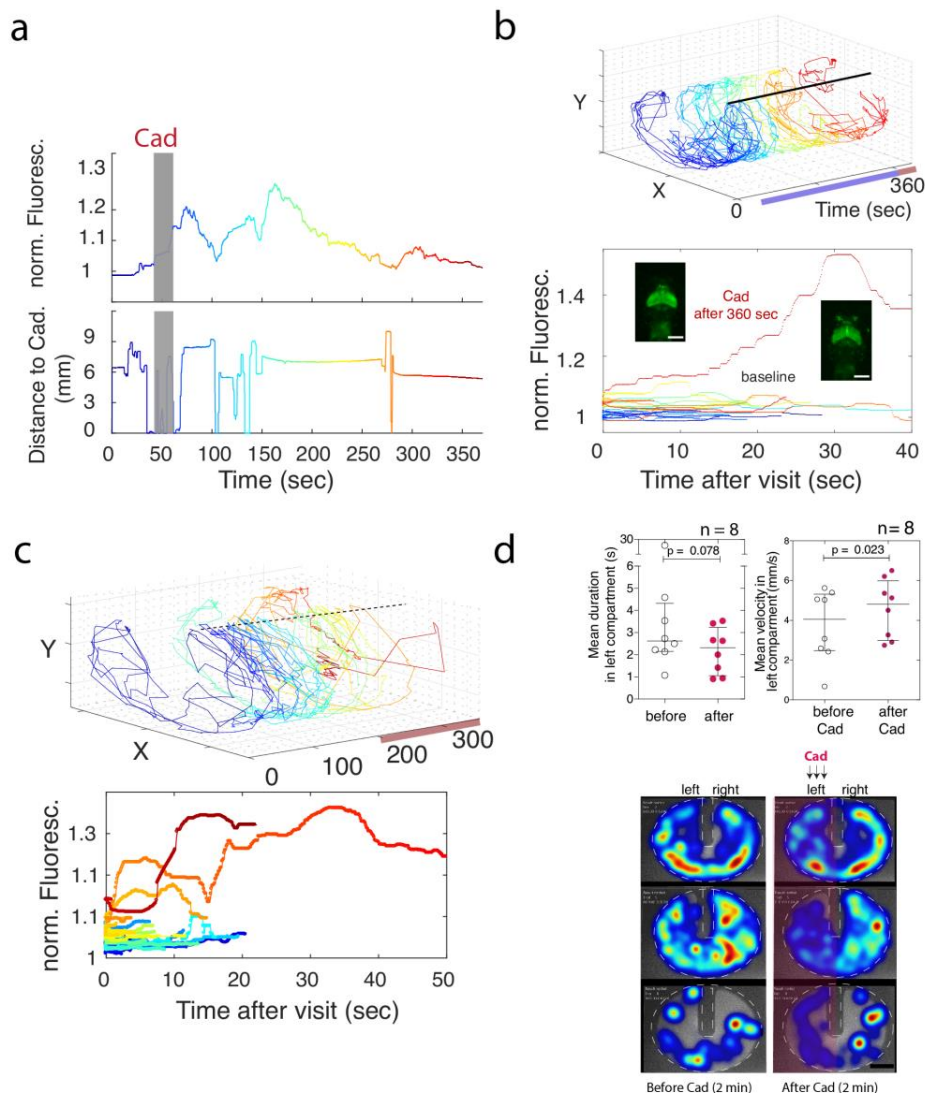
Supplementary Figure 11

Further characterization of neurobehavioral effects of cadaverine.

(**a**) Fluorescent signal changes recorded in the olfactory epithelium in the experiment shown in Figure 1e,f plotted here continuously over the entire duration of the experiment together with the distance of the fish to the cadaverine port at each point in time (color coding as in Figure 1f). (**b**) Control experiment in which water was injected instead of cadaverine with identical duration and settings to the experiment shown in Figure 1f,g. After the end of the 360 second baseline observation period, cadaverine was injected. Data are plotted analogously to Figure 1 and **a**. White scalebar represents 200 μm. (**c**) Additional cadaverine stimulation experiment run with a longer baseline than that shown in Figure 1f and showing again multiple visits to the cadaverine port with subsequent activations of oe. (**d**) The behavioral analyses show the median and the interquartile range of the mean duration of visits, as well as the mean swimming velocity in the left compartment before and after Cadaverine (Cad) delivery (100 μM). Cad reached the compartment via diffusion from a reservoir on the rim of the arena wall connected to the arena via a thin conduit (Wilcoxon matched-pairs signed rank tests, p = 0.0781, two-tailed (mean duration) and p = 0.023, two-tailed. (**e**) Representative heat maps of the behavioral traces for 3 different individuals during 2 minutes before (left) and after (right) delivery of cadaverine to the left compartment (purple shading in d). Black scalebar represents 2 mm.
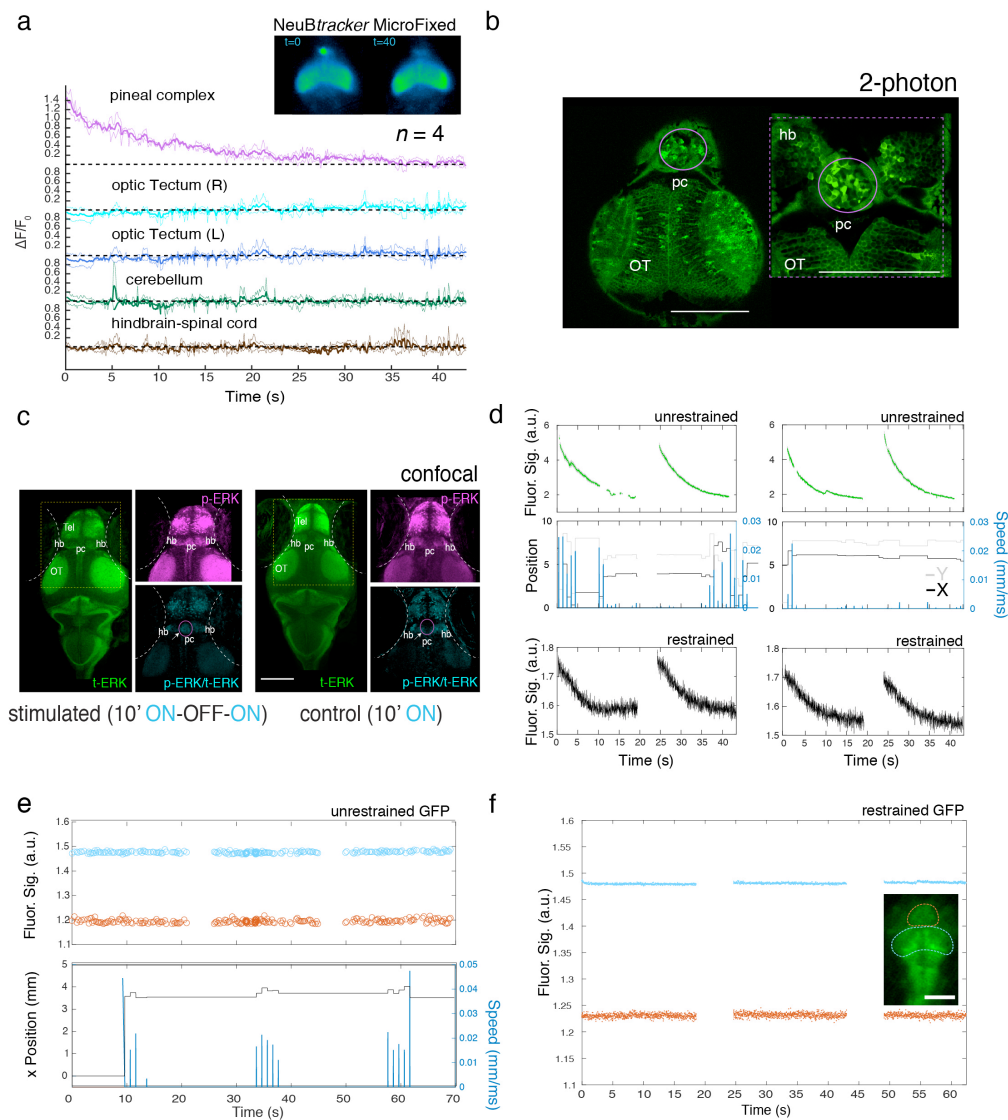
Supplementary Figure 12

Comparison of light-dependent pineal complex activity in freely moving and restrained animals

(**a**) Fluorescence signal changes obtained on NeuB*tracker* in MicroFixed configuration corresponding to the behavioral data shown in Figure 3 b,c. The signal from the different ROIs is averaged over 4 animals with bounds of one standard deviation in dashed lines (fitted time constant: 11.9 ± 1.1 seconds.) (**b**) Single plane through *pc* (two-photon microscopy; inset shows magnification) as anatomical reference. (**c**) Staining with the neural activity marker phosphorylated ERK (p-ERK, red), total ERK (t-ERK, green) and their ratio (p-ERK/t-ERK, cyan) from a fish imaged on NeuBtracker with ten cycles of 50 s ON/10 s OFF for 10 min. (**d**) Fluorescent signal changes (green traces) in the pineal complex (*pc*) during two cycles of light ON/OFF stimulation selected from the 10 cycles shown as average in Figure 3a from a short period in which the larva tg(*gSA2AzGFF49A;UAS:GCaMP7a*, 6 dpf) was relatively stationary (right) compared with a phase with swimming activity (left side) as seen from the plot of the concurrently recorded x- and y-position of the larva and its swimming speed (middle panel). The bottom panel shows as a reference the *pc* signal obtained from a restrained larva (embedded in agar, black trace). (**e,f**) To confirm the quality of image registration and control for any instrument-dependent effects on the signal changes, we performed the same experiment but using larvae expressing GFP *tg(*HuC:Gal4;UAS:eGFP*)* instead of a calcium indicator either freely swimming (e) or embedded in agar (f). The fluorescent signal traces are plotted from the ROIs indicated in the inset in (f). Scalebars represent 200 μm.
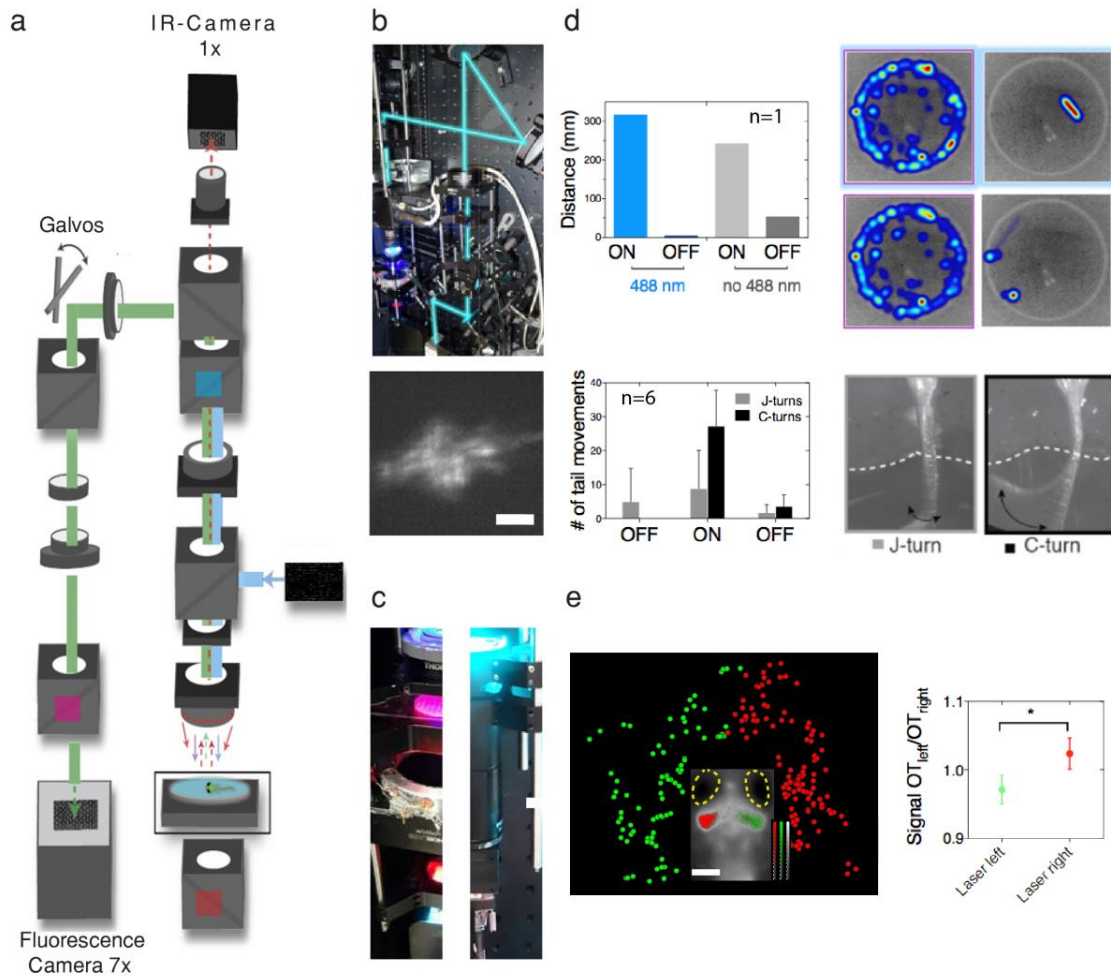
Supplementary Figure 13

Alternative optical paths for using NeuB*tracker* for imaging and stimulation

(**a**) Simplified schematic showing additional options for optical ports in NeuB*tracker* here shown in MicroFixed configuration. (**b**) Example of coupling a 488 nm laser instead of the LED as an excitation light source. Efficient excitation of a GCAMP6 tg(*HuC:H2B-GCaMP6s*) could also be achieved with a laser but speckle patterns were apparent (which could be removed by a rotating diffuser or alternatively used for structured illumination approaches). (**c**) The transparent bottom of the arena and the use of an NIR illumination ring rather than a table afford direct coupling of a video projector to provide visual stimulation to the animal. (**d**) A 405 nm laser was coupled via the galvanometric mirrors to provide a visual stimulus to the animal. During periods in which the laser spot was moved to repeatedly approach the head, the fish swam a longer distance than during periods in which the 405 nm laser was off. This was the case with and without a 488 nm laser turned on in the background. These data are consistent with data we obtained from fish immobilized in agar in which illumination of the head with the 405 nm laser lead to an increase in the number of specific tail deflections that can be characterized as C-turns (indicative of aversion) and J-turns by videography conducted with an IR camera. Individual counts from 6 individuals are shown with median and interquartile range. (**e**) In this experiment, the 405 nm laser spot was moved in a semi-circular path in a left-right-left trajectory in front of the head of a tg(*gSA2AzGFF49A;UAS:GCaMP7a*, 7 dpf) larva as indicated by color-coding for relative position. Neuronal activations were elicited in the optic tectum contralateral to the relative location of the laser spot (the color overlay over the co-registered frames in gray shows the ratio of the average fluorescence between frames in which the laser spot was located on the left and frames in which it was positioned on the right relative to the location of the fish head). The plot (median and interquartile range) shows a significant difference ($p < 0.01$, Wilcoxon matched-pairs signed rank test) of the ratio of the average fluorescence intensity of the left and right OT in frames with laser spots presented on the left (green) or right (red) of the fish respectively.

	Description	Company	Part Name / ID
Illumination	IR - LED	Roithner Laser Technik	12x ELD-1060-525
	IR - LED Holder	Custom Made	Ring for LED placement
	GCaMP-Exc.	MountainPhotonics	UHP-T-LED-460 Ultra High Power Blue LED Light Source
Obj.	1x Objective	Nikon	HR Plan Apo WD 54
	1x Objective	Nikon	CFI P-Achromat UW 1x/ 0.04/ 3,20
	Tube Lens	Thorlabs	ITL200 Infinity-Corrected Tube Lens
1x/IR	IR Camera	Ximea	MQ013RG-E2
	1:3 Relay	Thorlabs	1:3.33 Matched Achromatic Pair, B Coated
	1:5 Relay	Thorlabs	150 & 50 mm Achrom. Doublet pairs
3D Scanning System	Galvo (XY)	Thorlabs	GVS312/M - 2D Large Beam (10 mm) Diameter Galvo System
	ETL (Z)	Optotune	Fast electrically tunable lens EL-10-30-C-VIS-LD
Scanning Relay and Magnification	1 Telesc. Lens	Thorlabs	2x 100mm, 60mm Achrom. (Plössl Configuration)
	2 Telesc. Lens	Thorlabs	f=150 mm, Ø2" Achromatic Doublet
	Zooming System	Leica	Z16 Apo
	1 Telesc. Lens	Thorlabs	f=50 mm, Ø1" Achromatic Doublet,
	2 Telesc. Lens	Thorlabs	f=200 mm, Ø2" Achromatic Doublet
Fluor. Acq.	Camera	Andor	Zyla5.5-USB3 (or Neo sCMOS)
Manipulation Laser	Laser	Coherent	407 nm / 50 mW
	Alignment Mirrors	Thorlabs	Kinematic Mirror Mount for Ø2" Optics
	Coupling Lens	Thorlabs	f=200 mm, Ø2" Achromatic Doublet
Controllers	Main (PC)	Terra	i7-3770, 32GB RAM, Scorpio PCI-SSD@ 2GB/s
	for Galvo Mirrors	National Instruments	USB-9263, 4-Channel, ±10 V, 16-Bit Analog Voltage Output Module
	for Green LED	Arduino	Uno
Filters	Filters/Dichroics	Chroma Technology	ET470/40x, T495lpxr, (LED coupling) T770lpxr, ET780lp, (IR Camera) zt405rdc (stimulation laser coupling) ET525/50m (Fluorescence Camera)
	Filter Cubes	Thorlabs	30 mm Cage-Compatible Fluorescence Filter Cube
Example pieces for mechanical support	Rails	Thorlabs	Extended Dovetail Rail Carrier
	Bases	Thorlabs	Standard Ø1/2" Post Holders
	Post	Thorlabs	Ø12.7 mm Graduated Optical Post
	Rods	Thorlabs	ER Assembly Rods
	Cage Syst. Holder	Thorlabs	30 mm to 60 mm Cage Plate Adapter, M4 Tap
	Sliding Mount	Thorlabs	Removable Filter Holder
	Pivoting Mount	Thorlabs	Pivoting, Quick-Release, Ø1" Optic Mount
	Kin. Lens Mounts	Thorlabs	XY Translating Lens Mount
Add-ons	Motorized Stage	Zaber	Motorized linear slide, 150 mm travel, RS-232
	Alternative GCaMP Excitation	Coherent	OBIS 488 nm- LX 150 mW (coupled through ZT488dcrb)
	500FPS camera	Ximea	MQ003MG-CM

Supplementary Table 1 | Components of NeuB*tracker*. Components that are used only in one configuration are highlighted in green for the MacroZoom configuration and yellow for the MicroFix configuration. A complete parts list can be found on www.neubtracker.org.

A Letters of Approval for the manuscripts reproduction from Publishers

Apart from our effort as authors of the manuscript, the publishers have contributed to different degrees to the presented here articles, including editorial feedback, coordinating peer-review process, copy-editing and typesetting. Thus we have requested their approval for including them in this Dissertation the manuscripts. In the next four pages, we include letters of approval from each of the publisher of the papers we include in this Dissertation. The letters from the Optical Society of America(OSA) and Society of Photo-Optical Instrumentation Engineers (SPIE) were acquired through e-mail communication with the responsible office. For the Institute of Electrical and Electronics Engineers(IEEE) and Nature Methods manuscripts, we used the online forms from RightsLink©.

Request for using my: 10.1364/OL.39.003919 article on cummulative PhD Disseration

pubscopyright <copyright@osa.org>   Tue, Nov 21, 2017 at 10:15 PM
To: Panagiotis Symvoulidis <symvou@gmail.com>, pubscopyright <copyright@osa.org>

Dear Panagiotis Symvoulidis,

Thank you for contacting The Optical Society.

For the use of material from Panagiotis Symvoulidis, Karin M. Jentoft, P. Beatriz Garcia-Allende, Jürgen Glatz, Jorge Ripoll, and Vasilis Ntziachristos, "Steady-state total diffuse reflectance with an exponential decaying source," Opt. Lett. 39, 3919-3922 (2014):

As long as the copyrighted material is included within the body, section or chapter, of the thesis, and is not posted separate from the thesis, OSA considers your requested use of its copyrighted materials to be permissible within the author rights granted in the Copyright Transfer Agreement submitted by the requester on acceptance for publication of his/her manuscript. If the entire article is being included, it is requested that the **Author Accepted (or preprint)** version be the version included within the thesis and that a complete citation of the original material be included in any publication. This permission assumes that the material was not reproduced from another source when published in the original publication.

The **Author Accepted** version is the preprint version of the article that was accepted for publication but not yet prepared and/or formatted by The Optical Society or its vendors.

Let me know if you have any questions.

Kind Regards,

Rebecca Robinson

Rebecca Robinson

November 21, 2017

Authorized Agent, The Optical Society

From: Panagiotis Symvoulidis [mailto:symvou@gmail.com]
Sent: Monday, November 20, 2017 7:21 AM

RightsLink®

IEEE Requesting permission to reuse content from an IEEE publication

Title: Serial sectioning and multispectral imaging system for versatile biomedical applications

Conference Proceedings: 2014 IEEE 11th International Symposium on Biomedical Imaging (ISBI)

Author: P. Symvoulidis

Publisher: IEEE

Date: April 2014

Copyright © 2014, IEEE

Thesis / Dissertation Reuse

The IEEE does not require individuals working on a thesis to obtain a formal reuse license, however, you may print out this statement to be used as a permission grant:

Requirements to be followed when using any portion (e.g., figure, graph, table, or textual material) of an IEEE copyrighted paper in a thesis:

1) In the case of textual material (e.g., using short quotes or referring to the work within these papers) users must give full credit to the original source (author, paper, publication) followed by the IEEE copyright line © 2011 IEEE.
2) In the case of illustrations or tabular material, we require that the copyright line © [Year of original publication] IEEE appear prominently with each reprinted figure and/or table.
3) If a substantial portion of the original paper is to be used, and if you are not the senior author, also obtain the senior author's approval.

Requirements to be followed when using an entire IEEE copyrighted paper in a thesis:

1) The following IEEE copyright/ credit notice should be placed prominently in the references: © [year of original publication] IEEE. Reprinted, with permission, from [author names, paper title, IEEE publication title, and month/year of publication]
2) Only the accepted version of an IEEE copyrighted paper can be used when posting the paper or your thesis on-line.
3) In placing the thesis on the author's university website, please display the following message in a prominent place on the website: In reference to IEEE copyrighted material which is used with permission in this thesis, the IEEE does not endorse any of [university/educational entity's name goes here]'s products or services. Internal or personal use of this material is permitted. If interested in reprinting/republishing IEEE copyrighted material for advertising or promotional purposes or for creating new collective works for resale or redistribution, please go to http://www.ieee.org/publications_standards/publications/rights/rights_link.html to learn how to obtain a License from RightsLink.

If applicable, University Microfilms and/or ProQuest Library, or the Archives of Canada may supply single copies of the dissertation.

BACK   CLOSE WINDOW

Request for using my: 10.1117/1.JBO.20.9.096009 article on cummulative PhD Disseration

Nicole Harris <nicoleh@spie.org>   Mon, Nov 20, 2017 at 5:39 PM
To: Panagiotis Symvoulidis <symvou@gmail.com>

Dear Panos,

Thank you for seeking permission from SPIE to reprint material from our publications. As author, SPIE shares the copyright with you, so you retain the right to reproduce your paper in part or in whole.

   Publisher's permission is hereby granted under the following conditions:

      (1) the material to be used has appeared in our publication without credit or acknowledgment to another source; and

      (2) you credit the original SPIE publication. Include the authors' names, title of paper, volume title, SPIE volume number, and year of publication in your credit statement.

Sincerely,

Nicole Harris

Administrative Editor, SPIE Publications

1000 20th St.

Bellingham, WA 98225

+1 360 685 5586 (office)

nicoleh@spie.org

SPIE is the international society for optics and photonics. http://SPIE.org

SPIE.

From: Panagiotis Symvoulidis [mailto:symvou@gmail.com]
Sent: Monday, November 20, 2017 4:24 AM
To: reprint_permission <reprint_permission@spie.org>
Subject: Request for using my: 10.1117/1.JBO.20.9.096009 article on cummulative PhD Disseration

[Quoted text hidden]

RightsLink®

SPRINGER NATURE

Title: NeuBtracker—imaging neurobehavioral dynamics in freely behaving fish

Author: Panagiotis Symvoulidis, Antonella Lauri, Anca Stefanoiu, Michele Cappetta, Steffen Schneider et al.

Publication: Nature Methods

Publisher: Springer Nature

Date: Oct 2, 2017

Copyright © 2017, Springer Nature

Author Request

If you are the author of this content (or his/her designated agent) please read the following. If you are not the author of this content, please click the Back button and select no to the question "Are you the Author of this Springer Nature content?".

Ownership of copyright in original research articles remains with the Author, and provided that, when reproducing the contribution or extracts from it or from the Supplementary Information, the Author acknowledges first and reference publication in the Journal, the Author retains the following non-exclusive rights:

To reproduce the contribution in whole or in part in any printed volume (book or thesis) of which they are the author(s).

The author and any academic institution, where they work, at the time may reproduce the contribution for the purpose of course teaching.

To reuse figures or tables created by the Author and contained in the Contribution in oral presentations and other works created by them.

To post a copy of the contribution as accepted for publication after peer review (in locked Word processing file, of a PDF version thereof) on the Author's own web site, or the Author's institutional repository, or the Author's funding body's archive, six months after publication of the printed or online edition of the Journal, provided that they also link to the contribution on the publisher's website. Authors wishing to use the published version of their article for promotional use or on a web site must request in the normal way.

If you require further assistance please read Springer Nature's online author reuse guidelines.

For full paper portion: Authors of original research papers published by Springer Nature are encouraged to submit the author's version of the accepted, peer-reviewed manuscript to their relevant funding body's archive, for release six months after publication. In addition, authors are encouraged to archive their version of the manuscript in their institution's repositories (as well as their personal Web sites), also six months after original publication.

v1.0

BACK   CLOSE WINDOW